DESIGN OF REVERSIBLE "SMART" SURFACES FOR BIOMEDICAL AND NANOTECHNOLOGICAL APPLICATIONS

by

Thanh-Nga T. Tran

Bachelor of Science (Honors)
California Institute of Technology, 1996

Submitted to the Harvard-MIT Division of Health Sciences and Technology
in Partial Fulfillment of the Requirements for the Degree of

DOCTOR OF PHILOSOPHY

at the

MASSACHUSETTS INSTITUTE OF TECHNOLOGY

September 2003

Signature of author: _____
Harvard-MIT Division of Health Sciences & Technology
September 4, 2003

Certified by: _____
Robert S. Langer
Kenneth J. Germeshausen Professor of Chemical and Biomedical Engineering
Thesis Advisor

Accepted by: _____
Martha L. Gray
Edward Hood Taplin Professor of Medical and Electrical Engineering
Co-director,Harvard-MIT Division of Health Sciences and Technology

This doctoral thesis has been examined by a committee as follows:

Professor Robert S. Langer _____
Chair and Thesis Advisor
Kenneth J. Germeshausen Professor of Chemical and Biomedical Engineering

Professor Paula T. Hammond _____
Thesis Reader
Associate Professor, Chemical Engineering
ISN Facilities and Space Coordinator

Professor Klavs Jensen _____
Thesis Reader
Lammot du Pont Professor of Chemical Engineering
Professor of Materials Science and Engineering

Professor Martha L. Gray _____
Edward Hood Taplin Professor of Medical and Electrical Engineering
Co-director,Harvard-MIT Division of Health Sciences and Technology

DESIGN OF REVERSIBLE "SMART" SURFACES FOR BIOMEDICAL AND NANOTECHNOLOGICAL APPLICATIONS

by

Thanh-Nga T. Tran

Submitted to the Harvard-MIT Division of Health Sciences and Technology on September 4, 2003 in Partial Fulfillment of the Requirements for the Degree of Doctor of Philosophy in Medical Engineering

ABSTRACT

Chapter 1. An Introduction to Self-Assembled Monolayers & Surface Characterization

A brief summary of the formation, structure, and characterization techniques of self assembled monolayers (SAMs) is described. The characterization techniques include contact angle goniometry, ellipsometry, grazing-angle Fourier-transform infrared spectroscopy (FT-IR), X-ray photoelectron spectroscopy (XPS), cyclic voltammetry (CV), sum-frequency generation spectroscopy (SFG), and atomic force microscopy (AFM).

Chapter 2. A Reversibly Switching Surface

The design of surfaces that exhibit dynamic changes in interfacial properties such as wettability in response to an electrical potential is described. The change in wetting behavior was caused by surface-confined, single-layered molecules undergoing conformational transitions between a hydrophilic and a moderately hydrophobic state. Reversible conformational transitions were confirmed both at a molecular level using sum-frequency generation spectroscopy and at a macroscopic level using contact angle measurements. This type of surface design enables amplification of conformational transitions at a molecular level to macroscopic changes in surface properties without altering the chemical identity of the surface. Such reversibly switching surfaces may open new opportunities in interfacial engineering.

Chapter 3. A Synthetic Chemical Route for the Formation of Homogeneously-Mixed Self-Assembled Monolayers

A novel way to produce self-assembled monolayers (SAMs) uniformly mixed on the molecular length scale is described. Initially, a precursor SAM was formed from molecules that are derived from 16-mercaptohexadecanoic acid (MHA) and contain a globular end group. Self-assembly of these molecules resulted in a SAM that is densely packed with respect to the space-filling end groups, but shows low-density packing with respect to the hydrophobic chains. Subsequent cleavage of the space-filling end groups established a low-density SAM of MHA. A mixed monolayer of MHA and *n*-butanethiol was formed by backfilling the low-density monolayer of MHA with the corresponding alkanethiol. The new "mixed" SAM was characterized by optical ellipsometry, contact angle goniometry, X-ray photoelectron spectroscopy (XPS), Fourier Transform Infrared Spectroscopy (FT-IR), cyclic voltammetry (CV), and reductive desorption voltammetry. The results indicate a uniformly mixed monolayer as compared to a SAM generated by coadsorption of mixtures of the same MHA and *n*-butanethiol molecules. This approach provides a way to produce SAMs that are uniformly mixed using a synthetic chemical route, which affords considerable flexibility in composition and also in the ratio of the different molecules in the mixed SAM.

Chapter 4. Design of Oligonucleotide Arrays Using Homogeneously Mixed Self – Assembled Monolayers

We have employed two quantitative techniques, quart-crystal microbalance with dissipation monitoring (QCM-D) and surface plasmon resonance imaging (SPR) to quantify the hybridization efficiency of a 25-mer oligonucleotide probe to two different surfaces: a dense 16-mercaptohexadecanoic acid self-assembled monolayer (MHA SAM) and a homogeneously-mixed (HM) SAM generated from the method described in Chapter 3 that allows for regular spacing of functional –COOH groups. This reduced density of functional groups led to reduced attachment of oligonucleotide probes to the surface, increasing the area per probe, and allowed more space in which complimentary sequence can bind. Reducing the density of immobilized probes led to the improvement in hybridization efficiency as demonstrated in both SPR and QCM-D results, which are comparable to previous reports. Our method paves the way for customizing binding efficiency and target probe density based on the distance between functional groups. By changing the headgroup size of the precursor monolayer, different distances between functional group can be formed, allowing for an ability to tailor distances between molecules. This method may allow for improvement in DNA array technology.

Chapter 5. Long-Term Stability of Self-Assembled Monolayers in Biological Media

The study of long term stability of self-assembled monolayer (SAM) in biological media is of importance in evaluating its usefulness for applications in implantable biochips, biosensors, or biological microelectromechanical system (bioMEMs) devices for drug delivery. To minimize biofouling effects, researchers have investigated protein/cell adhesion resistant surface-bound materials such as poly(ethylene glycol) or oligo(ethylene glycol) terminated self-assembled monolayers. However, no long term study in biological media has been done. To address the issue of moderate to long-term stability of SAMs for bioMEMS device modification, alkanethiol and oligo(EG) terminated alkanethiol monolayers were prepared and studied after immersion in either phosphate buffer saline (PBS) or calf serum. Here, undecanethiol ($C_{11}H_{23}SH$) and tri(ethylene glycol) terminated undecanethiol ($HO(C_2H_4O)_3C_{11}H_{22}SH$) self-assembled monolayers (SAMs) on clean gold surfaces were prepared and characterized. The SAMs were then immersed into either phosphate buffered saline (PBS) or calf serum. The SAM samples were emmersed and investigated using several analytical techniques at numerous points over the next 35 days. Contact angles and current densities in voltammetry changed dramatically for the PBS samples over the time period, particularly after 21 days. Results indicate substantial loss of the integrity of the SAM. Similar alterations with time were observed for the calf serum samples in both contact angle and voltammetry measurements. X-ray photoelectron spectroscopy indicates that the likely origin is desorption of the alkanethiol moiety as evidenced by appreciable loss of the S 2p signal after 35 days. Additionally, this work may serve as a starting point for further studies of surface chemical modification methods for moderate to long-term minimization of biofouling for in vivo applications.

Thesis Supervisor: Robert S. Langer, Sc.D.
Title: Kenneth J. Germeshausen Professor of Chemical and Biomedical Engineering

DEDICATION

In memory of my beloved and dearly-missed father and teacher, Chieu Q. Tran

To my dear and loving mother and brother, Quy and Dinh-Yen

ACKNOWLEDGEMENTS

I would never have imagined that I would be here today, without the support and love of so many people. So in reality, this thesis does not solely belong to me. It is a part of all those who have devoted their love's labor and effort in lifting my wings each stage of my life, in believing in me, and in giving me nourishment both physically and emotionally.

With deepest gratitude and respect that I acknowledge my advisor, Dr. Robert Langer, who has shown such tremendous support and positive encouragement throughout my thesis work. Thank you, Bob, for showing such faith and belief in me, and for supporting me through all the challenges of research. You do not know how much it means to me to hear that you know much more about me than simply what I do in lab. Thank you! I also would like to acknowledge my former advisor, Dr. Elazer Edelman, for sharing some of my most difficult moments after the death of my father, for sharing his life's experiences with me, and for allowing me the freedom to spread my wings and supporting my decision to change research project. I would like to thank Dr. Paul Laibinis for the generous use of his FT-IR, Dr. George Whitesides for the use of his QCM-D, Dr. Paul Weiss and Rachel Smith for their time and help and the generous use of their STM, and my thesis committee members, Drs. Klavs Jensen and Paula Hammond, for their inputs, advice and guidance. I would not have been able to make it without the help and friendship of the CMSE Experimental Surface Analysis Coordinator, Libby Shaw and the staff at the Microsystems Technology Laboratories.

Much of this work was not done alone, but with the help of so many members of the Langer Lab as well as UROP students. I would like to thank Nolan Flynn, who spent countless hours with me over electrochemistry, who shared with me baby Potter's cute pictures, who pored over (and over and over) the manuscripts without complaint. For Joerg Lahann and Samir Mitragotri, thank you for getting me excited about the project and for all the support you have shown as we worked as a team. I am very grateful to David Lavan, Mad Scientist, for his microfabrication expertise, his wit, his funny anecdotes and help with so many questions that got me through this mad, mad, mad, mad lab life. I would also like to acknowledge Yadong Wang, Bianca Baroli, Eric Crumpler,

Erin Lavik, Tommy Thomas, Mariah Hahn and other past and present members of E25-345 for their tolerance of my use of smelly chemicals and my music, for making me laugh and cry with them, and for helping me through the ups and downs of research. I would like to thank Jenny Mu for being my teddy bear, for giving me a shoulder to cry on and a warm hug when I need it most. For my officemates, especially Ying Chau, Hua Tang, and Betty Yu, thank you for putting up with my messes, for listening to me griping about experiments not working, for late night talks. I am much in debt to Insung Choi for his advice on SAMs and help with the manuscripts, Molly Stevens for showing me how to use the QCM-D, and Connie Beal, Ilda Thompson and Nancy Parkinson for help with all the administrative issues. I would like to thank my many UROP students for help with so many measurements over the years. And to my other labmates, many whom I have consulted and collaborated with, especially Bianca, Sangyong, Omid, Ali, Kahpyang, Jiehyun, Dr. Yang, and many others who have helped me along the way, a sincere and heartfelt thank you!

To my friend Patsy, thank you for being there for me in every way, weathering all the storm of life with me. I want to thank my friends Giao, Christina, June, Tiffany, Prista, Anatole, Attma, Arnold, Thomas amongst so many others that I cannot all name here who have provided me with so much emotional support, understanding and help throughout the years. To my friends in E25-518 (Cathy, Patty, Domingo, Jennifer, Ron, Fred, Keiko), and at the MEC (Patty and Linda), thank you all for all your help and hugs! To my dear family, near and as far away as in Vietnam and Paris, my heartfelt gratitude for loving me and supporting me. I wouldn't have made it without you.

But most of all, this thesis is dedicated in memory of my dear father, who was my soul mate and friend, and whose love has kept me going through my darkest times and who has helped me be the person I am today. Daddy, I miss you dearly, each and everyday of my life, and I hope that you are proud of me. To my mother Quy and brother Dinh-Yen, I only want to say that I love you more than anything, and I thank you for all the tender loving and unwavering support you have shown me throughout my life, from the smallest to biggest things, for being there when I needed you the most, for helping me through the hardships of life as well as sharing with me its joy and simple pleasures. You are the reasons I am here today, and live for in the future.

TABLES OF CONTENTS

LIST OF FIGURES

CHAPTER ONE

CHAPTER TWO

CHAPTER THREE

CHAPTER FOUR

CHAPTER FIVE

LIST OF SCHEMES

CHAPTER ONE

CHAPTER THREE

CHAPTER FOUR

LIST OF TABLES

CHAPTER ONE

CHAPTER THREE

CHAPTER ONE

AN INTRODUCTION TO SELF-ASSEMBLED MONOLAYERS AND THEIR CHARACTERIZATION TECHNIQUES

1.1. Introduction

Organized molecular assemblies or self-assembled monolayers (SAMs) have recently excited interest in the scientific communities for their potentials as biological sensors,[1-4] microelectronic devices,[5, 6] optoelectronic devices,[7, 8] nonlinear optical material, optical switches, high density memory devices, or their potential uses in microfabrication,[6, 9-12] nanotechnology,[13-17] chemical sensors,[18-20] nonlinear optical materials.[21-24] Although there are many different systems of SAMs based on different organic components and supports such as silicon and silver, the best developed systems are those of alkanethiolates on gold films.[25] The thiol compounds chemisorp onto gold surface from solution and form adsorbed alkanethiolates with the loss of a hydrogen. The alkane compound can be modified to incorporate a variety of functional groups such as hydrophilic and hydrophobic groups,[26, 27] aromatic compounds,[28, 29] peptide sequences,[30, 31] fullerene balls.[32, 33] Hence, SAMs can used for a variety of applications, influencing such properties as wettability, hydrophobicity, hydrophilicity and offering protection against corrosion,[34-37] biological sensing properties,[1, 38, 39] cellular adhesion[30, 40-43] amongst many.[25, 44]

There have been many attempts at controlling the surface properties of SAMs, most often in photoswitching applications,[45] for chemically selective coating,[46] in redox changes, or pH induced changes, etc.[47] Molecular recognition and functional group complementarity are essential in the design and preparation of chemical or biological sensors, and analyte-selective chromatographics supports.[1, 20, 27, 48-51] The advantages of SAMs films are their relative ease of preparations as well as their structural order allows surface properties to be fine tuned and interfaces to be designed for analyte binding as

well as signal transduction.[25] The design of a chemically selective coating that can be reversibly attached to a sensor interface is of much interest. More importantly, the design of a universal surface that will reversibly change properties via an external switch is of great interest for its potential in chemical, biological sensor applications as well as cell adhesion, chemical separations, nanotechnology devices.

Self assembled monolayers have many potential uses in surface engineering such as semiconductor surface patterning,[6, 15, 17, 52-58] transducer technology such as optical, piezoelectric, and other forms of chemical sensors,[19, 20, 59, 60] and electroanalytical chemistry where redox reactions can be used to detect biomaterials.[61-65] SAMs may play an important role in miniaturization of analytical instrumentation, which may have considerable importance in the biomedical analytical area, and in the molecular level understanding of surface phenomena as they offer the ability to systematically modify surfaces in a predictable manner and to study their properties. By using molecularly engineered surfaces, a better understanding of molecules-surface interaction can be achieved.

The main goal of this research project is primarily to develop an understanding of the basic phenomena regarding controlling SAMs interfacial properties by modifying surface functionalities, and of the feasibility of controlling surface properties via external forces such as an applied electrical potential. The ultimate goal is to develop a universal surface that will reversibly change wettability either in response to external solvent conditions, or via an external switch such as an applied electrical potential. This was accomplished by several complimentary methods: (1) synthesis and characterization of new compounds, (2) controlling surface density of the self-assembled molecules, (3) modeling the SAMs

surfaces and making predictions on the energetics and ability of such novel compounds to self-assemble, (4) development of methods to characterize the novel surfaces, (5) development of applications.

The basic questions this thesis addresses are: (ia) can the chemical and physical properties of the interface be controlled, by purposefully designing interfacial molecular structures; which leads to (ib) can the density of the surface be controlled at a molecular level (ii) can surface properties such as hydrophobicity/hydrophilicity be further controlled by the application of an external force field, e.g. electrostatic forces; (iii) what are the proper physical characteristics of these supramolecular assemblies, e.g. in terms of surface energies, conformation, order/disorder, crystallinity and fluidity, etc; (iv) what are the potential applications; (v) what are the long term effects of SAMs in biological media. The main interest of the project lies along the controlled establishment of self-assembling supramolecular structures at solid/solution interface, and in the development of applications of these functionalized surfaces in the selective absorption/desorption of proteins, cells, drugs, enzymes, etc. in a controllable manner. The project focused on establishing a platform on which further applications can be developed, i.e. the building of engineered molecules containing thiol groups as a low density self-assembling monolayers on gold surfaces that possesses desired interfacial properties and molecular orientation. We also established the feasibility of using external force to induce a switch in surface properties (e.g. hydrophilic/hydrophobic). This switch is connected to a conformational reorientation of a stable oriented layer of the engineered molecules.

This thesis is divided into five chapters. Chapter One contains an introduction to self-assembled monolayers (SAMs) and the characterization techniques used in subsequent

work described herein. Chapter Two is the development of the reversibly switching surface proof-of-principle, which focused on addressing questions (ia), (ib), and (ii) mentioned above. Chapter Three is a characterization chapter that addresses question (iii) above, but also outlines an application for the system developed in forming homogeneously mixed SAMs. Chapter Four addresses question (iv) and describes a potential use of the homogeneously mixed SAMs for formation of oligonucleotide array. Finally, Chapter Five describes the long-term effects of SAMs in biological media, addressing question (v).

1.2. Self-assembled monolayers (SAMs) on gold

The concept of self-assembly in nature is a relatively old one. Many proteins in our bodies, crystal units, and viral particles all undergo a spontaneous process called self assembly to form supramolecular architecture made of interlocking components, a sort of natural "Lego" units. However, the field of synthetic self-assembled monolayers have only been undergoing tremendous growth in the last 15-20 years. The most studied SAMs have been that of alkanethiolates on gold. SAMs offer unique opportunities to increase the fundamental understanding of self-organization, structure-property relationships, and interfacial phenomena as they allow for tailored changes in the head and tail groups, allowing study of phenomena such as those affected by competing intermolecular, molecular-substrates, and molecule-solvent interactions such as ordering, growth, wetting, adhesion, lubrication, and corrosion.[25]

SAMs are relatively easy to form. Scheme 1.1 demonstrates how such a monolayer may be formed.

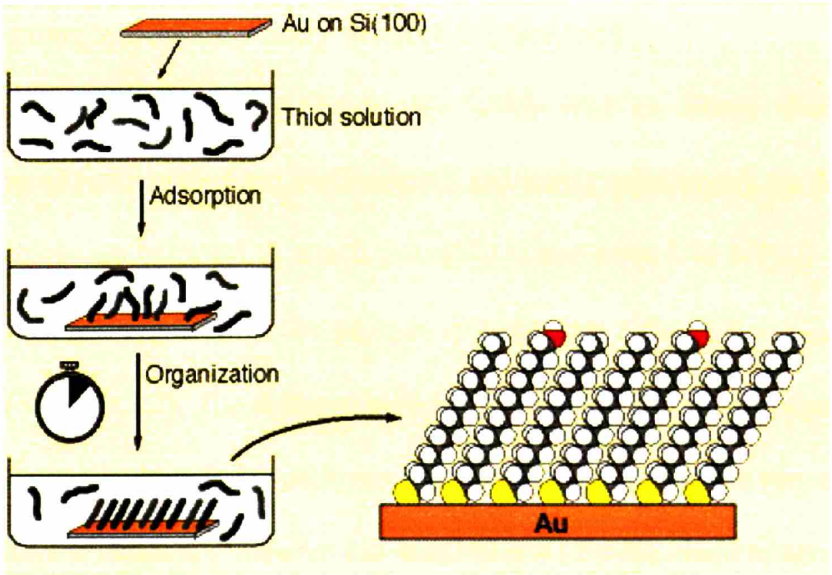

Scheme 1.1.

Formation of self-assembled molayer: adsorption and organization.[a]

[a]Figure adapted from: http://www.ifm.liu.se/Applphys/ftir/sams.html

Chemisorption of alkanethiols as well as of di-*n*-alkyl disulfides on clean gold gives indistinguishable monolayers, probably by forming the Au(I) thiolate (RS^-) species. In the alkanethiol case, the reaction maybe considered as the oxidative addition of the S-H bond to the surface, followed by a reductive elimination of the hydrogen.

$$R\text{-}S\text{-}H + Au^0_n \rightarrow R\text{-}S^-Au^+Au^0_n + \tfrac{1}{2} H_2 \quad (1.1)$$

The absorbing species has been shown to be the thiolate by several studies by XPS,[66, 67] IR,[68] and other techniques. The bond energy of the thiolate group to gold is quite strong, approximately 44 kcal/mol[25] and contributes to the stability of the SAMs together with the van der Waals forces between adjacent methylene groups, which amount to 1.4-1.8 kcal/mol. The latter forces add up to significant strength for alkyl chains of 10-20 methylenes and play an important role in aligning the alkyl chains parallel to each other in a nearly all-trans configuration. At low temperatures, typically 100 K, the order is nearly perfect, but even at room temperature there are only few gauche defects, concentrated to the outermost alkyl units. Though clean, freshly evaporated Au substrates give the best results, the adsorption of most alkanethiols to Au is sufficiently strong to displace weakly adsorbed contaminants.

It has been clearly shown that SAMs with an alkane chain length of 12 or more methylene units form well-ordered and dense monolayers on Au(111) surfaces.[69-71] The thiols are believed to attach primarily to the three-fold hollow sites of the gold surface, losing the proton in the process and forming a the $(\sqrt{3} \times \sqrt{3})R30°$ overlayer structure (Scheme 1.2). The distance between pinning sites in this geometry is 4.97 Å, resulting in an available area for each molecule of 21.4 $Å^2$. Since the van der Waals diameter of the alkane chain is somewhat too small (4.6 Å) for the chain to completely occupy that area,

the chains will tilt, forming an angle of approximately 30° with the surface normal.[25] Depending on chain length and chain-terminating group, various superlattice structures are superimposed on the ($\sqrt{3} \times \sqrt{3}$)R30° overlayer structure. The most commonly seen super-lattice is the c(4 × 2) reconstruction, where the four alkanethiolate molecules of a unit cell display slightly different orientations when compared with each other.

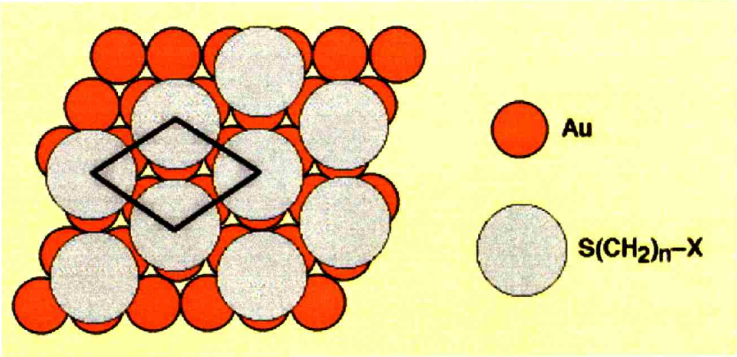

Scheme 1.2. A schematic model of the ($\sqrt{3} \times \sqrt{3}$)R30° overlayer structure formed by alkanethiolate SAMs on Au(111)[b]

[b] http://www.ifm.liu.se/Applphys/ftir/sams.html

1.3. CHARACTERIZATION TECHNIQUES

1.3.1. Contact angle Goniometry

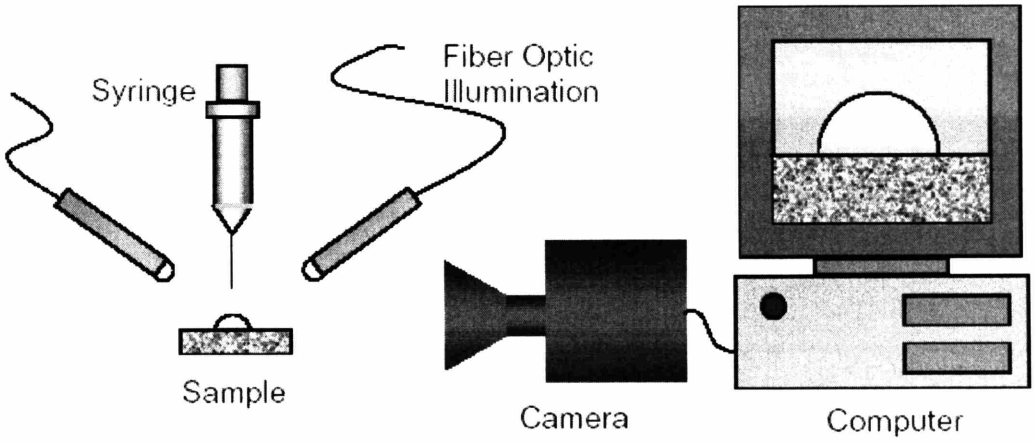

Scheme 1.3. Set-up for a contact angle experiment.[c]

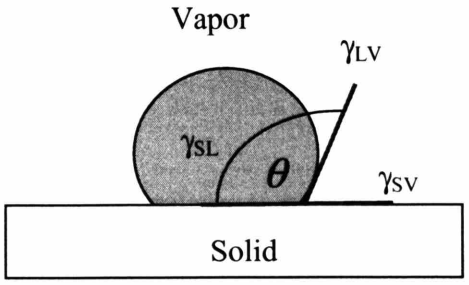

Scheme 1.4. A sessile drop in equilibrium on a solid surface forming a contact angle, θ

The set-up for a contact angle experiment is shown in Scheme 1.3. It consists of a syringe containing the liquid of interest, fiber optic cables to illuminate the surface, a CCD camera connected to a computer where the image can be analyzed. The liquid is

[c] http://poohbah.cem.msu.edu/courses/cem419/

pumped through the syringe and drop onto the surface for static measurements. Contact angle is defined as the angle formed at a point on the line of contact of three phases, of which at least two are condensed phases, by the tangents to the curves obtained by intersecting a plane perpendicular to the line of contact with each of three phases. One of the phases must be a liquid, another phase may be solid or liquid and the third phase may be gas or liquid. In the case where the liquid drops onto a solid as demonstrated in Scheme 1.4, the contact angle is the angle between the liquid vapor and solid-vapor interfaces made by the tangent to the liquid and the solid. The governing equation for measuring contact angle is Young's equation (Eq 1.2) where γ_{SV} is the surface free energy of the solid in contact with vapor, γ_{SL} is the surface free energy of the solid covered with liquid, γ_{LV} is the surface free energy of the liquid-vapor interface, and θ is the contact angle.

$$\gamma_{SV} - \gamma_{SL} = \gamma_{LV}\cos\theta \qquad (1.2)$$

Experimentally, when a liquid is contacted with a solid and another phase, it is usually observed that the contact angle does not reach its equilibrium value instantaneously. The same is true when liquid in contact with a solid is displaced. Therefore, one distinguishes an advancing and a receding contact angle respectively. Advancing and receding contact angles are measured as the drop is expanding (advancing contact angle) by advancing or contracting (receding contact angle) the drop quasistatically over the surface. Almost always the advancing angle is greater than the receding, the difference is called hysteresis. A small hysteresis can indicate a well-ordered, crystalline SAM. Large hysteresis may indicate increased roughness or molecular and chemical heterogeneity.

There are at least three possible reasons for contact angle hysteresis. First is contamination: the drop may become contaminated as it moves across the surface. This will change the surface tension of the liquid. This may also clean or contaminate the surface. Second, surface roughness: on a rough surface, the drop may spread over different portions of the surface. The less polar portions may affect advancing angles while the receding angle may be affected by polar regions.[72] Third, surface reconstruction: the surface itself may change in the presence of the liquid. For example, the hydrophobic group of a monolayer may become slightly buried when using water to measure contact angles. Given the above reasons, a small difference (<5 degrees) between advancing and receding angles suggests that the surface is free of contamination, well organized, and smooth.

1.3.2. Ellipsometry

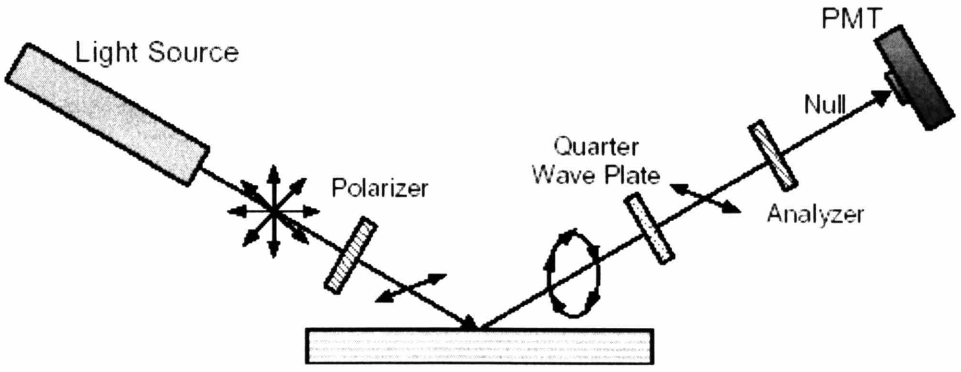

Scheme 1.5. The null rotating element ellipsometer. Adapted from H.G. Tompkins "A User's Guide to Ellipsometry" 1993.[73]

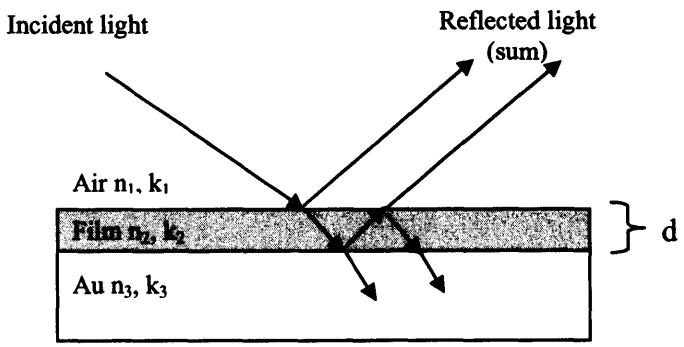

$n_1 = 1, k_1 = 0 \quad n_2 = 1.5, \; k_2 = 0$

n_3 and k_3 – substrate values measured in different experiment

Scheme 1.6. Calculation of thickness using ellipsometry.

Ellipsometry is perhaps the most common method to determine the thickness and refractive index of thin organic films. The polarization condition of an electromagnetic wave is altered by reflection from a surface. In general, both the phase and the relative amplitude of the Cartesian components of light are changed. These changes are reflected in the ellipsometric quantities Δ and Ψ which can be used to determine the complex dielectric response (refractive index) and thickness of overlayers on a reflective surface. When a plane-polarized light interacts with a surface at some angle, it is resolved into its parallel and perpendicular components (*s*- and *p*-polarized respectively), the phase and amplitude of which are modulated in different ways as the light reflect from the surface. Elliptically polarized light is the sum of the *s*- and *p*-polarized components. Ellipsometry estimates the thickness of the thin organic layer between the substrate and air by measuring the ratio, *r*, between the reflection coefficients of the *p*-and *s*-polarized light, r_p and r_s.

In a typical null ellipsometer (single wavelength – Scheme 1.5), monochromatic light from a He-Ne laser is plane-polarized (p = angle of polarization) and impinges on the

surface (Scheme 1.6). The resulting elliptically polarized light is changed by the compensator to plane-polarized (a = angle of polarization, which is determined by the analyzer). These two angles (p and a) give the phase shift between the parallel and perpendicular components (Δ), and the change in ratio of the amplitudes of the two components ($\tan\Psi$) as:

$$e^{i\Delta}\tan\Psi = \frac{E_{reflected(p)}/E_{reflected(s)}}{E_{incident(p)}/E_{incident(s)}} \tag{1.3}$$

where $\Delta = 2p + \pi/2$ and $\Psi = a$. For a clean surface, Δ and Ψ are related to the complex index of refraction of the surface via:

$$n^s(\text{complex}) = n^s(1 - i\,k^s) \tag{1.4}$$

where n^s is the refractive index and k^s is the extinction coefficient. Experimental data is obtained taking the measurements before and after the deposition of an organic film, and is expressed as:

$$\delta\Delta = \Delta_o - \Delta \tag{1.5}$$

$$\delta\Psi = \Psi_o - \Psi \tag{1.6}$$

where the suffix o denotes the clean substrate values.

Typically, the refractive index of the film has to be estimated if the film is less than 50 Å, and a refractive index of 1.50 is often used for simple alkanethiol monolayer with chain length greater than C_9 and 1.45 for monolayer with chain length less than C_9 with other values being used for different molecular structures.[25]

1.3.3. Grazing-angle Fourier-Transform Infrared Absorption Spectroscopy (FT-IRAS or FT-IR)

Infrared reflectance spectroscopy has developed into one of the primary methods of monitoring chemical structure and molecular orientation of thin films and monolayers adsorbed onto metal surfaces.[74] At a high (grazing) angle of incidence the intensity of a reflected *p*-polarized infrared light beam is enhanced at a metal surface so that even submonolayer quantities of chemisorbed species can be observed in the *p*-polarized FTIR reflectance spectrum. In contrast, at a high angle of incidence an s-polarized reflected infrared beam has virtually no intensity at the metal surface. This polarization disparity leads to strong selection rules at the surface, and has been used to deduce the average molecular orientation and conformation for monolayers of long chain alkyl molecules adsorbed onto metals.

One convenient method of checking a SAM for well-ordered and dense structure is infrared reflection-absorption spectroscopy (IRAS). The CH stretching vibrations of the alkyl chain are very sensitive to packing density and to the presence of gauche defects, which makes them ideally suited as probes to determine SAM quality. In particular, the antisymmetric CH_2 stretching vibration at ~2918 cm^{-1} is a useful indicator. For a densely packed, crystalline SAMs of exceptional quality; the CH_2 stretches would appear from 2916 to 2917 cm^{-1}. For normal, densely packed SAMs, the CH_2 stretch would be at around 2918 cm^{-1}. And for a heavily disordered, "spaghetti-like" SAM, it would be at approximately 2926 cm^{-1} or above.[67]

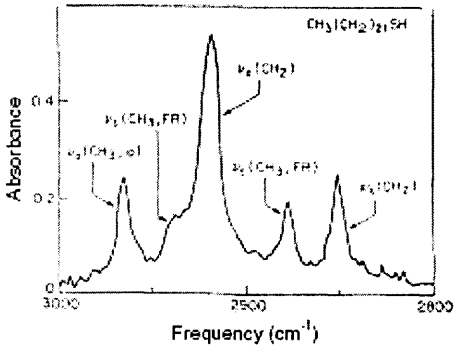

Scheme 1.7.

FTIR spectrum of the C-H stretch region of an alkanethiol monolayer on gold

The absorbance frequency is dependent upon the degree of organization as shown in the following table:

Peak positions (cm^{-1})

Group	Mode	Crystalline	Liquid	$CH_3(CH_2)_{17}SH$ on Au
$-CH_2-$	ν_a	2918	2924	2917
	ν_s	2851	2855	2850

Table 1.1. Comparison of Liquid and Crystalline State- CH_2- Absorbance Frequencies with Annealed Monolayers Values.[75]

As the monolayers anneal, the $-CH_2-$ absorption frequency decreases from a value characteristic of a disordered liquid state to one indicative of a more ordered crystalline-like state.

1.3.4. X-ray Photoelectron Spectroscopy (XPS)

XPS is the surface analytical tool of choice when surface composition and its depth profile are under study. In an XPS experiment, the sample is exposed to X-ray radiation. The energy of the incoming X ray ($h\nu$) minus the energy of the core electrons (E_b or

binding energy, which is characteristic of a particular electron in a particular atom), is equal to the energy of the ejected electron, E_k.

$$E_k = h\nu - E_b \quad (1.7)$$

The experimentally measured energies of the photoelectrons are given by:

$$E_k = h\nu - E_b - E_w \quad (1.8)$$

where E_w is the work function of the spectrometer

Hence, determining E_b will give atomic identification and since the number of electrons ejected is proportional to the number of atoms present, composition can be derived quantitatively. Since the presence of chemical bonding will alter the energy state of the atom in study and cause shift in binding energy, the high resolution spectra of an atom may give information on its chemical nature and hence information about the various types of carbon-carbon or carbon-oxygen bond in the sample (Scheme 1.8). Also, grazing electron take-off geometry (angle-resolved XPS) can emphasize the contribution of different atoms at different depth, and hence, is an excellent way to study compositional depth distribution in a film.[74] The strength of XPS is its ability to identify different chemical states. This ability is useful in a range of physical studies, for example, oxidation/corrosion products, adsorbed species, and thin-film growth processes. Analysis of insulators is possible with the Kratos Axis ULTRA, the XPS used in this project. XPS is also capable of semi-quantitative analysis. Exact quantities are difficult to obtain as XPS is very sensitive to contaminants, and therefore, it is difficult to get the exact mass or composition.

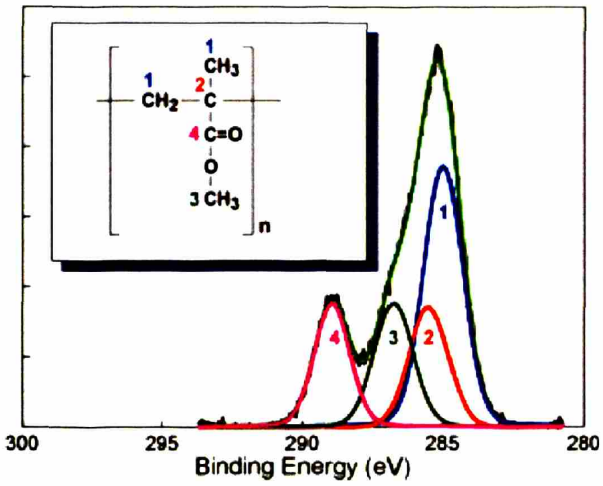

Scheme 1.8. An example of a high resolution XPS spectrum of carbon that can distinguish chemical state of carbon in a chemical compound, illustrating the power of XPS to detect presence of chemical bonding.

1.3.5. Cyclic Voltammetry

Electrochemical techniques are probably the most sensitive probes of monolayer defects. Infrared spectroscopy, ellipsometry, contact-angle measurements, and QCM studies are all more or less bulk measurements. Cyclic voltammetry (CV) and impedance measurements, however, are extremely sensitive to defects in a monolayer. If 99% of a surface is covered by a wellformed monolayer, most techniques will be representative of that 99%. CV and impedance measurements, however, will show evidence of defect areas.

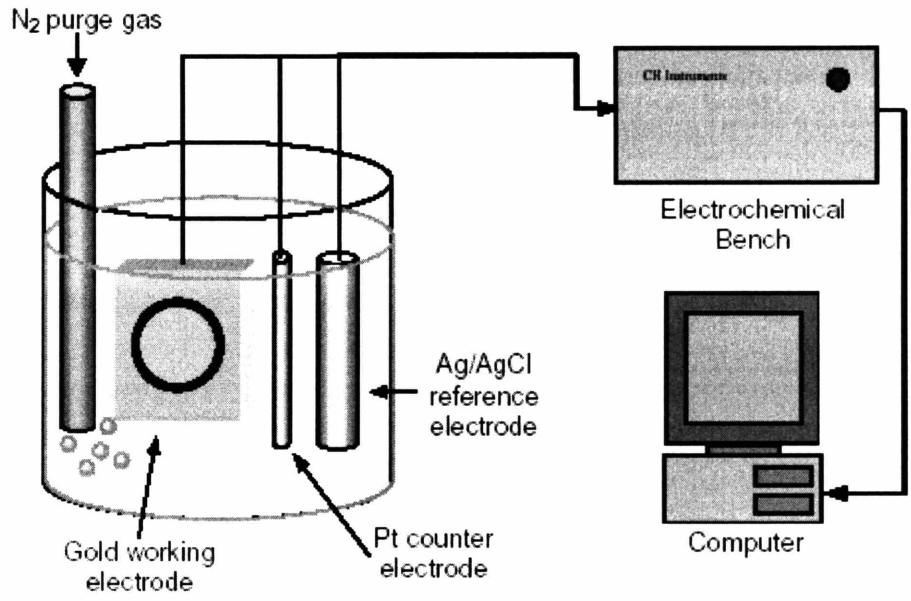

Scheme 1.9. Typical set-up for a cyclic voltammetry experiment.[d]

A typical set-up for the cyclic voltammetry experiment is shown in Scheme 1.9. It consists of a gold working electrode containing the SAM of interest, a counter electrode (often made of platinum wire), and a Ag|AgCl|saturated KCl reference electrode. The solution often contains a redox active probe, the most common being the Ferri/Ferrocyanide, $Fe(CN)_6^{3-/4-}$.

Figure 1.1 describes the process that occurs in simple electrode reactions. In the case of reduction, a species (O) capable of receiving an electron from the electrode diffuses to the surface, receives an electron and diffuses away from the surface. Current at the surface is generated by the transfer of electrons from the electrode to the redox species while current in solution is carried by migration of ions. A transient current can flow even in the absence of charge-carrying species (or a redox couple) in solution because the

[d] http://poohbah.cem.msu.edu/courses/cem419/

electrode-solution interface behaves as a capacitor. As the potential of the electrode is varied, ions move to the surface to form a double-layer as shown in Figure 1.1.

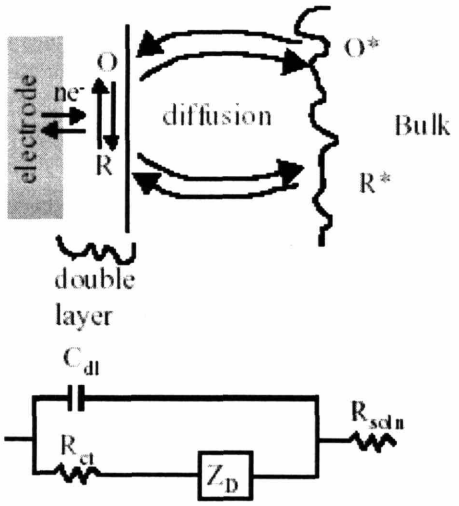

Figure 1.1 Electrochemical system that includes electron transfer along with its equivalent circuit where C_{dl} = double layer capacitance, R_{ct} = charge transfer resistance, Z_D = diffusional impedance.[e]

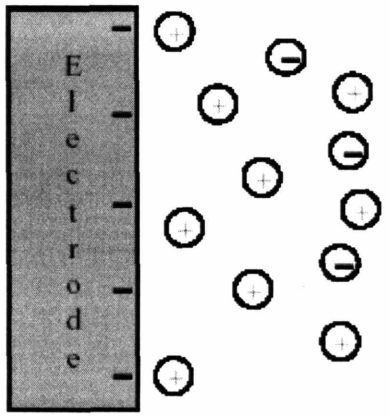

Figure 1.2. Schematic diagram of an electrical double layer.[f]

Strictly speaking, an electrode-solution interface in the absence of a redox couple is not a pure parallel-plate capacitor; however, it behaves rather like one and a parallel-plate capacitor model is often adequate to describe electrochemical systems. The use of this model allows us to learn about the behavior of electrodes in the absence of a redox

[e] http://poohbah.cem.msu.edu/courses/cem419/

[f] http://poohbah.cem.msu.edu/courses/cem419/

couple. For a simple parallel plate capacitor, charge on the capacitor, Q, is proportional to the voltage drop across the capacitor, E:

$$Q = CE \tag{1.9}$$

The proportionality constant C is the capacitance of the medium. The simplest description of electrochemical capacitance is the Helmholtz model given by:

$$\frac{C}{A} = \frac{\varepsilon\varepsilon_0}{l} \tag{1.10}$$

where ε is the dielectric constant of the material separating the parallel plates, ε_0 is the permittivity of free space, l is the separation between the plates, and A is the area of the electrode. This model does not adequately describe all electrochemical interfaces as the capacitance can depend on both potential and the supporting electrolyte, although it still is a helpful construct.

Capacitance is a crucial factor in electrochemical experiments because it gives rise to current during the charging of the capacitor, henceforth referred to as charging current. To calculate the magnitude of this current, we differentiate equation (1.9) with respect to t and assume that capacitance is constant:

$$\frac{dQ}{dt} = C\frac{dE}{dt} \tag{1.11}$$

where dQ/dt = i = current and dE/dt = ν = potential scan rate and hence:

$$i = C\nu \tag{1.12}$$

From this expression, we can measure the current at steady state while applying a ramping voltage at a given scan rate, and hence, determine the capacitance of the system. If there is no possibility for electron transfer between the solution and the electrode (in

the case of no redox couple) this is the only current that we will observe as illustrated in the figure below.

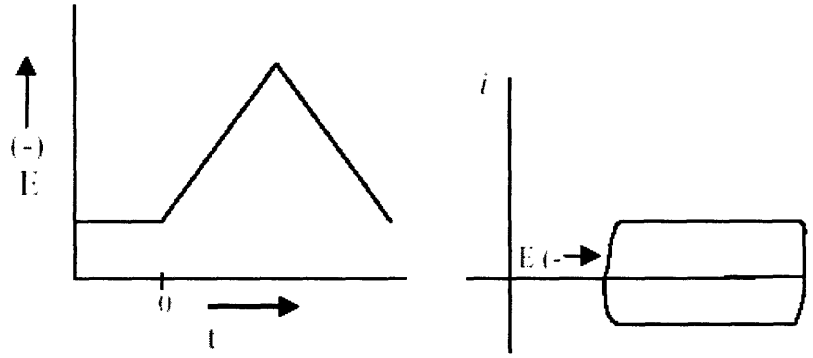

Figure 1.3. Schematic explanation of a cyclic voltammetry experiment in the absence of a redox couple.[g]

1.3.6. Cyclic Voltammetry with an Active Redox Couple

Most of the cyclic voltammetry technique, however, is used with a redox couple, most often when the capacitive current is small compared to the current from electron transfer (Faradaic current). Faradaic current depends on two things: the kinetics of electron transfer and the rate at which the redox species diffuses to the surface. One of the most common redox couple is the ferro/ferricyanide system ($Fe(CN)_6^{3-/4-}$). For this redox couple, the kinetics of electron transfer are reasonably fast, so it can be assumed that at least for the moment that at the surface, the concentrations of $Fe(CN)_6^{3-}$ and $Fe(CN)_6^{4-}$can be described by the Nernst equation (eq. 1.13):

[g] http://poohbah.cem.msu.edu/courses/cem419/

$$E = E^{0'} - 0.0592 \log\left(\frac{\left[Fe(CN)_6^{-4}\right]}{\left[Fe(CN)_6^{-3}\right]}\right) \tag{1.13}$$

Where E is the applied potential and $E^{0'}$ is the formal electrode potential. One can see that as the applied potential becomes more negative the concentration of $Fe(CN)_6^{3-}$ must decrease at the electrode surface. It is being reduced to $Fe(CN)_6^{4-}$. This is a very sensitive method to detect defects in the monolayers as well as estimate surface coverage. For the system under consideration with an active redox couple (ie charge transfer between the surface and the solution) the circuit shown in Figure 1.1 can be simplified to be:

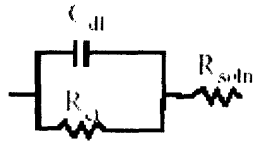

where C_{dl} = capacitance of the double layer = sum of monolayer and defect capacitance

R_{ct} = charge transfer resistance

R_{soln} = solution resistance

Figure 1.4. Circuit diagram for cyclic voltammetry with active redox couple.

First for the qualitative, pictorial explanation. If we assume that concentrations at the surface are governed by the Nernst equation, the concentration of the oxidized species at the surface will decrease as the potential becomes more negative. A lower concentration at the surface gives a higher concentration gradient (at least initially) so according to Fick's law of diffusion, we will have higher flux to the surface and hence a higher cathodic current. As we continue to make the potential more negative, the concentration at the surface will eventually go to zero. Simultaneously, the volume in the solution that is depleted of the oxidized species will increase and the concentration gradient will begin

to decrease. As the concentration gradient decreases, we will have less flux to the surface and current will begin to decrease. All of this will result in a current-voltage curve that looks like:

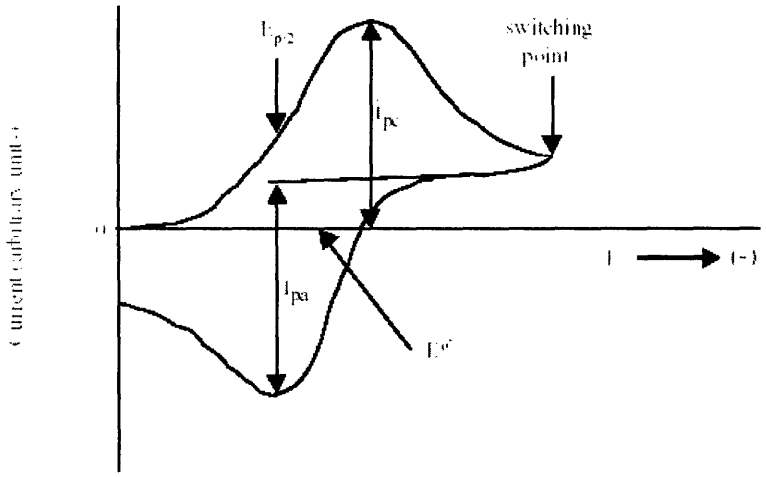

Figure 1.5. Current vs voltage curve for cyclic voltammetry with active redox couple.[h]

As we reverse the voltage scan, we still have a layer depleted of the oxidized species, though the surface concentration begin to rise, further decreases the current. Finally, a region where the anodic current begins to dominate, and a similar concentration profile is obtained for the reduced species. Peak negative current is achieved, and the current will further decrease in magnitude as the depletion layer for the reduced species increases.

Cyclic voltammetry with an active redox couple can be used to study the surface coverage as well as monolayer defects. For a monolayer of densely packed molecules, charge transfer between the solution and the surface will not be able to take place. However, upon formation of a low-density monolayer such as when the headgroup is

[h] http://poohbah.cem.msu.edu/courses/cem419/

cleaved from a monolayer formed from triphenyl ester precursor, which has a cleavable bulky headgroup (this will be discussed more in details in subsequent chapter, particularly, Chapter Three), passivation of ions can occur. Upon backfilling the low-density monolayer with a shorter chain alkanethiol, passivation will be reduced. A cartoon of this principle is shown in Scheme 1.10.

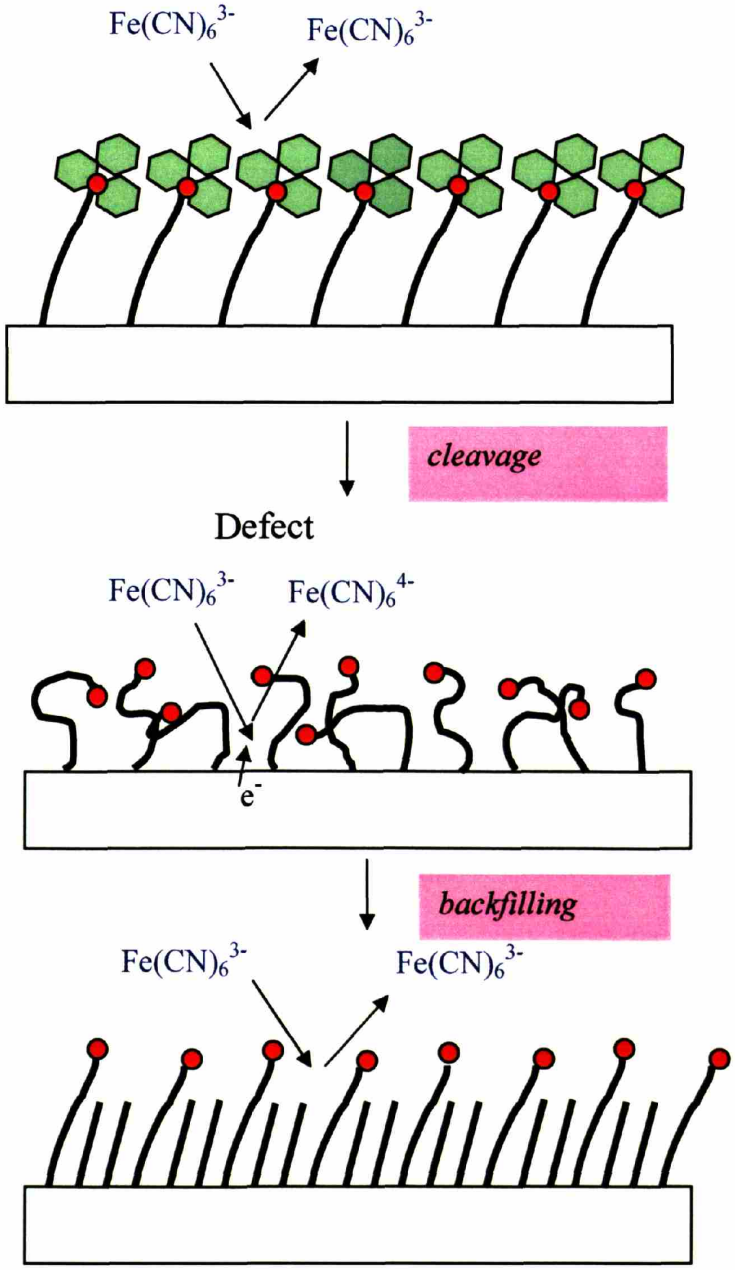

Scheme 1.10. Illustration of the changes in charge transfer passivation of a SAM that is formed from precursor molecules containing a bulky headgroup. This precursor SAM is inhibitive to electron passivation. Upon cleavage of the headgroup, a low-density monolayer is formed, which has high electron transfer to the redox couple. Backfilling of this low-density monolayer with a second alkanethiol reduces passivation due to the inablity of the redox couple to transfer/accept electron to the gold (Au) surface.

1.3.7. Atomic force microscopy (AFM)

Atomic force microscopy is one of many scanned probe microscopy techniques used to image the surface. AFM operates by measuring attractive or repulsive forces between a tip and the sample.[76] The atomic force microscope (AFM) probes the surface of a sample with a sharp tip, a couple of microns long and often less than 100 Å in diameter. The tip is located at the free end of a cantilever that is 100 to 200 μm long. Forces between the tip and the sample surface cause the cantilever to bend, or deflect. A laser beam is focused on the back of the cantilever, and the deflection of the cantilever translates to a deflection in the laser beam. A detector measures the cantilever deflection as the tip is scanned over the sample, or the sample is scanned under the tip. The measured cantilever deflections allow a computer to generate a map of surface topography. In non-contact mode, the AFM derives topographic images from measurements of attractive forces; the tip does not touch the sample.[77] AFMs can achieve a resolution of 10 pm, and unlike electron microscopes, can image samples in air and under liquids.

In principle, AFM resembles the record player as well as the stylus profilometer. However, AFM incorporates a number of refinements that enable it to achieve atomic-scale resolution:

- Sensitive detection

- Flexible cantilevers
- Sharp tips
- High-resolution tip-sample positioning
- Force feedback

Several forces typically contribute to the deflection of an AFM cantilever. The force most commonly associated with atomic force microscopy is an interatomic force called the van der Waals force. The dependence of the van der Waals force upon the distance between the tip and the sample is shown in Figure 1.6 below:

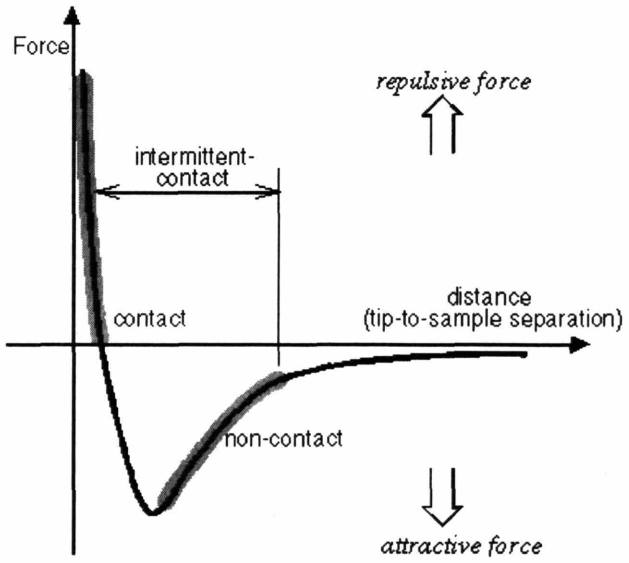

Figure 1.6. Interatomic force vs. distance curve.[i]

[i] AFM- Measuring Interaction Molecular Sources - National Research Laboratory http://stm2.nrl.navy.mil/how-afm/how-afm.html

The AFM can be operated in three modes: contact, non-contact, and tapping. For contact mode, an AFM tip makes soft "physical contact" with the sample. The tip is attached to the end of a cantilever with a low spring constant, lower than the effective spring constant holding the atoms of the sample together. As the scanner gently traces the tip across the sample, the contact force causes the cantilever to bend to accommodate changes in topography.

In non-contact mode, the system vibrates a stiff cantilever near its resonant frequency (typically from 100 to 400 kHz) with an amplitude of a few tens of angstroms. The changes in resonant frequency of vibrational amplitude are detected as the tip comes close to the surface. However, the forces measured are much smaller than that of the contact mode, although it offers advantages in preventing sample degradation, and in working with soft or elastic samples.

For tapping mode, the vibrating cantilever tip is brought closer to the sample so that at the bottom of its travel it just barely hits, or "taps" the sample. Tapping mode overcomes problems associated with friction, adhesion, electrostatic forces, and other difficulties that an plague conventional AFM scanning methods by alternately placing the tip in contact with the surface to provide high resolution and then lifting the tip off the surface to avoid dragging the tip across the surface. Tapping mode imaging is implemented in ambient air by oscillating the cantilever assembly at or near the cantilever's resonant frequency using a piezoelectric crystal. The tip is made to oscillate at a high amplitude when not in contact with the sample by the motion of the piezo crystal. Image is obtained when the oscillating tip is brought close to the sample until it lightly touches the sample surface, at a frequency of 50,000 to 500,000 cycles per second. The reduction in the oscillation

amplitude caused by contact with the sample is measured and translated to surface topography. The oscillation amplitude, which is maintained by a feedback loop to keep a constant amplitude and force on the sample via adjusting the tip-sample separation, is measured by the dectector and input to the AFM controller electronics.

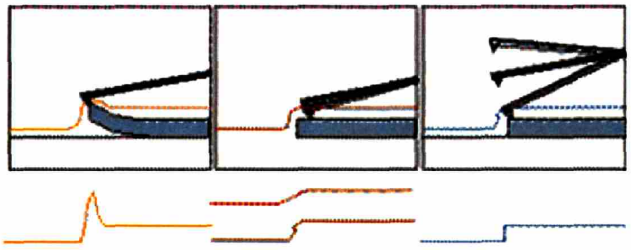

Figure 1.7. Illustration of the different types of AFM mode: contact (left), non-contact (middle), and tapping (right).[j]

1.3.8. Sum Frequency Spectroscopy

A prerequisite for a successful control of interfacial properties is the availability of methods to characterize structures and processes at interfaces. Throughout the past decades surface science has developed a wealth of techniques to investigate interfacial processes. However, most techniques are restricted to vacuum since they are based on massive particles (ion, electrons, atoms), whereas most problems relevant to technology are non-vacuum interfaces such as liquid/solid, high-pressure gas/solid or even solid/solid. Techniques which are capable of analyzing interfaces *in situ* are highly

---

[j]Source: Introduction to AFM - University of Guelph , http://www.chembio.uoguelph.ca/educmat/chm729/afm/details.htm

needed. At the same time information on a molecular scale is desired. During the past two decades there has been a significant development in such *in situ* techniques one class being nonlinear optical techniques such as second harmonic generation (SHG) and sum frequency generation (SFG).

Sum frequency generation (SFG) is a non-linear spectroscopic method which is powerful for its ability to probe structure of the liquid interface *in situ*. This is a three wave mixing process that originates from the rapid change of index of refraction which occurs at an interface. Two input waves, sufficiently intense, will interfere and generate a nonlinear polarization at the sum and difference frequencies. With the two input waves at the same frequency (ω), the generated polarization oscillates at the harmonic frequency (2ω) – this is the second harmonic generation. If the two input waves are at different frequencies ω_1 and ω_2, then the outputs are at the sum ($\omega_1 + \omega_2$) and difference ($\omega_1 - \omega_2$) frequencies. If one of the inputs is an infrared frequency, then the sum frequency is resonance enhanced when a vibrational mode of the interfacial molecules matches the frequency of the input. Dectection of the vibrational resonances is facilitated is SF is in the visible region.[78]

Non Linear Optics at Interfaces

Intense electromagnetic waves with electric fields E_i at frequencies ω_i impinging on matter create a polarization

$$P_{tot} = \alpha^{(1)} \bullet E + \chi^{(2)}:E_1E_2 + ... \qquad (1.14)$$

where $\alpha^{(1)}$ and $\chi^{(2)}$ are the first and second order polarizability, respectively. As the direction of the incident electric field, E, and the polarization is not the same, the first

order response, $\alpha^{(1)}$, is a matrix that describes Raleigh and Raman scattering. The second order response is a tensor. In addition to the linear term, higher order terms that lead to the generation of waves with new frequencies by coupling of the incoming waves, become significant. The first nonlinear term gives rise to a signal whose intensity is given by

$$I(\omega = \omega_1 + \omega_2) \propto \left|\chi^{(2)}\right|^2 I(\omega_1) I(\omega_2) \tag{1.15}$$

where $\chi^{(2)}$ is the susceptibility which characterizes the material and $I(\omega_{1/2})$ are the intensities of the incoming beams. Mixing gives rise to sum frequency generation (SFG) with a signal of intensity $I(\omega_1 + \omega_2)$. The degenerate case of a single frequency ($\omega_1 = \omega_2$) is called second harmonic generation (SHG). Due to its symmetry properties $\chi^{(2)}$ must vanish under inversion and, thus, an intrinsically high interface sensitivity of SHG and SFG results for centro-symmetric or amorphous media. Combining a visible beam with an IR beam which is tunable in the range of the molecular vibrations (IR-vis SFG) an interface vibrational spectroscopy becomes possible which in contrast to linear IR spectroscopy is highly interface specific. The high intensities required for second harmonic and sum frequency generation at interfaces are achieved using pulsed lasers with pulse durations ranging from nano to femtoseconds. This also allows for studying dynamics at interfaces.[k]

As a second order nonlinear optical process, SFG is intrinsically interface-specific because it is electric-dipole-forbidden in a centrosymmetric bulk but necessarily allowed at an interface where the inversion symmetry is broken. Molecules at an interface can be

---

[k] http://ch-www.st-andrews.ac.uk/staff/mb/mb_index.html

selectively probed via their resonances in SFG. Observed resonances in the infrared yield the interfacial vibrational spectrum whose polarization dependence allows us to deduce orientational information of different parts of the molecules at interface.[79]

1.4. Summary

This chapter covers the basic theories behind the characterization techniques employed in subsequent chapters as well as basic introduction to self-assembled monolayer. Specific experimental details in using these characterization techniques will be discussed in details in subsequent chapters.

In conclusion, self-assembled monolayers are easy to form, stable, rugged framework for tail groups that support a wide degree of chemical manipulation. The study of SAM has expanded the field of surface chemistry and defined new questions as well as contributed to the sophistication and sensitivity of analytical techniques. SAM offers exciting new possibilities in engineering smooth surfaces and fine-tuning their chemical properties at molecular levels and also in the developing new biosensors, chemical sensors, as well as improving the understanding of modern theories of wetting, spreading, adhesion, friction, molecular recognition and related phenomena.

1.5. References

1. Chaki, N.K. & Vijayamohanan, K. Self-assembled monolayers as a tunable platform for biosensor applications. *Biosens. Bioelectron.* **17**, 1-12 (2002).

2. Bianchi, N. et al. Biosensor technology and surface plasmon resonance for real-time detection of HIV-1 genomic sequences amplified by polymerase chain reaction. *Clinical and Diagnostic Virology* **8**, 199-208. (1997).

3. Boncheva, M., Scheibler, L., Lincoln, P., Vogel, H. & Aakerman, B. Design of Oligonucleotide Arrays at Interfaces. *Langmuir* **15**, 4317-4320 (1999).

4. Nakamura, F. et al. Preparation of a Branched DNA Self-Assembled Monolayer toward Sensitive DNA Biosensors. *Nano Lett.*, ACS ASAP.

5. Abbott, N.L. et al. Molecular self-assembly and micromachining. *NATO ASI Series, Series E: Applied Sciences* **239**, 293-301 (1993).

6. Chen, C.S., Mrksich, M., Huang, S., Whitesides, G.M. & Ingber, D.E. Micropatterned surfaces for control of cell shape, position, and function. *Biotechnol. Prog.* **14**, 356-363 (1998).

7. Kim, J., Chang, S. & Muramatsu, H. In situ optoelectrochemical approach for the dynamic property study of polypyrrole thin film by quartz crystal combined with UV-visible advanced design. *J. Electrochem. Soc.* **146**, 4544-4550 (1999).

8. Willner, I. Photoswitchable biomaterials: en route to optobioelectronic systems. *Acc. Chem. Res.* **30**, 347-356 (1997).

9. Wilbur, J.L., Kumar, A., Biebuyck, H.A., Kim, E. & Whitesides, G.M. Microcontact printing of self-assembled monolayers: applications in microfabrication. *Nanotechnology* **7**, 452-457 (1996).

10. Tien, J., Terfort, A. & Whitesides, G.M. Microfabrication through Electrostatic Self-Assembly. *Langmuir* **13**, 5349-5355 (1997).

11. Lee, W.B., Oh, Y., Kim, E.R. & Lee, H. Nanopatterning of self-assembled monolayers on Si-surfaces with AFM lithography. *Synth. Met.* **117**, 305-306 (2001).

12. Gorman, C.B., Biebuyck, H.A. & Whitesides, G.M. Use of a Patterned Self-Assembled Monolayer To Control the Formation of a Liquid Resist Pattern on a Gold Surface. *Chem. Mater.* **7**, 252-254 (1995).

13. Biebuyck, H.A., Larsen, N.B., Delamarche, E. & Michel, B. Lithography beyond light: microcontact printing with monolayer resists. *IBM Journal of Research and Development* **41**, 159-170 (1997).

14. Chen, C.S., Ostuni, E., Whitesides, G.M. & Ingber, D.E. Using self-assembled monolayers to pattern ECM proteins and cells on substrates. *Methods in Molecular Biology (Totowa, New Jersey)* **139**, 209-219 (2000).

15. Demers, L.M. et al. Direct patterning of modified oligonucleotides on metals and insulators by dip-pen nanolithography. *Science (Washington, DC, U. S.)* **296**, 1836-1838 (2002).

16. Geyer, W. et al. Electron induced chemical nanolithography with self-assembled monolayers. *J. Vac. Sci. Technol., B* **19**, 2732-2735 (2001).

17. Kumar, A., Biebuyck, H.A. & Whitesides, G.M. Patterning Self-Assembled Monolayers: Applications in Materials Science. *Langmuir* **10**, 1498-1511 (1994).

18. Grassi, J.H. & Georgiadis, R.M. Temperature-Dependent Refractive Index Determination from Critical Angle Measurements: Implications for Quantitative SPR Sensing. *Anal. Chem.* **71**, 4392-4396 (1999).

19. Michalitsch, R. & Laibinis, P.E. Adsorption-mediated electrochemical sensing of halides. *Angew. Chem., Int. Ed.* **40**, 941-944 (2001).

20. Ziegler, C. Cell-based biosensors. *Fresenius' Journal of Analytical Chemistry* **366**, 552-559 (2000).

21. Chan, W., Burnham, S., Chidsey, C.E.D. & Scott, J.C. Using self-assembled monolayers to modify electrode interfaces in organic light-emitting diodes. *Polym. Prepr. (Am. Chem. Soc., Div. Polym. Chem.)* **38**, 936 (1997).

22. Bradley, R., Georgiadis, R., Kevan, S.D. & Richmond, G.L. Nonlinear optical spectroscopy of Ag(111) in electrolyte and in vacuum. *Report*, 43 pp. (1993).

23. Katz, H.E. et al. Electrical and nonlinear optical properties of zirconium phosphonate multilayer assemblies. *Proceedings of SPIE-The International Society for Optical Engineering* **1560**, 370-376 (1991).

24. Putvinski, T.M. et al. Self-assembly of organic multilayers with polar order using zirconium phosphate bonding between layers. *Langmuir* **6**, 1567-1571 (1990).

25. Ulman, A. Formation and structure of self-assembled monolayers. *Chem. Rev.* **96**, 1533-1554 (1996).

26. Bain, C.D., Evall, J. & Whitesides, G.M. Formation of monolayers by the coadsorption of thiols on gold: variation in the head group, tail group, and solvent. *J. Am. Chem. Soc.* **111**, 7155-7164 (1989).

27. Castner, D.G. Chemical modification of surfaces. *Methods of Surface Characterization* **4**, 209-238 (1998).

28. Buckel, F., Effenberger, F., Yan, C., Golzhauser, A. & Grunze, M. Influence of aromatic groups incorporated in long-chain alkanethiol self-assembled monolayers on gold. *Adv. Mater. (Weinheim, Ger.)* **12**, 901-905 (2000).

29. Arnold, R., Azzam, W., Terfort, A. & Woell, C. Preparation, Modification, and Crystallinity of Aliphatic and Aromatic Carboxylic Acid Terminated Self-Assembled Monolayers. *Langmuir* **18**, 3980-3992 (2002).

30. Mrksich, M. A surface chemistry approach to studying cell adhesion. *Chem. Soc. Rev.* **29**, 267-273 (2000).

31. Ozkan, D. et al. Electrochemical detection of hybridization using peptide nucleic acids and methylene blue on self-assembled alkanethiol monolayer modified gold electrodes. *Electrochem. Commun.* **4**, 796-802 (2002).

32. Kelly, K.F., Shon, Y.S., Lee, T.R. & Halas, N.J. Scanning Tunneling Microscopy and Spectroscopy of Dialkyl Disulfide Fullerenes Inserted into Alkanethiolate SAMs. *J. Phys. Chem. B* **103**, 8639-8642 (1999).

33. Shon, Y.-S., Kelly, K.F., Halas, N.J. & Lee, T.R. Fullerene-Terminated Alkanethiolate SAMs on Gold Generated from Unsymmetrical Disulfides. *Langmuir* **15**, 5329-5332 (1999).

34. Zamborini, F.P. & Crooks, R.M. Corrosion Passivation of Gold by n-Alkanethiol Self-Assembled Monolayers: Effect of Chain Length and End Group. *Langmuir* **14**, 3279-3286 (1998).

35. Law, H.H., Sapjeta, J., Chidsey, C.E.D. & Putvinski, T.M. Protective treatments for nickel-based contact materials. *J. Electrochem. Soc.* **141**, 1977-1982 (1994).

36. Jennings, G.K., Munro, J.C., Yong, T.-H. & Laibinis, P.E. Effect of Chain Length on the Protection of Copper by n-Alkanethiols. *Langmuir* **14**, 6130-6139 (1998).

37. Jennings, G.K. & Laibinis, P.E. Self-assembled monolayers of alkanethiols on copper provide corrosion resistance in aqueous environments. *Colloids Surf., A* **116**, 105-114 (1996).

38. Feriotto, G., Borgatti, M., Mischiati, C., Bianchi, N. & Gambari, R. Biosensor technology and surface plasmon resonance for real-time detection of genetically modified Roundup Ready soybean gene sequences. *J. Agric. Food Chem.* **50**, 955-962 (2002).

39. Goepel, W. & Liedberg, B. Biosensors and bioelectronics special issue on \"artificial biosensing interfaces (a new European science foundation scientific program)\" workshop no. 1: \"surface modification and characterization\". *Biosens. Bioelectron.* **10**, 743 (1995).

40. Zhu, B., Eurell, T., Gunawan, R. & Leckband, D. Chain-length dependence of the protein and cell resistance of oligo(ethylene glycol)-terminated self-assembled monolayers on gold. *J. Biomed. Mater. Res.* **56**, 406-416 (2001).

41. Roberts, C. et al. Using mixed self-assembled monolayers presenting RGD and (EG)3OH groups to characterize long-term attachment of bovine capillary endothelial cells to surfaces. *J. Am. Chem. Soc.* **120**, 6548-6555 (1998).

42. Qian, X. et al. Arrays of self-assembled monolayers for studying inhibition of bacterial adhesion. *Anal. Chem.* **74**, 1805-1810 (2002).

43. Abdelghani-Jacquin, C., Abdelghani, A., Chmel, G., Kantlehner, M. & Sackmann, E. Decorated surfaces by biofunctionalized gold beads: application to cell adhesion studies. *European Biophysics Journal* **31**, 102-110. (2002).

44. Ulman Introduction to Ultrathin Organic Films - from Langmuir-Blodgett to Self-Assembly. (Academic Press, Boston; 1991).

45. Abbott, S., Ralston, J., Reynolds, G. & Hayes, R. Reversible wettability of photoresponsive pyrimidine-coated surfaces. *Langmuir* **15**, 8923-8928 (1999).

46. Sellergren, B., Swietlow, A., Arnebrant, T. & Unger, K. Consecutive Selective Adsorption of Pentamidine and Phosphate Biomolecules on a Self-Assembled Layer: Reversible Formation of a Chemically Selective Coating. *Anal. Chem.* **68**, 402-407 (1996).

47. Abrantes, L.M., Kalaji, M. & Viana, A.S. In situ ellipsometric study of redox induced orientation of a short chained ferrocenylalkylthiol monolayer self-assembled on gold. *Russ. J. Electrochem.* **38**, 39-43 (2002).

48. Ziegler, C. & Gopel, W. Biosensor development. *Curr. Opin. Chem. Biol.* **2**, 585-591. (1998).

49. Malmqvist, M. A surface plasmon resonance biosensor for characterization of biospecific interactions. *Nanofabrication and Biosystems*, 103-122 (1996).

50. Liedberg, B. & Cooper, J.M. Bioanalytical applications of self-assembled monolayers. *Immobilized Biomolecules in Analysis*, 55-78 (1998).

51. Joensson, U. et al. Introducing a biosensor based technology for real-time biospecific interaction analysis. *Annales de Biologie Clinique* **51**, 19-26 (1993).

52. Frutos, A.G., Brockman, J.M. & Corn, R.M. Reversible Protection and Reactive Patterning of Amine- and Hydroxyl-Terminated Self-Assembled Monolayers on Gold Surfaces for the Fabrication of Biopolymer Arrays. *Langmuir* **16**, 2192-2197 (2000).

53. Fuierer, R.R., Carroll, R.L., Feldheim, D.L. & Gorman, C.B. Patterning mesoscale gradient structures with self-assembled monolayers and scanning tunneling microscopy based replacement lithography. *Adv. Mater. (Weinheim, Ger.)* **14**, 154-157 (2002).

54. Herbert, C.B. et al. Micropatterning gradients and controlling surface densities of photoactivatable biomolecules on self-assembled monolayers of oligo(ethylene glycol) alkanethiolates. *Chemistry and Biology* **4**, 731-737. (1997).

55. Mrksich, M., Dike, L.E., Tien, J., Ingber, D.E. & Whitesides, G.M. Using microcontact printing to pattern the attachment of mammalian cells to self-assembled monolayers of alkanethiolates on transparent films of gold and silver. *Exp. Cell Res.* **235**, 305-313 (1997).

56. Yousaf, M.N., Houseman, B.T. & Mrksich, M. Using electroactive substrates to pattern the attachment of two different cell populations. *Proc. Natl. Acad. Sci. U. S. A.* **98**, 5992-5996 (2001).

57. Tan, J.L., Tien, J. & Chen, C.S. Microcontact Printing of Proteins on Mixed Self-Assembled Monolayers. *Langmuir* **18**, 519-523 (2002).

58. Rozsnyai, L.F. & Wrighton, M.S. Selective Electrochemical Deposition of Polyaniline via Photopatterning of a Monolayer-Modified Substrate. *J. Am. Chem. Soc.* **116**, 5993-5994 (1994).

59. Xia, N., Hu, Y., Grainger, D.W. & Castner, D.G. Functionalized poly(ethylene glycol)-grafted polysiloxane monolayers for control of protein binding. *Langmuir* **18**, 3255-3262 (2002).

60. Ketteree, T., Rickert, J., Bayer, E. & Gopel, W. Mass-sensitive detection of oligonucleotides by quartz crystal microbalance. *Chemical Sensors, Technical Digest of the International Meeting, 7th, Beijing, China, July 27-30, 1998*, 816-818 (1998).

61. Hickman, J.J. et al. Combining spontaneous molecular assembly with microfabrication to pattern surfaces: selective binding of isonitriles to platinum microwires and characterization by electrochemistry and surface spectroscopy. *J. Am. Chem. Soc.* **111**, 7271-7272 (1989).

62. Kuramitz, H., Sugawara, K. & Tanaka, S. Electrochemical sensing of avidin-biotin interaction using redox markers. *Electroanalysis* **12**, 1299-1303 (2000).

63. Roth, K.M., Lindsey, J.S., Bocian, D.F. & Kuhr, W.G. Characterization of Charge Storage in Redox-Active Self-Assembled Monolayers. *Langmuir* **18**, 4030-4040 (2002).

64. Steel, A.B., Herne, T.M. & Tarlov, M.J. Electrochemical Quantitation of DNA Immobilized on Gold. *Anal. Chem.* **70**, 4670-4677 (1998).

65. Steel, A.B., Levicky, R., Herne, T.M. & Tarlov, M.J. Electrochemical characterization and quantitation of DNA on gold. *Proc. - Electrochem. Soc.* **99-5**, 132-143 (1999).

66. Walczak, M.M., Chung, C., Stole, S.M., Widrig, C.A. & Porter, M.D. Structure and interfacial properties of spontaneously adsorbed n-alkanethiolate monolayers on evaporated silver surfaces. *J. Am. Chem. Soc.* **113**, 2370-2378 (1991).

67. Porter, M.D., Bright, T.B., Allara, D.L. & Chidsey, C.E.D. Spontaneously Organized Molecular Assemblies. 4. Structural Characterization of n-Alkyl Thiol

Monolayers on Gold by Optical Ellipsometry, Infrared Spectroscopy, and Electrochemistry. *J. Am. Chem. Soc* **109**, 3559 (1987).

68. Nuzzo, R.G., Zegarski, B.R. & Dubois, L.H. Fundamental studies of the chemisorption of organosulfur compounds on gold(111). Implications for molecular self-assembly on gold surfaces. *J. Am. Chem. Soc.* **109**, 733-740 (1987).

69. Wolf, K.V., Cole, D.A. & Bernasek, S.L. in Analytical Chemistry ACS ASAP.

70. Bain, C.D. & Whitesides, G.M. Formation of monolayers by the coadsorption of thiols on gold: variation in the length of the alkyl chain. *J. Am. Chem. Soc.* **111**, 7164-7175 (1989).

71. Porter, M.D., Bright, T.B., Allara, D.L. & Chidsey, C.E.D. Spontaneously organized molecular assemblies. 4. Structural characterization of n-alkyl thiol monolayers on gold by optical ellipsometry, infrared spectroscopy, and electrochemistry. *J. Am. Chem. Soc.* **109**, 3559-3568 (1987).

72. Chen, W. et al. Ultrahydrophobic and Ultralyophobic Surfaces: Some Comments and Examples. *Langmuir* **15**, 3395-3399 (1999).

73. Tompkins, H.G. A User's Guide to Ellipsometry. (Academic Press, Inc., San Diego; 1993).

74. Ulman, A. Characterization of Organic Thin Films. (Butterworth-Heinemann, 1995).

75. Porter, M.D., Bright, T.B., Allara, D.L. & Chidsey, C.E.D. Spontaneously Organized Molecular Assemblies. 4. Structural Characterization of n-Alkyl Thiol Monolayers on Gold by Optical Ellipsometry, Infrared Spectroscopy, and Electrochemistry. *J. Am. Chem. Soc.* **109**, 3559 (1987).

76. Binnig, G., Quate, C.F. & Gerber, C. Atomic force microscope. *Phys. Rev. Lett.* **56**, 930-933 (1986).

77. Albrecht, T.R., Grütter, P., Horne, D. & Rugar, D. Frequency modulation detection using high-Q cantilevers for enhanced force microscope sensitivity. *J. Appl. Phys.* **69**, 668-673 (1991).

78. Shultz, M.J., Schnitzer, C., Simonelli, D. & Baldelli, S. Sum Frequency Generation Spectroscopy of the Aquaeous Interface: Ionic and Soluble Molecular Solutions. *Int. Reviews in Physical Chemistry* **19**, 123-153 (2000).

79. Zhang, D., Ward, R.S., Shen, Y.R. & Somorjai, G.A. Environment-Induced Surface Structural Changes of a Polymer: An *in situ* IR + Visible Sum-Frequency Spectroscopic Study. *J. Phys. Chem. B* **101**, 9060-9064 (1997).

CHAPTER TWO

A REVERSIBLY SWITCHING SURFACE

2.1. Introduction

Interfacial properties such as wetting behavior are defined by the molecular-level structure of the surface (1). Diverse modification procedures have thus been used to permanently alter wettability (2-4). Control of wettability has been recently demonstrated by elegant methods including light-induced (5-6) and electrochemical surface modifications (7-9), such as oxidative desorption of molecules (10). These systems require chemical reactions in order to control wettability.

We demonstrate an alternative approach for dynamically controlling interfacial properties that utilizes conformational transitions (switching) of surface-confined molecules. Polymers have been shown to undergo conformational reorientations when changed from one solvent to another (11) or due to a temperature change (12-13) because of phase transitions between a well solvated and a poorly solvated state (14). In contrast, our approach maintains the system's environment unaltered (including solvent, electrolyte content, pH, temperature, and pressure) while using an active stimulus, such as an electrical potential, to trigger specific conformational transitions (e.g. switching from an all-trans to a partially gauche oriented conformation; see Fig. 2.1). Amplification of conformational transitions to macroscopically measurable changes requires synergistic molecular reorientations of ordered molecules. In principle, this is attainable using a single-molecular layer, such as a self-assembled monolayer (SAM) of alkanethiols on gold (15). However, the dense molecular packing in SAMs and the strong interactions between the CH_2-groups restrict dynamic molecular motions to the outermost atoms (16, 17). All in situ evidence so far indicates that applied electrical potentials have no effect on long chain alkanethiolate monolayers on gold within

the range of chemical stability of the SAM (18). In other words, conventional SAMs are too dense to allow conformational transitions and consequently do not allow for switching.

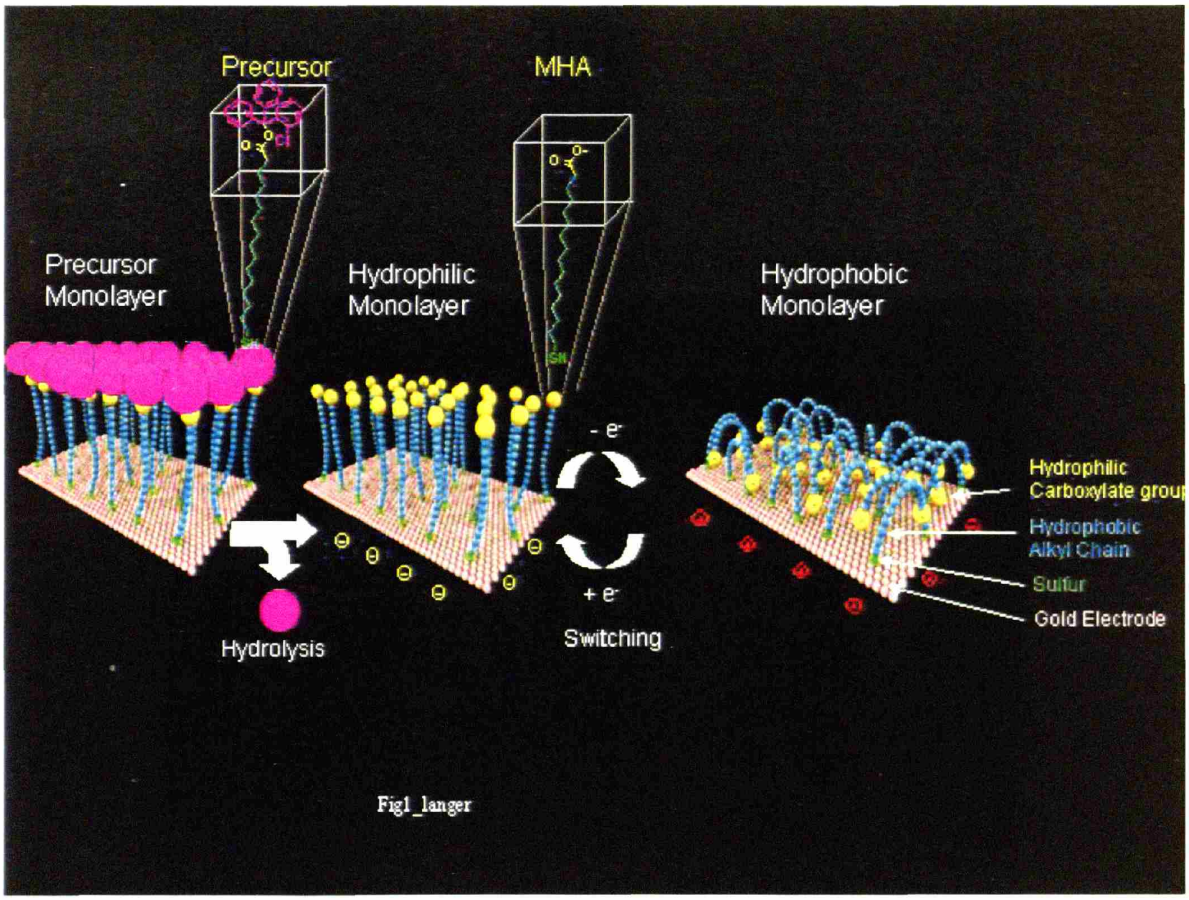

Figure 2.1 Idealized representation of the transition between straight (hydrophilic) and bent (hydrophobic) molecular conformations (ions and solvent molecules are not shown). The precursor molecule MAHE, characterized by a bulky end group and a thiol head group, was synthesized from MHA by introducing the (2-chlorophenyl)diphenylmethyl ester group.

To explore SAMs as a model system for switching, sufficient spatial freedom must be established for each molecule. Once a low-density SAM is created, preferential exposure of either hydrophilic or hydrophobic moieties of the SAM to the surrounding medium could be exploited for switching of macroscopic surface properties such as wettability.

(16-Mercapto) hexadecanoic acid (MHA) was chosen as a model molecule since it (a) self-assembles on Au(111) into a monolayer and (b) has a hydrophobic chain capped by a hydrophilic carboxylate group, thus potentially facilitating changes in the overall surface properties. To create a monolayer with sufficient spacing between the individual MHA molecules, we used a strategy that exploits synthesis and self-assembly of a MHA derivative with a globular end group, which results in a SAM that is densely packed with respect to the space-filling end groups, but shows low-density packing with respect to the hydrophobic chains. Subsequent cleavage of the space-filling end groups establishes a low-density SAM of MHA. The spatial dimensions of the precursor molecule to be utilized were adapted to match the optimum alkanethiolate density for conformational rearrangements.

The equilibrium low energy conformational state of each of the sparsely packed MHA molecules is all trans (all C-C-C-C torsion angles of the hydrophobic core are 180 degrees) (15). Upon applying an electrical potential, the negatively charged carboxylate groups experience an attractive force to the gold surface causing the hydrophobic chains to undergo conformational changes. This chain bending disrupts the all-trans conformational state and causes the aliphatic MHA chains to adopt a mixture of trans and gauche conformations. Thus, the 'bent' state of the MHA chains is characterized by an ensemble of molecules in mixed conformations to maximize the inter-molecular van der Waals contact and exposes the hydrophobic chains of the MHA molecules to the surrounding medium. To obtain a theoretical estimate of the packing density that would provide sufficient conformational freedom for optimal arrangement of the bent states of the MHA molecules, we performed molecular simulations of MHA monolayers, computing intra-molecular bonded interactions and inter- and intra-molecular non-bonded interactions. Electrostatic interactions and

influence of solvents have been ignored for simplicity, since the goal of the simulations was to understand the influence of the packing density on the conformational transitions of the MHA chains. Since alkanethiolates adsorbed on Au(111) build either a hexagonal ($\sqrt{3}x\sqrt{3}$)R30 or a c(4x2) superlattice, only certain area-per-molecule values were permitted (19). Simulations were conducted starting from assemblies of MHA molecules in bent states. Six assemblies with area-per-molecule values in the range between and 0.29 and 2.59 nm^2 were studied. These area-per-molecule values correlate with chain spacings between 0.58 and 1.73 nm for a hexagonal lattice. For small area-per-molecule values, relaxation of the highly constrained assemblies was dominant, resulting in a steep decline of the potential energy as S-S spacings were widened. Repulsive interactions did not permit creating an assembly of 0.22 nm^2, which is the area-per-molecule value of a regular SAM of MHA, so that the smallest studied area-per-chain was 0.29 nm^2. MHA molecules were confined on a hexagonal gold lattice (Au-Au distance of 0.29 nm) and sulfur and gold atoms were fixed in space. The intermolecular potential was adopted from literature (33-34) and the potential describing the interactions between carbon and sulfur atoms with the gold surface was selected to mimic the values reported by Hautman and Klein (35). Periodic boundary conditions were applied. The height of the periodic box was chosen to be large so that the molecules would not feel the presence of molecules above thus simulating a monolayer (10 nm). The simulations were performed under constant density and temperature conditions (NVT). The cutoff used for the non-bonded parameters was 0.65 – 0.7 nm. A smoothing function was used between 0.65 and 0.7 nm for the potential profile. Based on the vibrational frequency of the C-H bond (~3000 cm^{-1}; fastest motion in an organic chain), the time step of the simulation was chosen to be 0.01 picoseconds. The monolayer was first

subjected to energy minimization followed by molecular dynamics simulations. The system was heated at 1000 K for about 1 ps to allow the structure to overcome the energy barriers and sample a larger configurational space. This will ensure that the system is outside of any local equilibrium. The ensemble was then run at 300 K for about 100 picoseconds. The subsequent energy minimization (Truncated Newton) was deemed achieved either if RMS values below 0.01. For small area-per-molecule values, relaxation of the highly constrained assemblies was dominant resulting in a steep decline of the potential energy as S-S spacings were widened. The plot of the potential energy vs. area-per-molecule (Fig. 2.2) shows that steric constraints are reasonably low for area-per-molecule values of 0.65 nm^2 or higher. On the other hand, the spacing between the MHA molecules for an area-per-molecule value of 0.65 nm^2 still permits a significant overlap of MHA molecules, leading to favorable hydrophobic interactions between alkyl chains. Thus, even for the system with the widest S-S spacing of 1.73 nm, sufficient overlap of neighboring chains occurred and prevented the overall energy of the system to approach zero. We concluded from these simulations that an area-per-molecule of 0.65 nm^2 is optimum, since it supports significant steric relaxation while allowing for extensive chain overlap.

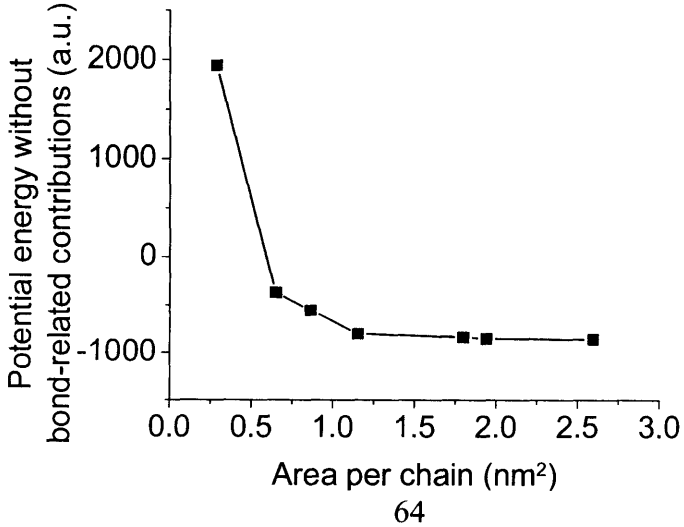

Fig. 2.2 Non-bonded interaction energy of MHA molecules vs. area-per-molecule. To evaluate the effect of the packing density on the conformational transitions and steric interactions of the MHA molecules, an assembly of 64 alkanethiolates that were forced into a bent molecular state (distance between sulfur and carbonyl carbon below 0.4 nm) was chosen as a starting point. Electrostatics were ignored since the goal of this simulation was to estimate the optimal geometrical spacing between the MHA molecules to allow for conformational transitions that provide switching capabilities to the monolayer. Nearest neighbor distances were set to be between 0.58 and 1.73 nm. A distance of 0.58 nm between two sulfur atoms corresponds to the densest packing we could establish with a bent assembly, while the distance of 1.73 nm was chosen as an upper limit to guarantee chain-chain overlap (an all-trans oriented chain of MHA has an approximate length of 2.24 nm). All alkanethiolates were confined on a hexagonal gold lattice (Au-Au distance of 0.29 nm) and sulfur and gold atoms were fixed in space. The intermolecular potential was adopted from literature (33-34) and the potential describing the interactions between carbon and sulfur atoms with the gold surface was selected to mimic the values reported by Hautman and Klein (35).

Based on these theoretical considerations, a MHA derivative with a globular end group ((16-mercapto) hexadecanoic acid (2-chlorophenyl) diphenylmethyl ester, MHAE) was synthesized. Its space-filling end group (approximately 0.67 nm^2) matched closely with the above-determined area of 0.65 nm^2. Self-assembly of MHAE on gold and subsequent removal of the acid-labile end groups resulted in a low-density SAM of MHA (20). The quantitative removal was verified by the absence of the signal of chlorine as detected by X-ray photoelectron spectroscopy (XPS). In addition, the characteristic signal of the Cl-triphenyl ester group at 1743 cm^{-1} in the infrared (IR) spectrum was no longer observed and the characteristic C=O peak appeared (21). We then exposed a low-density SAM of MHA to a solution of n-butanethiol immediately after cleavage of the bulky end group and conducted electrochemical desorption. For the mixed SAM formed from the low-density MHA backfilled by n-butanethiol, a single desorption peak was detected (orange line in Fig. 2.3). In contrast, two desorption peaks were found for phase-separated SAMs composed of MHA and

n-butanethiol formed via co-adsorption (blue line in Fig. 2.3), corresponding to the co-existence of two distinct phases (22). We concluded from this experiment that preparation of a SAM following the above-mentioned strategy resulted in a rather homogeneously distributed monolayer and not in a phase-segregated system. These results support the assumption that the low-density SAM consists of molecules that show increased spacing between individual molecules; the formation of MHA clusters is less likely.

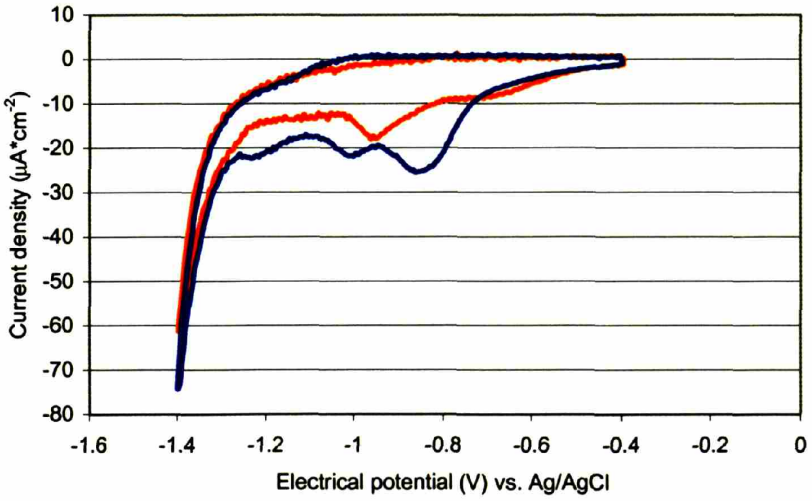

Fig. 2.3 Electrochemical desorption of two-component SAMs consisting of MHA and n-butanethiol in 0.1 M KOH with a sweep rate of 50 mV s^{-1}. Reductive desorption of two SAMs is shown that have been prepared following different procedures: (i) A Low-density SAM was prepared through self-assembly of (16-mercapto)hexadecanoic acid (2-chlorophenyl) diphenylmethyl ester on gold and subsequent cleavage of the ester bound. The resulting low-density SAM of MHA was subsequently incubated with n-butanethiol (1mM, ethanol) (orange line); (ii) A SAM on gold was prepared via co-adsorption of a 2:1 mixture of MHA and 3-mercaptopropionic acid (MPA) in ethanol. The MPA was selectively desorbed and the resulting monolayer was backfilled with n-butanethiol (blue line). Cyclic voltammetry of the SAMs was performed in a glass cell equipped with a supported gold film as the counter electrode, an Ag/AgCl reference electrode (Bioanalytical Systems, Inc), and a Gamry PC4-300 potentiostat. Working electrodes were fabricated from silicon wafers coated with silicon nitride using standard deposition techniques and photolithography, producing gold electrodes with a working surface area of 0.25 cm^2.

Prior to examining whether the low-density SAM of MHA undergoes conformational transitions in response to electric potentials, we confirmed the conformational freedom of the alkanethiolates by studying their response to changes in the chemical environment. Sum-frequency generation spectroscopy (SFG) was used for this purpose since it exploits a highly surface-sensitive nonlinear optical process (23). The intensity of a peak in the SFG spectrum is affected by the orientation of the adsorbed molecules. An ordered monolayer of all-trans oriented molecules is locally centrosymmetric and hence, by rule of mutual exclusion, its CH_2- modes are sum-frequency inactive. Gauche conformations break the local symmetry and give rise to SFG-signals of the CH_2-groups (24). Fig. 2.4 shows SFG spectra of the low-density SAMs of MHA that was deprotonated. When exposing the low-density SAM to an apolar medium such as air or toluene, the molecules were found to be in disordered conformations. This state was characterized by the presence of gauche conformations as indicated by SFG-signals of the CH_2-groups at wavelengths of 2925 and 2855 cm^{-1} (Fig. 2.4, green filled squares and black filled dots). When the same surface was brought in contact with a polar environment (acetonitrile or water), molecules straightened up, presumably by exposing their polar end groups to the solvent. SFG signals associated with the CH_2-groups were no longer detected. For the dense SAM of MHA, structural reorganizations were far less pronounced and were comparable to reported studies (25). Based on the detected conformational transitions in response to changes in the polarity of the surrounding medium, we concluded that only the low-density SAM provided sufficient chain mobility to allow conformational reorientations from a hydrophilic state (straight chains) to a hydrophobic state (bent chains).

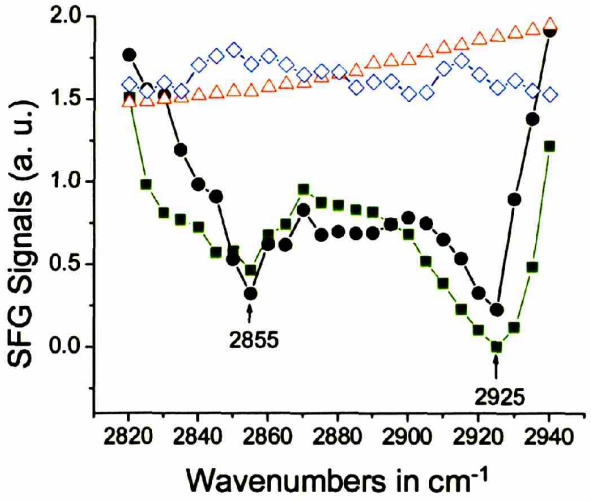

Fig. 2.4. In situ SFG spectra of the CH-stretch region (2820-2940 cm^{-1}) for the low-density SAM being exposed to air (green filled square), d^3-acetonitrile (red open triangle), d^2-water (blue open diamond) and d^8-toluene (black filled circle). Tunable mid-infrared light (1400-4000 cm^{-1}) was generated by difference frequency mixing of near-infrared light with the fundamental beam of the Nd:YAG pump laser in a $LiNbO_3$ or $AgGaS_2$ crystal. The near-infrared light was produced through optical parametric generation and amplification of 532-nm light in angle-tuned barium borate crystals. The infrared and visible beams were incident on the liquid/solid interface at 40° and 35° and have energy densities of 4 mJ/cm^2 and 15 mJ/cm^2, respectively. SFG spectra were an average of 10 scans with 5 cm^{-1} resolution. SFG signals were collected for 1 to 5 seconds at every 5 cm^{-1} interval. SFG data were normalized with respect to the reflected IR beam from the electrode to ensure that no false SFG peaks were observed due to strong IR absorption by the thin film of electrolyte above the electrode surface. The lines are drawn as a guide to the eye.

We next assessed switching induced by an active stimulus such as application of an electrical potential. Information regarding the prospective range of the electrical potential for switching may be obtained from basic energy considerations. First, alkanethiolates adsorbed on gold and exposed to a surrounding solution show electrochemical stability only in a relatively narrow range of electrical potential (–1.046 V to +654 mV w.r.t. standard Calomel electrode (SCE)) (26). Applied electrical potentials must be within this range of stability. Second, the change in Gibbs free energy of the system must be negative for a change in the

monolayer structure to occur. Using a basic model, we estimated a potential above about +150 mV (-118 mV w.r.t. SCE) to be required to satisfy the conditions of molecular reorientation in a low-density SAM (27).

A SFG spectrometer equipped with an electrochemical quartz cell (28) was used to assess the switching of the surface in response to electrical potentials (Figs. 2.5A and B). Without applied electrical potential, the SFG spectra recorded in acetonitrile (0.1 M cesium trifluoromethanesulfonate (CT)) were featureless in the range between 2820 and 2940 cm^{-1} signifying straight molecular conformations of an all-trans orientation. Slightly positive polarization of the gold surfaces (25 mV w.r.t. SCE), however, initiated simultaneous switching of the molecules indicated by characteristic CH_2-modes at wavelengths of 2855 and 2925 cm^{-1} (Fig. 2.5A). The presence of gauche conformations in the molecules implies that the molecules bend their negatively charged end groups toward the positively charged gold surface (Fig. 1). After the positive potential was turned off, the low-density SAM returned into an assembly of straight molecules with all-trans orientation, as SFG signals of the CH_2-groups were no longer detected. Switching was reversible with intensities of the SFG signals being nearly constant as the electrical potential was repeatedly applied. In contrast, the dense SAM of MHA did not show reorientations induced by an applied electrical potential, as the SFG signals remained unaltered when potential was applied (Fig. 2.5B).

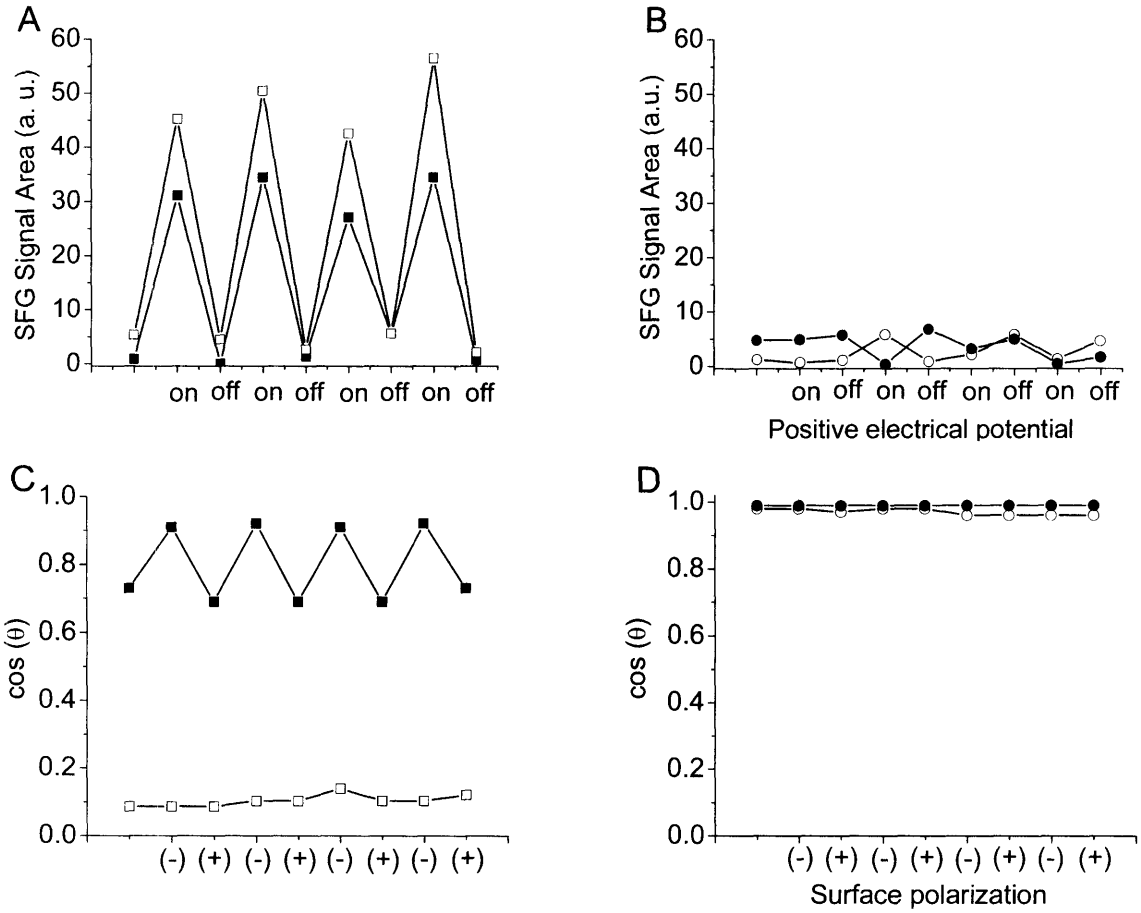

Fig. 2.5. Microscopic and macroscopic responses of the low-density SAM to an electrical potential as monitored by SFG and contact angle measurements. Relative SFG intensities (peak areas) of the CH_2-modes at wavelengths of 2855 cm^{-1} (full symbols) and 2925 cm^{-1} (open symbols) are shown for the low-density SAMs (**A**) and the dense SAMs (**B**) measured in d^3-acetonitrile (0.1 M CT) when a potential of +25 mV w.r.t. SCE was repeatedly applied to the system. Cosine of the advancing (open symbols) and receding (full symbols) contact angles for the low-density SAMs (**C**) and the dense SAMs (**D**) were determined while applying either +80 or -300 mV w.r.t. SCE to the underlying gold electrode. Four switch cycles were conducted and contact angles were measured with an aqueous solution (0.1 M CT, pH 11.5) at air using a goniometer (VCA-2500XE, AST) equipped with an electrometer (6517A, Keithley Inst.) and platinum and carbon fiber microelectrodes (Kation Scientific). Contact angles averaged at least 100 data points from nine samples with maximum errors of ±3°. The SAMs were examined for chemical integrity and deprotonation by IR spectroscopy after an electrical potential was applied. The lines are drawn as a guide to the eye.

We then addressed the question whether the observed rearrangements could be amplified into macroscopically detectable changes in surface properties. Advancing (open symbols) and receding (full symbols) contact angles for the low-density SAMs (Fig. 2.5C) and the dense SAMs (Fig. 2.5D) were determined, while applying either +80 or -300 mV w.r.t. SCE between the underlying gold electrode and a platinum-made microelectrode. Four subsequent switch cycles were examined and contact angles with an aqueous solution were measured. Fig. 2.5C indicates switching of the receding contact angles as the surface polarization was alternately changed. While the advancing contact angle was independent from the applied potential, the receding contact angle showed a sharp step whenever the polarization of the surface was changed (Fig. 2.5C, full square). The large hysteresis in contact angle can be caused by surface roughness or chemical heterogeneity of the surface (29). Since scanning force microscopy did not reveal significant differences in surface roughness between systems configured of molecules in bent and straight states (30), the assumption of a chemical discontinuity along the solid/air/liquid contact line best explains the large hysteresis in contact angles and the pronounced sensitivity of the receding contact angle. Following Neumann and Good's wettability model (31), the system reflects the behavior of a smooth, but chemically heterogeneous system that is composed of a low-energy area (area exposed to air) and a high energy-area (area exposed to solution). The observed changes in receding contact angle then signify molecular transitions at the high-energy area. SFG results support this assumption (cf. Fig. 2.4). The drop in contact angle was a reversible phenomenon as the assembly was switched several times between its hydrophilic (straight molecules) and hydrophobic state (bent molecules) (four times for the study shown in Fig. 2.5C). In contrast, switching was not observed for the dense SAM (Fig. 2.5D). We excluded the possibility of

electrochemically induced protonation, because it would affect both dense and low-density SAMs similarly (in addition, experiments were conducted at pH 11.5 to avoid protonation). It is important to point out that the applied electrical potentials were well above the estimated lower limit of electrical potentials that permits conformational transitions (27), but low enough to be within the potential window of greatest stability for SAMs of alkanethiolates on gold (26, 32). Thus, electrochemical reactions can be excluded as driving force for the observed changes in surface properties. We conclude that the observed switching in surface properties is microscopically driven by conformational transitions.

In summary, the study demonstrates reversible control of surface switching for a low-density monolayer. Due to synergistic molecular reorientations, amplification into macroscopic changes in surface properties is observed. Future research might be directed towards enhancement of macroscopic effects and development of alternative stimuli. The fact that controlled conformational reorientations of single-layered molecules induced observable changes in wettability raises hope that these findings may, with further study, have implications in dynamic regulation of macroscopic properties, such as wettability, adhesion, friction, or biocompatibility. Potential applications might include microfluidics, microengineering of smart templates for bioseparation or data storage, or the microfabrication of controlled-release devices.

2.2. Materials and Method

Synthesis of MHAE

Prior to esterification, selective protection of the thiol group was achieved by reacting purified MHA (5 mmol) with 1,1'-(chlorophenylmethylene)bis[4-methoxybenzene] (5.2 mmol) and triethylamine (6 mmol) in a mixture of tetrahydrofuran, acetic acid and water (5:4:1) for 14 h at room temperature under an argon atmosphere. After removal of the solvent under reduced pressure, the remaining residue was dissolved in ethyl ether. Extraction with ammonium bicarbonate (1 M) delivered 16-[[bis(4-methoxyphenyl)phenylmethyl]thio]hexadecanoic acid that was purified by column chromatography. Subsequently, the S-protected acid (4 mmol) was allowed to react with 1-chloro-2-(chlorodiphenylmethyl)benzene (5 mmol) and diisopropylethylamine (9 mmol) in methylene chloride for 14 h at room temperature to yield the S-protected ester. For deprotection of the thiol group, the S-protected ester (1 mmol) was dissolved in 20 ml of tetrahydrofuran and methanol (3:1) and 2 ml of an aqueous solution of sodium acetate (3 M). Silver nitrate (2 mmol) dissolved in a mixture of water and methanol (1:5) was added and the resulting suspension was stirred at room temperature for 1 hour. Subsequent centrifugation and re-suspension in 20 ml of the tetrahydrofuran/methanol mixture delivered a crude intermediate that was subsequently converted with dithioerythritol (2 mmol) in aqueous sodium acetate (3 M) for 5 h. The precipitate was filtered and the remaining filtrate was concentrated under reduced pressure. Extraction with ethyl acetate and subsequent column chromatography yielded (16-mercapto)hexadecanoic acid (2-chlorophenyl)diphenyl methyl ester. Only freshly prepared precursor was used for SAM formation on a flat Au(111)

substrate (root-mean square (RMS) roughness < 2 nm determined by scanning force microscopy).

16-[[bis(4-methoxyphenyl)phenylmethyl]thio]hexadecanoic acid. ^{1}H NMR (300 MHz, $CDCl_3$, TMS): δ= 1.18-1.39 (m, 22H, C<u>H</u>$_2$), 1.37 (q, 2H, C<u>H</u>$_2$-CH_2COO), 1.62 (q, 2H, C<u>H</u>$_2$-CH_2S), 2.05 (s, 1H), 2.14 (t, 2H, C<u>H</u>$_2$COO), 2.34 (t, 2H, C<u>H</u>$_2$S), 3.78 (s, 6H, OC<u>H</u>$_3$), 6.80 (d, 4H, C<u>H</u>), 6.81 (q, 2H, C<u>H</u>), 7.16-7.31 (compl., 5H, CH), 7.37-7.40 (compl., 2H, CH); ^{13}C NMR (75 MHz, $CDCl_3$, TMS) δ= 14.44, 21.31, 24.92, 28.89, 29.30, 29.47, 29.49, 29.68, 29.82 (double), 29.84 (double), 29.87 (double), 32.37, 34.24, 55.44 , 60.68, 113.27, 126.61, 127.99, 129.63, 130.90, 137.75, 145.93, 158.12; MS (electrospray): m/z $[M-H]^-$ = 589.34.

16-[[bis(4-methoxyphenyl)phenylmethyl]thio]hexadecanoic acid (2-chlorophenyl) diphenyl methyl ester. ^{1}H NMR (300 MHz, $CDCl_3$, TMS): δ= 1.18-1.39 (m, 22H, C<u>H</u>$_2$), 1.37 (q, 2H, C<u>H</u>$_2$-CH_2COO), 1.69 (q, 2H, C<u>H</u>$_2$-CH_2S), 2.05 (s, 1H), 2.19 (t, 2H, C<u>H</u>$_2$COO), 2.56 (t, 2H, C<u>H</u>$_2$S), 3.79 (s, 6H, OC<u>H</u>$_3$), 6.81 (d, 4H, C<u>H</u>), 6.81 (q, 2H, C<u>H</u>), 7.70-7.36 (compl., 19H, C<u>H</u>), 7.39-7.43 (compl., 2H, C<u>H</u>); ^{13}C NMR (75 MHz, $CDCl_3$, TMS) δ= 35.37, 35.51, 36.67, 36.54, 52.19, 129.21, 131.96, 132.68, 133.13, 133.51, 135.71, 136.54, 136.84, 139.78, 140.69, 142.50, 168; MS (electrospray): m/z $[M-H]^-$ = 865.37.

(16-mercapto)hexadecanoic acid (2-chlorophenyl)diphenyl methyl ester. ^{1}H NMR (300 MHz, $CDCl_3$, TMS): δ= 1.32 (s, 22H, C<u>H</u>$_2$), 1.63 (compl., 4H, C<u>H</u>$_2$-CH_2COO, C<u>H</u>$_2$-CH_2S), 2.53 (compl., 4H, C<u>H</u>$_2$COO, C<u>H</u>$_2$S), 3.50 (q, 1H), 7.18-7.36 (compl., 14H, C<u>H</u>); ^{13}C NMR (75 MHz, $CDCl_3$, TMS) δ= 35.37, 35.51, 36.67, 36.54, 52.19, 129.21, 131.96, 132.68,

133.13, 133.51, 135.71, 136.54, 136.84, 139.78, 140.69, 142.50, 168; MS (electrospray): m/z $[M-H]^-$ = 563.27.

2.3. References and Notes

1. P. G. deGennes, *Rev. Mod. Phys.* **57**, 827 (1985).

2. G. M. Whitesides, P. E. Laibinis, *Langmuir* **6**, 87 (1990).

3. P. E. Laibinis, C. D. Bain, R. G. Nuzzo, G. M. Whitesides, *J. Phys. Chem.* **99**, 7663 (1995).

4. M. K. Chaudhury, G. M. Whitesides, *Science* **256**, 1539 (1992).

5. S. Abbott, J. Ralston, G. Reynolds, R. Hayes, *Langmuir* **15**, 8923 (1999).

6. K. Ichimura, S-K. Oh, M. Nakagawa, *Science* **288**, 1624 (2000).

7. N. L. Abbott, C. B. Gorman, G. M. Whitesides, *Langmuir* **11**, 16 (1995).

8. M. Byloos, H. Al-Maznai, M. Morin, *J. Phys. Chem. B* **105**, 5900 (2001).

9. A. Iannelli, J. Merza, J. Lipkowski, *J. Electroanal. Chem.* **376**, 49 (1994).

10. B. S. Gallardo *et al.*, *Science* **283**, 57 (1999).

11. M. D. Wilson, G. M. Whitesides, *J. Am. Chem. Soc.* **110**, 8718 (1988).

12. G. De Crevoisier, P. Favre, J. Corpart, L. Leibler, *Science* **285**, 1246 (1999).

13. Y. G. Takei *et al.*, *Macromolecules* **27**, 6163 (1994).

14. T.P. Russell, *Science* **297**, 964 (2002).

15. Y. Xia, G. M. Whitesides, *Angew. Chem. Int. Ed.* **37**, 550 (1998).

16. M. H. Schoenfisch, J. E. Pemberton, *Langmuir* **15**, 509 (1999).

17. R. Anderson, M. Gatin, *Langmuir* **10**, 1638 (1994).

18. T. Li, I. Chao, M. A. Hines, J. A. Todd, P. Guyot-Sionnest, *Langmuir* **11**, 493 (1995).

19. Y. Tao, *J. Phys. Chem. B* **102**, 2935 (1998).

20. A low-density monolayer was prepared by (a) immersing Au (111) in a solution of MHAE (1mM, ethanol) and (b) removing the acid-labile end group by incubation in trifluoroacetic acid (40% in ethanol). The thickness of the SAM of MHAE was 2.05 (±0.1) nm as examined by ellipsometry. Formation of islands of adsorbed thiolates was ruled out by cyclic voltammetry (Gamry PC4-300 potentiostat, polycrystalline Au counter and Ag/AgCl reference electrodes, scan rate: 50 mV/s, 10 cycles, scan range: -0.2 to 0.5 V w.r.t. Ag/AgCl) revealing a shielding of the gold surface by the SAM of MHAE that was comparable to dense SAMs (36).

21. In air, the low-density monolayer collapsed into a disordered configuration with a thickness of 1.1 (±0.1) nm as confirmed by ellipsometry. This value was significantly lower than the thickness of a dense SAM (2.03 (±0.1) nm) and indicated the loss of two-dimensional order due to increased spacing between the adsorbed molecules. The collapsed structure was also characterized by IR spectroscopy, which revealed general features of a disordered monolayer, such as the red shift of the methylene bands from 2921 and 2852 cm^{-1} (dense SAMs of MHA) to 2929 and 2858 cm^{-1}. Furthermore, we detected an increased static contact angle with water of 62° as compared to 10° measured for the dense SAMs of MHA. The carboxylic acid group was deprotonated under argon atmosphere by incubation with a degassed aqueous cesium hydroxide solution (0.1 M) and completeness was verified by IR spectroscopy (BioRad FTS 175, grazing angle of 80°) revealing the absence of the carbonyl signals at 1742 and 1716 cm^{-1} and the presence of signals at 1550 and 1440 cm^{-1}. The low-density SAM showed chemical stability, as it remained unaltered after exposure to ambient conditions for four weeks (confirmed by XPS, IR, and cyclic voltammetry).

22. K. Shimazu, T. Kawaguchi, T. Isomura, *J. Am. Chem. Soc.* **124**, 652 (2002).

23. Y. R. Shen, *Nature* **337**, 519 (1989).

24. T. H. Ong, P. B. Davies, C. D. Bain, *Langmuir* **9**, 1836 (1993).

25. S. M. Stole, M. D. Porter, *Langmuir* **6**, 1199 (1990).

26. W. R. Everett, I. Fritsch-Faules, *Anal. Chim. Acta* **307**, 253 (1995).

27. In a first order approximation, we neglected interactions between the gold surface and solvent or electrolyte molecules, implicating that their net energetic contributions are comparably small. We then assumed the negatively charged end groups to act as dynamically mobile acceptors dictating the molecular reorientations and assumed the change in Gibbs free energy upon transition of the system to an electrified state ($N \rightarrow E$) as follows:

$$\Delta g_{total}\big|_{N\rightarrow E} = \Delta g_{\text{int}}\big|_{N\rightarrow E} + \Delta g_{sur}\big|_{N\rightarrow E} + g_{ele} \qquad (1)$$

where, Δg_{int} is the change in the Gibbs free energy associated with internal reorganization of the molecules, Δg_{sur} reflects the intermolecular interactions of the hydrocarbon chains and their interactions with the surrounding solvent molecules, and g_{ele} describes the electrostatic component associated with attractive forces between the gold surface and the carboxylate groups. Since steric hindrance between the chains is minimal in the low-density SAM, gauche conformations associated with chain bending mainly account for Δg_{int}. Δg_{int} can be approximated as $0.9nkT$ with n being the number of gauche-oriented bonds (37). Δg_{sur} primarily originates from exposure of methylene groups to the surrounding aqueous environment that were embedded in the hydrophobic environment prior to application of an electrical potential. This term is approximated by $1.5mkT$, where m is the number of methylene groups exposed to the aqueous surrounding due to application of electric field (38). Assuming further that at least two bonds need to be gauche-oriented in order to observe a detectable change in contact angle, the required contribution from the electrostatic field based on equation [1] is $|g_{ele}| > 4.8kT$. The electrostatic contribution of the free energy can be approximately described by $e\psi_o$, where e is the electronic charge and ψ_o is the surface potential (37).

28. S. Baldelli, N. Markovic, P. Ross, Y. R. Shen, G. Somorjai, *J. Phys. Chem.* **103**, 8920 (1999).

29. Y.L. Chen, A. Helm, J.N. Israelachvili, *J. Phys. Chem.* **95**, 10736 (1991).

30. Scanning force microscopy did not reveal significant differences in surface roughness between systems configured of molecules in bent (root-mean square (RMS) roughness = 1.9 nm) and straight states (RMS roughness = 1.5 nm). The different states were realized by conducting scanning force microscopy of a low-density SAM in toluene and water, respectively. Our experiments indicated that surface roughness is predominately caused by the intrinsic surface roughness of the gold surface (RMS roughness < 2nm). All RMS values refer to an area of 500x500 nm^2. Refer to Fig. 2.6 for detailed information.

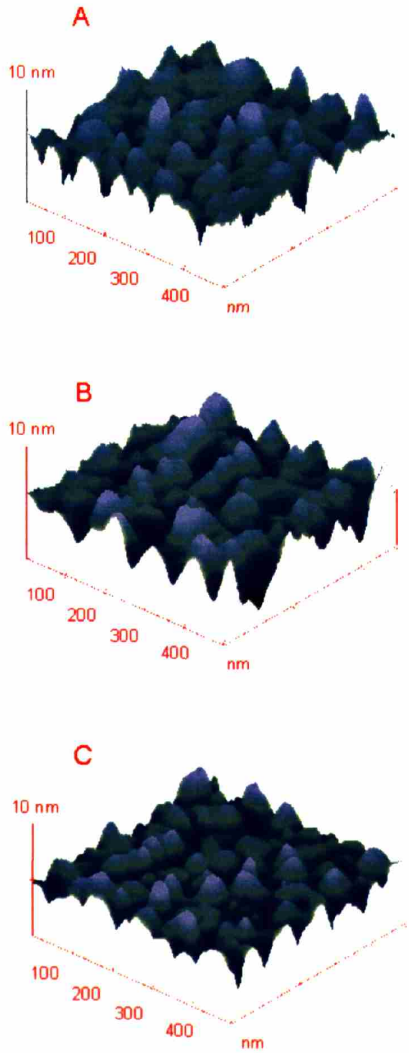

Fig. 2.6. Scanning force micrographs (500x500 nm^2) of a representative area of the low-density SAM of MHA acquired in toluene (A) and water (B). An image of the underlying gold surface conducted in air is shown as a reference (C). The experiments were performed in tapping mode on a NanoScope III Dimension (Digital Instruments, Santa Barbara) equipped with an environmental chamber for liquid handling. Data were processed using Nanoscope III 4.31r6 software (Digital Instruments, Santa Barbara).

31. A.W. Neumann, R.J. Good, *J. Colloid Interface Sci.* **38**, 341 (1972).

32. H. O. Finklea, S. Avery, M. Lynch, T. Furtsch, *Langmuir* **3**, 409 (1987).

33. W. D. Cornell *et al.*, *J. Am. Chem. Soc.*, **117**, 5179 (1995).

34. S. J. Weiner *et al.*, *J. Am. Chem. Soc.* **106**, 765 (1984).

35. J. Hautman, M. L. Klein, *J. Chem. Phys.* **91**, 4995 (1989).

36. F. P. Zamborini, R. M. Crooks, *Langmuir* **14**, 3279 (1998).

37. N. Aydogan, B. S. Gallardo, N. L. Abbott, *Langmuir* **15**, 722 (1999).

38. M. H. Abraham, *J. Chem. Soc., Faraday Trans. 1* **80**, 153 (1984).

CHAPTER THREE

A SYNTHETIC CHEMICAL ROUTE FOR THE FORMATION OF HOMOGENEOUSLY MIXED SELF-ASSEMBLED MONOLAYERS

3.1. Introduction

The formation of self assembled monolayers (SAMs) containing homogeneously mixed multicomponent alkanethiol derivatives is of interest in the design of oligonucleotide arrays, in electroanalysis, in the study of electron transfer mechanism, and in exploring the molecular-level basis of wettability, adhesion, and frictional properties.[1-4] Mixed or multicomponent SAMs are often formed by immersing the substrate into a solution containing a mixture of the self-assembling molecules.[5-9] This process can be controlled by varying factors such as solvent, temperature, and mole fractions of the components in solution. However, factors such as rate of competitive adsorption, reversibility of adsorption, and exchange between molecules in solution and in the mixed SAMs are more difficult to control.[10] These factors lead to a process that often involves numerous trial and error experiments to obtain the desired surface composition[2,8,11] due to differences in adsorption rate of the two species.[12,13] The tendency of adsorbates to form single-component domains or "islands" makes it difficult to obtain a homogenously mixed monolayer. These micron-sized domains are characterized by the presence of two peaks in voltammograms for the reductive desorption of the mixed SAMs.[11,14-17] For applications where periodic molecular spacing is desired, a homogenously mixed monolayer and the ability to spatially control its composition are of importance.

Several approaches to form mixed SAMs have been reported. One approach involves the chemisorption of bifunctional adsorbates such as unsymmetrical alkyl sulfides or disulfides,[18,19] or unsymmetrical spiroalkanedithiols, 2-octyl-2-pentadecylpropane-1,3-dithiol,[20] onto gold to yield complex interfaces. Both methods are generally limited to creating monolayers with a 1:1 molecular ratio of the two components. Recent effort has shown that a homogenously mixed SAM can also be formed from a multi-step

electrochemical method.[2] Shimazu *et. al* used underpotential deposition (UPD) to create a low-density layer of Pb atoms on Au, followed by the formation of a SAM onto the Pb-Au surface. Desorption of the Pb atoms created vacant sites onto which a second alkanethiol was absorbed to form a mixed monolayer. This approach made major strides in the creation of two-component SAMs that were homogeneously mixed over short length scales.[2]

Here we report a novel route for the formation of homogeneously mixed SAMs, employing a strategy that exploits the synthesis and self-assembly of a 16-mercaptohexadecanoic acid (MHA) derivative containing a globular end group opposite to the thiol moiety. Scheme 1 illustrates the formation process. The SAM of Cl-triphenyl methyl ester precursor (16-CTC) is a monolayer that shows low-density packing with respect to the hydrophobic chains due to the spatial restrictions of the space-filling endgroups (Scheme 3.1, Step 1). Subsequent cleavage of endgroups establishes a low-density SAM of MHA (Scheme 3.2, Step 2). Backfilling the low-density assembly with a second alkanethiol leads to formation of a mixed monolayer of two different components (Scheme 3.3, Step 3). Characterization of the resulting SAM with optical ellipsometry, contact angle goniometry, X-ray photoelectron spectroscopy (XPS), Fourier-transform infrared spectroscopy (FT-IR), cyclic voltammetry (CV), and reductive desorption voltammetry indicates the formation of a homogeneously mixed SAM. This method presents several advantages over complimentary techniques. For example, our method can incorporate molecules that would normally form islands in coadsorption. It also has an advantage over other methods in allowing for molecules with a variety of endgroups to be mixed, not just alkanethiols with different chain lengths. Our method can also overcome some of the disadvantages associated with the UPD method. For example, a

SAM formed from our technique should allow a wider compositional ratio of mixed samples to be achieved by changing the headgroup size of the initial adsorbate.

The reported approach represents a novel way to produce SAMs that are uniformly mixed using a synthetic chemical route that exploits the low-density SAM as a platform for formation of mixed SAMs. This method affords considerable flexibility in varying the composition and the ratio of different molecules in the mixed SAM.

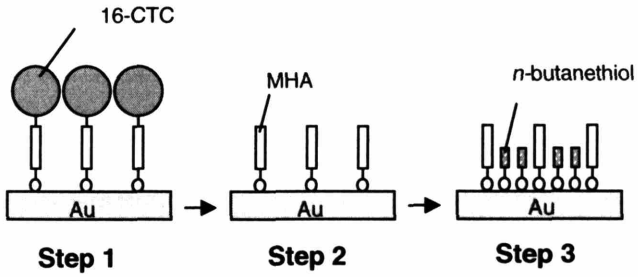

Scheme 3.1. Simplified schematic of the formation of the homogeneously mixed monolayer via attachment of Cl-triphenyl methyl precursor 16-CTC (Step 1), formation of low density monolayer (Step 2), and backfilling to form a mixed monolayer (Step 3).

3.2. Experimental Section

Materials. Silicon(111) wafers (SiliconQuest) were used for gold deposition. Hexadecane, methanol (MeOH), anhydrous ethanol (reagent grade), and hexadecanethiol (HDT), dichloromethane (DCM), triethylamine, diisopropylethylamine (DIPEA), 16-mercaptohexadecanoic acid (MHA), tetrahydrofuran (THF), acetic acid (99.99%), dimethoxytrityl chloride (DMT), dithioerythritol (DTE), silver nitrate, and potassium ferricyanide were from Aldrich and used as received. MHA was purified via column chromatography (silica, ethyl acetate:hexane (2:5)) prior to use. Chlorotrityl chloride

(CTC, Novabiochem) was used as received. Deionized water was purified with a Millipore-Q system (MilliQ).

Synthesis of Cl-Triphenyl Methyl Ester Precursor (16-CTC). The synthesis of the precursor was briefly described previously.[21] The synthetic route is presented in Scheme 2. The thiol group of 16-mercaptohexadecanoic acid was selectively protected by reacting MHA (I, 5 mmol, 1.44 g) with dimethoxytrityl chloride (3.5 mmol, 1.86 g), and triethylamine (6 mmol, 840 μL) in a mixture of THF, acetic acid, and MilliQ water (5:4:1) for 14 hours under an argon atmosphere. After the solvent was removed *in vacuo*, the product was redissolved in diethyl ether and washed with an aqueous solution of ammonium bicarbonate (1 M, 3 × 100 mL). The organic phase was dried over Na_2SO_4 and evaporated to dryness under vacuum. The crude product was purified via column chromatography (silica, hexane:ethyl acetate:methylene chloride (6:2:1)) to yield the S-protected acid (II). Subsequently, the S-protected acid (4 mmol, 2.36 g) was allowed to react with chlorotrityl chloride (5 mmol, 1.57 g) and DIPEA (9 mmol, 1.57 mL) in DCM for 14 h at room temperature to yield the S-protected ester (III). The product was purified via column chromatography (silica, hexane:ethyl acetate:methylene chloride (6:2:1)). For deprotection of the thiol group to yield Cl-triphenyl methyl ester precursor (16-CTC), the S-protected ester (1 mmol, 0.869 g) was dissolved in 20 mL of THF and methanol (3:1) and 2 mL of an aqueous solution of sodium acetate (3 M). Silver nitrate (2 mmol, 340 mg) dissolved in a mixture of water and methanol (1:5) was added and the resulting suspension was stirred at room temperature for 1 h. Subsequent centrifugation and re-suspension in 20 mL of the THF/methanol mixture delivered a crude intermediate that was subsequently converted with dithioerythritol (2 mmol, 0.308 g) in 3 mL aqueous sodium acetate (3 M) for 5 h. The precipitate was filtered, and the remaining filtrate was

concentrated under reduced pressure. The solid was then dissolved in mixture of ethyl acetate and water (1:1). The aqueous phase was extracted with ethyl acetate (3 × 50 mL) and the organic phase was washed with water (3 × 50 mL). The combined organic phase was dried over Na_2SO_4 and evaporated to dryness under vacuum. Subsequent column chromatography (silica, ethyl acetate:hexane (2:5)) yielded Cl-triphenyl methyl ester (16-CTC) with the following properties: ^{1}H NMR (300 MHz, $CDCl_3$, TMS): δ= 1.32 (s, 22H, C$\underline{H}_2$), 1.63 (compl., 4H, C$\underline{H}_2$-CH_2COO, C$\underline{H}_2$-CH_2S), 2.53 (compl., 4H, C$\underline{H}_2$COO, C$\underline{H}_2$S), 3.50 (q, 1H), 7.18-7.36 (compl., 14H, C$\underline{H}$); ^{13}C NMR (75 MHz, $CDCl_3$, TMS) δ= 33.37, 33.51, 36.67, 36.54, 52.19, 129.21, 131.96, 132.68, 133.13, 133.51, 133.71, 136.54, 136.84, 139.78, 140.69, 142.50, 168; ESI-MS: m/z $(M-H)^-$ = 563.27 (theoretical 563.28).

Preparation of SAMs. Substrates were prepared by evaporation of titanium (100 Å) as an adhesion layer and gold (1000 Å) on test grade silicon wafer (SiliconQuest) that was precoated with a 3000 Å layer of Si_3N_4 as an electrically insulating layer. The evaporation was carried out in a Temescal Semiconductor Products VES 2550 electron beam evaporator under high vacuum (10^{-7} Torr). The root-mean square roughness of the surface as determined by atomic force microscopy (AFM) with the Nanoscope IIIa Scanning Probe Microscope (Digital Instruments) using tapping mode in air was approximately 15 Å. Substrates were either used fresh or cleaned for 1 min in piranha solution (7:3, H_2SO_4:H_2O_2), washed 3 times in MilliQ water and absolute ethanol, and blown dry under a stream of nitrogen; *caution: "piranha" solution reacts violently with organic materials, and should be handled carefully.* The substrates were immersed in 1 mM solutions of the adsorbates in anhydrous ethanol and allowed to equilibrate for a minimum of 16 h. The resultant SAMs were rinsed with ethanol and dried under a filtered stream of nitrogen.

To prepare the low-density SAMs, the ester group on the 16-CTC SAMs was cleaved in 50% trifluoroacetic acid in ethanol for 1 min. The resultant monolayers were sonicated in ethanol for 1 min, washed exhaustively with MilliQ water and ethanol and blown dry in a filtered stream of nitrogen. Formation of the mixed SAM was performed by immersing the low-density SAM for 2–5 min in 1 mM ethanolic solution of *n*-butanethiol. The mixed monolayer was rinsed exhaustively in ethanol, sonicated for 1 min in ethanol, rinsed in water and ethanol, and dried in a filtered stream of nitrogen.

Contact Angle Measurements. Water advancing, receding, and static contact angles were measured at ambient temperature using a goniometer (VCA-2500XE, AST). To measure the advancing and receding contact angles, the angle of a water droplet that formed at the end of a blunt-tipped syringe made with the surface was examined. Advancing and receding angles are defined as the angle formed between the film-droplet interface and the tangent to the droplet at its intersection with the substrate as the volume of the drop is being altered via a syringe.

Ellipsometric Measurements. Thickness measurements were carried out on a Gaertner Ellipsometer Model L3W26C.830 equipped with a 632.8-nm helium-neon laser. Monolayer thicknesses were determined with incident and reflected light at 70° to the surface normal and assuming that $n_f = 1.3$.[22] Optical constants were measured prior to deposition and used to calculate thickness of the molayer after deposition. The variation in the measured thickness among 3–4 spots on any sample was ± 2 Å. Reported thicknesses were the average of at least five independent experiments in which each sample was characterized by ellipsometry at three distinct locations on its surface.

Reflectance Infrared Spectroscopy (Grazing Angle FT-IR). IR spectra were obtained in a single reflection mode with a Bio-Rad FTS 175 infrared spectrometer and Universal

Reflectance Attachment, which allowed for *p*-polarized light to reflect off the sample with an angle of incidence at 80° from the surface normal. The spectrometer was equipped with a narrow-band mercury-cadmium-telluride (MCT) detector cooled with liquid nitrogen. Background spectra were taken using gold substrates coated with octadecanethiol-d_{37} and 1024 scans of both sample and reference were used to obtain good signal to noise ratio at a resolution of 2 cm^{-1} after triangular apodization.

Electrochemistry. Cyclic voltammetry (CV) of the SAMs was performed in a glass cell with a supported gold film as the counter electrode, Ag|AgCl as a reference electrode (Bioanalytical Systems, Inc), and a Gamry PC4-300 potentiostat. Working electrodes consisted of 2 pads, a rectangular pad (0.5 cm × 0.75 cm), and a square pad (0.5 cm × 0.5 cm), connected by a 0.1 mm wire 0.5 cm long. This electrode design was chosen in order to simultaneously prepare a series of electrodes with the same geometrical area. The electrodes were fabricated using standard lithographic techniques, producing electrodes with an Au working surface area of 0.25 cm^2 or 0.375 cm^2 on Si_3N_4 coated Si wafers. The voltammetric experiment was carried out in a 1 M KCl solution containing 0.1 mM $Fe(CN)_6^{-3}$. The scan rate was 50 mV/s. Typically up to 10 cycles were recorded with a scan range of −0.2 to 0.5 V versus a Ag|AgCl|saturated KCl electrode.

Electrochemical Reductive Desorption. All experiments were conducted in a nitrogen-filled glove bag to minimize interference from dissolved oxygen. A low-density SAM of MHA prepared from its 16-CTC precursor was incubated with *n*-butanethiol (1 mM, ethanol) for 2 min. Another SAM on gold was prepared via co-adsorption of a 2:1 mixture of MHA and 3-mercaptopropionic acid (MPA) in ethanol. The MPA was selectively desorbed and the resulting monolayer was backfilled with *n*-butanethiol. [23] Electrochemical desorption of two-component SAMs consisting of MHA and *n*-

butanethiol was performed in deoxygenated 0.1 M KOH with a scan rate of 50 mV/s in a glass cell equipped with a supported gold film as the counter electrode, an Ag|AgCl reference electrode, and a Pine Mode AFRDE bipotentiostat interfaced to a PC using a custom-made DAQCard-6024E (National Instruments) and a LabVIEW program. Working electrodes were fabricated as described above.

X-ray Photoelectron Spectroscopy (XPS). XPS spectra were obtained using a Kratos AXIS Ultra Imaging X-ray Photoelectron Spectrometer with a monochromatic Al K_α X-ray source operated at 1400 V and a 160 mm concentric hemispherical energy analyzer. The spot size was 300 × 700 μm. Take-off angle of 90 degree was used.

3.3. Results and Discussion

The procedure for formation of the mixed SAM is presented in Scheme 3.1. Step 1 is the adsorption of a Cl-triphenyl methyl precursor, 16-CTC. Step 2 is the cleavage of a 16-CTC monolayer and formation of a low-density monolayer of MHA molecules. Step 3 is a backfilling step in which *n*-butanethiol molecules adsorb onto accessible Au sites, resulting in a mixed SAM.

3.3.1. Synthesis and characterization of 16-CTC monolayers (Step 1)

Synthesis. The synthesis of the 16-CTC precursor was carried out according to the route shown in Scheme 3.2. The protection of the thiol group, II, had good yield and was purified as described. The protection of the acid group was much lower in yield (III), and subsequent deprotection of the thiol group gave about 15-25% yield. Compound II was an orange-color oil that became a clearer, more yellowish oil upon purification.

Compound III was also a yellowish oil. The final product, 16-CTC (IV) was a white solid.

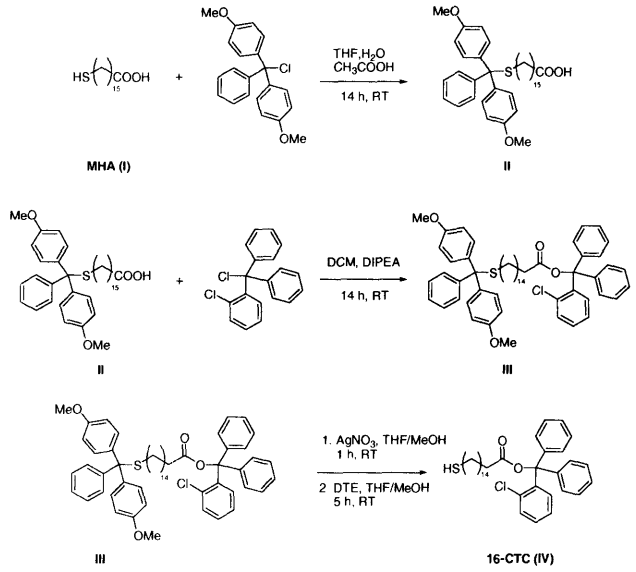

Scheme 3.2. Synthetic route for the Cl-triphenyl methyl ester precursor (16-CTC)

Formation of 16-CTC Monolayers. The water contact angles for the 16-CTC monolayers were 86 ± 3°, 96 ± 3°, and 72 ± 3° for static, advancing, and receding values, respectively. These values are significantly higher than those observed for the acid terminated MHA (10°).[21] This result indicates a substantial increase in hydrophobicity of the 16-CTC monolayer due to presence of the hydrophobic triphenyl group. The static angle was also similar to that obtained for dimethoxytrityl chloride group (DMT) tethered to a mercaptoundecanol SAM on Au where researchers measured a contact angle of 61°.[24]

The thickness of the monolayers measured by ellipsometry was 23 ± 2 Å, whereas those of MHA and HDT monolayers were 20 ± 1 and 18 ± 2 Å, respectively. Based on

this result, the thickness of the CTC headgroup was derived to be about 3–5 Å, a reasonable estimate given that the DMT group, a similar molecule to CTC, has a thickness of about 5 Å.[24]

To determine structural information regarding the 16-CTC monolayer, Fourier-transform infrared spectroscopy (FT-IR) was used. The CH_2 stretching vibrations of the alkyl chain are very sensitive to packing density and to the presence of gauche defects, which makes these vibration modes ideally suited as probes to determine the quality of SAMs. In particular, the asymmetric CH_2 stretching ($\upsilon_a^{CH_2}$) vibration at ~2918 cm^{-1} is a useful indicator.[25] For a densely packed, crystalline SAM of exceptional quality, the $\upsilon_a^{CH_2}$ band would appear between 2916 and 2917 cm^{-1}. For normal, densely packed SAMs, the $\upsilon_a^{CH_2}$ band would be near 2918 cm^{-1}. For a disordered, "spaghetti-like" SAM, it would be at 2926 cm^{-1} or above.[25] As shown in Figure 3.1A, the FT-IR spectrum of 16-CTC monolayer (solid line) shows CH_2 vibrations at 2924 and 2855 cm^{-1}, suggesting moderate disorder along the alkyl chains. These bands are reproducible at higher frequencies than those of MHA SAM (dashed line), which appear at 2920 and 2852 cm^{-1}. The decrease in crystallinity of the 16-CTC SAM is likely due to the spatial limitations exerted by the bulky headgroup, preventing the close-packing of the chains. This increased chain-to-chain separation can also lead to weaker interchain van der Waals stabilization and further decreases the conformational order in the 16-CTC films. Other differences between the 16-CTC and MHA SAMs include the presence of aromatic CH stretches at 3071 and 3030 cm^{-1} (Figure 3.1A) and of an ester bond at 1746 cm^{-1} (Figure 3.1B) in the 16-CTC spectrum as opposed to the two peaks at 1743 and 1720 cm^{-1}, which are from the non-hydrogen-bonded and hydrogen-bonded –C=O stretches of –COOH groups, respectively, in the MHA SAM.[26,27]

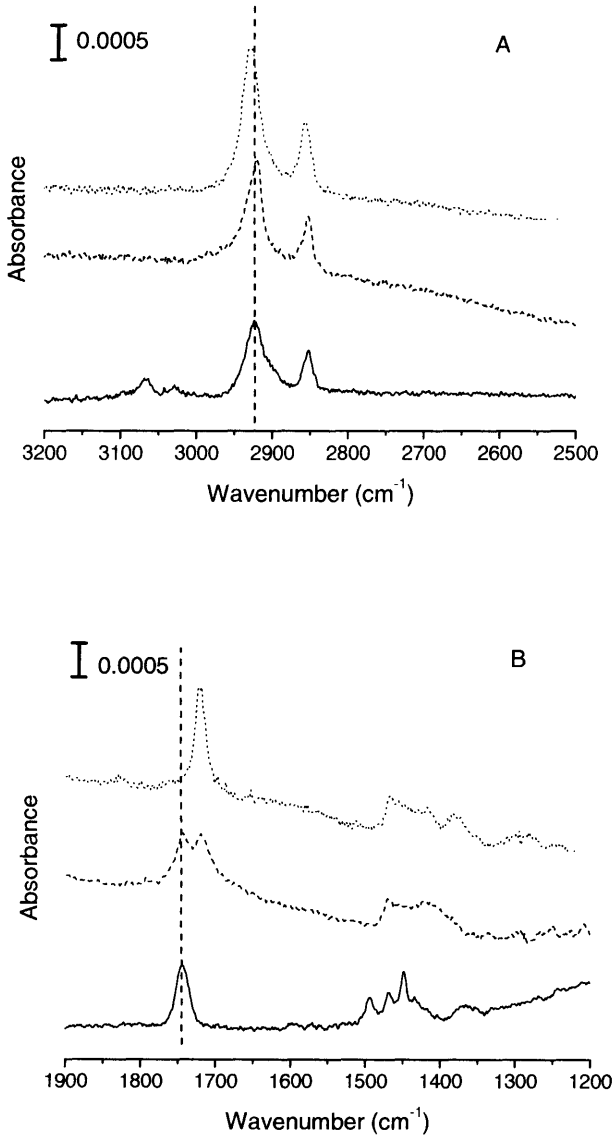

Figure 3.1. FT-IR spectra of 16-CTC (solid line), MHA (dashed line), and cleaved 16-CTC (dotted line) in high (A) and low (B) frequency regions. Vertical lines at 2924 cm^{-1} (A) and 1720 cm^{-1} (B) are included to aid spectral comparison.

Table 3.1. Composition results obtained from XPS.

Sample	C	O	S	Cl
16-CTC	92.42	4.44	1.35	1.79
theoretical[a]	*89.74*	*5.13*	*2.56*	*2.56*
16-CTC cleaved	86.63	9.24	4.13	0.00
MHA	87.47	10.43	2.18	0.00
theoretical[a]	*84.21*	*10.53*	*5.26*	*0.00*
16-CTC cleaved + butanethiol	88.24	8.21	3.55	0.00
butanethiol	94.46	2.41	3.13	0.00

[a]Theoretical values represent simple atomic percentages, ignoring attenuation of electron signal through the SAM.

The 16-CTC SAM was subjected to compositional analysis using XPS, a sensitive technique in determining the relative atomic composition, the substrate attachment chemistry,[28-30] and the local chemical environment in the SAM. Table 1 displays the XPS compositional results for the monolayers. There was good correlation between the theoretical and calculated atomic composition of the 16-CTC SAM. The difference may be due to the attenuation of the sulfur and chlorine signal by the bulky aromatic rings. The sulfur seems to be more screened than chlorine as is expected from its increased attenuation by the alkyl chain.

The presence of defects in the monolayer was investigated by cyclic voltammetry with a redox active probe, ferri/ferrocyanide ($Fe(CN)_6^{3-/4-}$). The ability of a SAM to block electron transfer between the gold electrode and an electroactive probe in solution is a very useful tool to measure the nature and extent of structural defects in SAMs.[31] For a densely packed monolayer prepared by using alkanethiols on gold electrodes, there is minimal charge transfer that occurs between the redox couple and the metal surface, giving rise to a very small current in cyclic voltammetry.[25] However, if there are any defects such as pinholes or gross defects, an increase in current will be recorded. Cyclic

voltammograms for the 16-CTC monolayer (solid line) as compared to a dense layer of MHA (dashed line) are shown in Figure 3.2. The 16-CTC monolayer was very effective at preventing charge transfer between the Au and the $Fe(CN)_6^{3-/4-}$ redox active probe. The 16-CTC monolayer actually performed slightly better at inhibiting charge transfer than the MHA sample at comparable incubation time, perhaps due to the ability of the aromatic group to prevent the penetration of the bulky $Fe(CN)_6^{3-/4-}$ species into the monolayer. This result combined with FT-IR results shows that although the 16-CTC monolayer is not densely packed with respect to the methylene chains, it is effective at blocking electrochemical reactions at the Au surface.

These characterization methods demonstrate that a monolayer of 16-CTC molecules is uniformly adsorbed with no gross defects. FT-IR, ellipsometry, and XPS results support the presence of aromatic rings and chlorine group as found in the CTC headgroup, and demonstrate that the monolayer is of low density with respect to the methylene chains and is densely packed with respect to the space-filling end-groups.

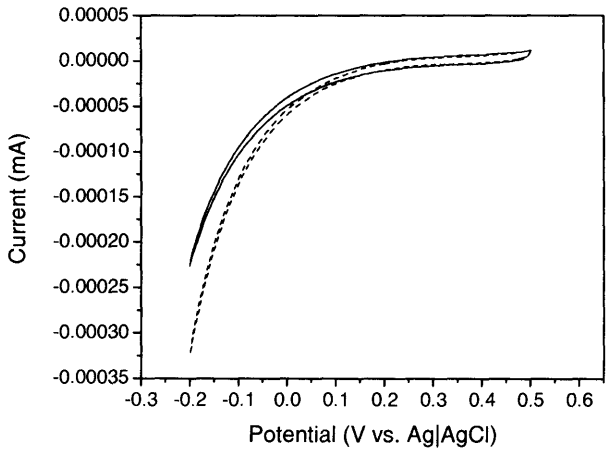

Figure 3.2. Cyclic voltammograms of $Fe(CN)_6^{3-/4-}$ redox couple at 16-CTC (solid line) and dense MHA (dashed line) SAMs on gold at a scan rate of 50 mV/s.

3.3.2. Formation of low-density monolayers (Step 2)

Formation of low-density monolayers. After cleavage of the CTC head group, water contact angles of the 16-CTC SAM decreased to 55 ± 3° (static), 80 ± 5° (advancing) and 52 ± 5° (receding), with the difference between advancing and receding angle (hysteresis) of approximately 28°. These values are ~20° lower than that for the 16-CTC monolayer but are substantially higher than for a dense MHA layer where the contact angle was 10° (static) and hysteresis was less than 10°. This difference between cleaved 16-CTC and dense MHA is attributed to the low-density monolayer exhibiting a mixture of hydrophilic acid groups and hydrophobic carbon chains at the interface, giving rise to a chemically heterogeneous surface. This idea is supported by molecular modeling and FT-IR characterization performed in our lab, which showed that the low-density monolayer consisted of molecules that were in relatively random and disordered conformation, exposing both the hydrophilic acid group as well as the hydrophobic methylene backbone in air.[21] In addition, the spacing between molecules would not allow for dense and ordered packing of molecules since strong chain-chain interactions are prevented. A heterogeneous system in the SAM is formed when a water droplet from the contact angle goniometer contacts the low-density SAM. This system consists of a low-energy area (area exposed to air) and a high-energy area (area exposed to water), following Neumann and Good's wettability model.[32] Here, the assumption of a chemical discontinuity along the solid/air/liquid contact line best explains the large hysteresis. The significantly reduced receding contact angle observed signifies molecular transitions at the high-energy area due to the molecular rearrangement of MHA molecules upon exposure to water. This molecular rearrangement involves the MHA molecules straightening from a random conformation to expose their hydrophilic carboxylic acid group to the water

surface, reducing the receding contact angle and leading to a large hysteresis. Langmuir suggested a similar phenomenon where the contact angle hysteresis of water on monolayer surfaces was due to the flipping of surfactant molecules on becoming exposed to water, rendering the surfaces hydrophilic and reducing the receding angle.[33] This is especially true for cases where water can penetrate into the adsorbed layer and drastically change its structure and dynamics.[34] In the case of cleaved 16-CTC, the monolayer is a low-density one, where water can easily penetrate and "pull out" the hydrophilic groups, especially when the monolayer surface has already been exposed to the liquid, as in the case of the receding contact angle.

The ellipsometric thickness of the low-density monolayer was 11 ± 1 Å. This value was significantly lower than the thickness of a dense 16-CTC monolayer (23 ± 2 Å). If the 16-CTC molecule was to just lose the CTC head group and retained a somewhat extended conformation, the thickness would be that of an MHA monolayer, around 19 Å. Cleavage of the headgroup alone would not lead to such a huge change in ellipsometric thickness since its size is likely around 3–5 Å as discussed above. However, the fact that the thickness of the cleaved 16-CTC SAM was so much lower is indirect evidence that the monolayer collapsed upon removal of the supporting CTC head groups. For the purpose of control, the HDT and MHA monolayers were also subjected to cleavage conditions. However, there were no detectable changes in thickness or contact angle upon exposure to TFA.

FT-IR was employed to further characterize the low-density monolayer. Figure 3.1 shows the FT-IR spectrum of cleaved 16-CTC (dotted line). As expected, the FT-IR spectra display the general features of a highly disordered SAM, such as the red shift of the methylene bands to 2929 and 2856 cm^{-1}. The removal of the bulky headgroups shifts

the 16-CTC monolayer from a moderately disordered state to a highly disordered state ($\upsilon_a^{CH_2}$ mode shifts from 2924 to 2929 cm^{-1}). The ester peak at 1746 cm^{-1} disappeared (see solid line in Fig. 1B) and was replaced by the C=O peak at 1720 cm^{-1}. Complete cleavage is also demonstrated by the loss of the aromatic C-H (3030 and 3071 cm^{-1}) and C=C (1448, 1468, and 1495 cm^{-1}) stretches. The CH_2 scissor mode near 1469 cm^{-1} [35] is now evident after the removal of the C=C modes between 1400 and 1500 cm^{-1} in the spectrum for 16-CTC.

XPS further supports the removal of the CTC headgroup evident by the loss of chlorine signal in the low-density SAM (Table 1). Furthermore, the carbon to oxygen ratio of the low-density monolayer is very similar to that of a dense MHA SAM. The lack of chlorine signal and the reduction in the C:O ratio indicate that the bulky aromatic group was removed upon cleavage. Although the sulfur (S) signal is still reduced relative to its theoretical value based on elemental composition, the sulfur content is substantially higher than that observed with MHA. This increase in sulfur signal relative to MHA is likely due to the low density of the molecules in the cleaved monolayer, which reduces the extent of attenuation in XPS.

The most dramatic change in the monolayer's property was observed in cyclic voltammetry. Figure 3.3 shows the cyclic voltammogram for the low-density monolayer (solid line) as compared to that of bare gold (dashed line) and dense MHA SAM (dotted line). There is a large difference between the spectra for the 16-CTC monolayer and the low-density analog, which exhibited the redox peaks similar to bare gold. Since the molecules in the low-density monolayer are widely spaced apart, the inhibition of the electron transfer from the gold electrode to the redox active species $Fe(CN)_6^{3-/4-}$ is reduced, resulting in a cyclic voltammogram similar to that of bare gold. However, there is a

slight difference in the peak-to-peak separation between that of the bare gold (77.4 mV) and the low-density monolayer (84.9 mV). Although this difference is not large, it may indicate some slight barrier to redox reaction from the presence of the low-density SAM. Evidence of similar behavior has been seen with short chain alkanethiol systems.[36,37]

These results indicate that the CTC headgroups have been removed. The resulting monolayer is composed of loosely-packed, highly disordered MHA molecules on the Au surface as demonstrated by FT-IR and electrochemical analysis.

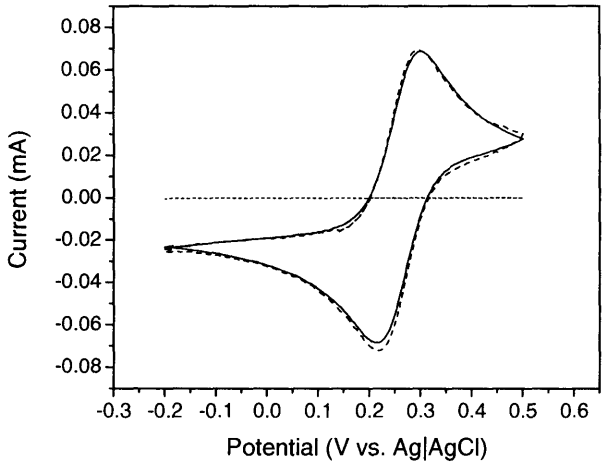

Figure 3.3. Cyclic voltammograms of $Fe(CN)_6^{3-/4-}$ redox couple at a cleaved 16-CTC SAM (solid line), bare gold (dashed line), and high density MHA SAM (dotted line) on gold at a scan rate of 50 mV/s.

3.3.3. Formation of mixed monolayers (Step 3)

Mixed monolayers formed from incubating the low-density SAM with *n*-butanethiol were characterized with contact angle measurements. The static, advancing, and receding contact angles for the mixed monolayers were: 58 ± 5°, 84 ± 5°, and 57 ± 5° respectively. Large contact angle hysteresis was observed, which is attributable to the molecular heterogeneity. We can use the Israelachvili equation to assess the different group contributions to the wettability where the chemical heterogeneity is not in the form of discrete patches but is of atomic or molecular dimensions:[38-40]

$$(1+\cos\theta)^2 = f_1(1+\cos\theta_1)^2 + f_2(1+\cos\theta_2)^2 \quad (1)$$

$$f_1 + f_2 = 1 \quad (2)$$

where θ_1, and θ_2 are the advancing contact angles of the pure homogeneous surfaces of 1 and 2 respectively, and θ is the contact angle of the mixed surface containing components 1 and 2. This equation was used to calculate the molecular ratio of the two components in the mixture.

The contact angle measured experimentally for the mixed monolayer system (θ = 84°) and the values for the pure MHA (θ_1 = 10°) and pure *n*-butanethiol (θ_2 = 110°) monolayers were used in eq. (1) and (2) to determine the mole fraction of MHA (f_1) and *n*-butanethiol (f_2). Solving these equations resulted in values of 0.78 and 0.22 for *n*-butanethiol and MHA respectively. These value correspond to a deposition of 3.4 *n*-butanethiol molecules for every MHA molecule in the low-density monolayer. This method of calculation is a first-order approximation. For more rigor, the specific intermolecular forces appropriate to a particular system would probably need to be considered.[38] The molecular rearrangements of the headgroup should also be considered. Also, this system is for a

dense SAM, whereas our system is at least moderately disordered. Previous study has shown that monolayer surfaces containing a high concentration of OH groups on a mobile organic chain is not stable over time, and that the OH groups could stabilize by reorganization and adsorption of contaminants.[41] Hence, there may be an increase in contact angle associated with a similar rearrangement of the –COOH headgroups in the low-density monolayer to minimize surface energy.

The thickness of the monolayers measured by ellipsometry remained relatively unchanged at about 11 ± 2 Å after exposure of the low-density SAM to *n*-butanethiol. This is expected since the *n*-butanethiol molecules are only 2–3 Å in length and will not be sufficiently long to cause a change in thickness of the overall low-density monolayer.

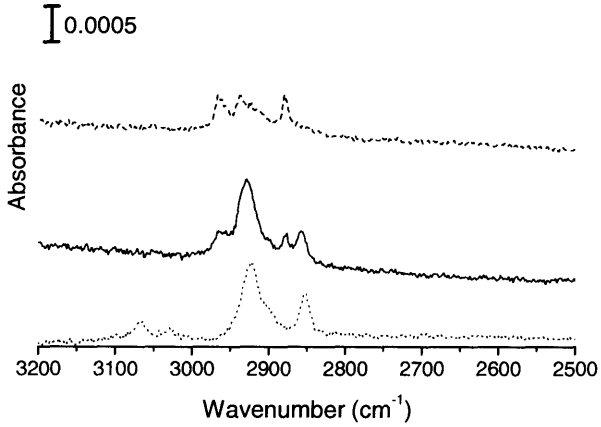

Figure 3.4. FT-IR spectra of 16-CTC after cleavage and backfill with *n*-butanethiol (solid line) and *n*-butanethiol (dashed line). The spectrum for MHA (dotted line) is also shown for comparison.

Figure 3.4 shows the FT-IR spectra of the low-density monolayer backfilled with *n*-butanethiol (solid line) and pure *n*-butanethiol (dashed line). The pure *n*-butanethiol SAM has peaks at 2879 cm^{-1}, 2924 cm^{-1}, 2936 cm^{-1}, and 2966 cm^{-1}. These bands correspond to the symmetric CH_3, asymmetric CH_2, symmetric CH_3, and asymmetric, in-plane CH_3 vibrations, respectively, based on standard assignments.[29] The mixed monolayer spectrum (Figure 3.4, solid line) continue to be dominated by the asymmetric and symmetric CH_2 vibrations at ~2930 cm^{-1} and 2859 cm^{-1}, respectively. The broadened peak at 2930 cm^{-1} is most likely due to the combined CH_2 vibrations from the MHA and the *n*-butanethiol and indicates a still highly disordered SAM. This is due to the fact that *n*-butanethiol SAM itself is highly disordered, and backfilling of the *n*-butanethiol for a short time into a disordered, low-density MHA system will not improve ordering in the mixed SAM.[42] However, two new bands were observed at 2967 cm^{-1} and 2876 cm^{-1}. These bands likely correspond to the symmetric and asymmetric, in-plane CH_3 modes as described for *n*-butanethiol above. The final CH_3 mode at 2936 cm^{-1} is likely obscured by the intense $\upsilon_a^{CH_2}$ mode at ~2930 cm^{-1}. The presence of the CH_3 bands after exposure to *n*-butanethiol is further evidence of the inclusion of the molecule into the low-density MHA monolayer.

Table 1 shows compositional results from XPS characterization of the low-density monolayer backfilled with *n*-butanethiol as compared to a pure *n*-butanethiol SAM. After exposure of the low-density SAM to *n*-butanethiol, several changes in composition were apparent. The carbon content increased while the oxygen and sulfur content decreased. All these changes were consistent with the values expected from inclusion of *n*-butanethiol into the monolayer based on XPS results from the pure *n*-butanethiol system.

Figure 3.5 shows the CV of the mixed SAM of MHA and *n*-butanethiol (solid line) and that for dense *n*-butanethiol SAM (dashed line). Exposure of the low-density MHA monolayer to *n*-butanethiol has greatly reduced the current from that seen with the low-density monolayer itself (Figure 3.3, solid line). The current is also substantially lower than that observed for the pure *n*-butanethiol SAM (Figure 3.5, dashed line). The lower current for the mixed monolayer is likely the result of the combined effects of short-chain *n*-butanethiol with the low-density MHA monolayer. Although the same degree of passivation as the initial 16-CTC monolayer was not achieved (see Figure 3.2, solid line), the voltammetric signature of the mixed SAM indicates that no significant gross defects or pinhole defects exist in the monolayer. This extent of passivation by the mixed SAM system indicates a well-formed system despite the geometric constraints of the backfilling process.

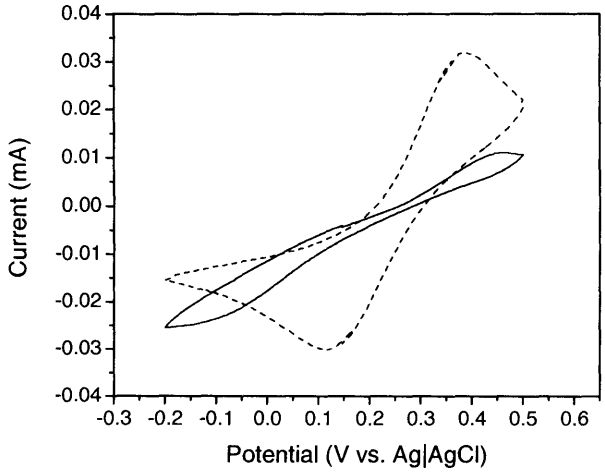

Figure 3.5.Cyclic voltammograms of $Fe(CN)_6^{3-/4-}$ redox couple at a 16-CTC SAM after cleavage and backfilling with *n*-butanethiol (solid line) compared with voltammograms for a dense *n*-butanethiol (dashed line) SAM.

Electrochemical desorption. Previous studies have shown that if mixed monolayers are constructed from a solution of mixed thiols, separate single component domains likely form.[2,14-16] Upon electrochemical desorption, the voltammetry shows two peaks, one at the characteristic desorption voltage of each of the respective single component monolayers. However, if a uniformly mixed monolayer with domain size less than 15 nm^2 is formed, a shift in the peaks will occur so that the mixed monolayer will show a single peak between that of the two original components.[2,11] This method will elucidate whether the single component domains exist in a low-density monolayer backfilled with shorter chain alkanethiols.

Electrochemical desorption experiments were conducted using the low-density monolayer backfilled with *n*-butanethiol. Figure 3.6 shows the reductive desorption results from the low-density backfilled monolayer (solid line) and the MHA/*n*-butanethiol mixture (dashed line) formed from the adsorption method outlined in the experimental section. As the desorption potential is dependent on chain length, a longer alkanethiol is desorbed at a more negative potential. With the MHA/*n*-butanethiol system, *n*-butanethiol desorbs first at –0.85 V followed by MHA at –1.01 V. These values match those seen for single component SAM of *n*-butanethiol and MHA (Figure 3.3.7). Previously researchers have attributed the presence of two peaks to the existence of phase-segregated domains over 15 nm^2.[2,14-16] For the mixed SAM formed from the low-density MHA backfilled by *n*-butanethiol, a single desorption peak was detected (solid line in Fig. 5). There is a small shoulder appearing at the most negative potential for the MHA/*n*-butanethiol sample. The origin of this subwave is unclear but it is probably due to the heterogeneity in the crystallinity of the substrate surface[43-46] and in the packing of thiol molecules.[47,48] We have observed this phenomenon in other SAM surfaces used in

electrochemical desorption such as that of *n*-butanethiol. We concluded from this experiment that preparation of a SAM following the above-mentioned strategy resulted in a homogeneously distributed monolayer and not in a phase-segregated system. These results support the assumption that the low-density SAM consists of molecules that show increased spacing between individual molecules; the formation of MHA clusters is less likely.

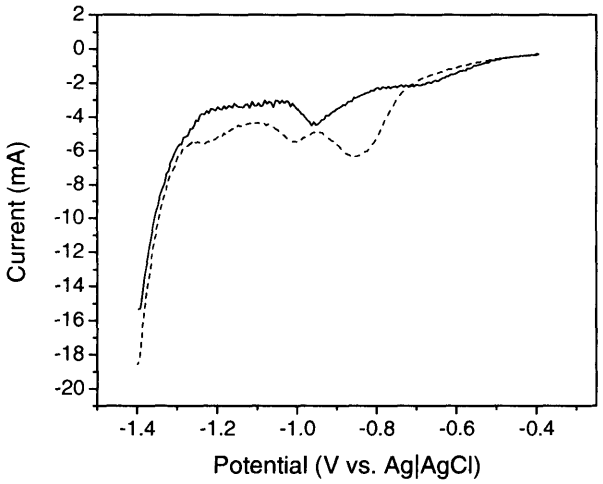

Figure 3.6. Reductive desorption of low density MHA backfilled with *n*-butanethiol (solid line) and MHA:*n*-butanethiol formed as outlined in the experimental section. Both voltammograms were recorded in a 0.1 M KOH solution with a scan rate of 50 mV/s.

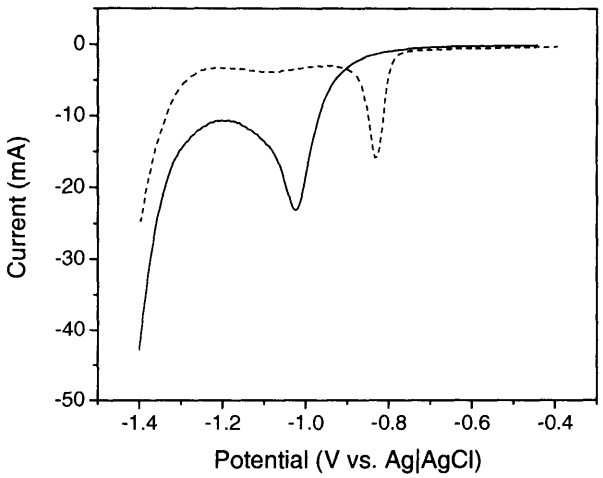

Figure 3.7. Reductive desportion voltammetry of pure MHA (solid line) and pure *n*-butanethiol (dashed line) monolayers.

3.4. Conclusions

A novel method involving use of a synthetic chemical route to form low-density and homogeneously mixed monolayers was reported here. The route is via synthesis of a precursor molecule, 16-CTC, which contains a bulky head group, and subsequent assembly of these molecules on gold surfaces. Characterization of the monolayer showed dense packing with respect to the space filling CTC group and low-dense packing with respect to the alkane chains. Upon cleavage of the ester bond, the monolayer collapsed to a highly disordered state, which resembled a low-density SAM of MHA molecules. This low-density monolayer had vacant Au sites that could be occupied by molecules such as *n*-butanethiol via backfilling. Homogeneity of this mixed monolayer was demonstrated via electrochemical desorption, where a single peak was observed as opposed to two peaks arising from phase separation.

This is a new concept where molecular and structural control of the monolayer's architecture was achieved via a synthetic method. The ability to modulate the microenvironment around a single adsorbed molecule gives flexibility in controlling charge transfer mechanism, in studying single molecule array of devices, and in providing a designer's platform for building well-ordered surface chemical and biological functionalities such as proteins, nucleic acid, or small organic molecules. This method also gives considerable flexibility in allowing for the formation of homogenously mixed SAM of molecules that would normally phase-separate and can also serve as a useful model system to explore interfacial phenomena. Good control over composition at a molecular level is achieved, together with the possibility that adjustment of the size of the headgroup would also give some degree of lateral control in constructing mixed monolayers. By varying the size of the globular end group and also changing the type of the backfilling thiol the composition and also the ratio of the different molecules in the mixed SAM can be altered. Supramolecular chemistry can be done on the monolayer in which DNA, proteins, other molecules can be attached, spaced apart on the surface at a reduced density. Further study is underway for use of this platform in oligonucleotide array application.

3.5. References and Notes

1. Shon, Y.-S., Lee, S., Colorado, R., Jr., Perry, S. S. & Lee, T. R. Spiroalkanedithiol-Based SAMs Reveal Unique Insight into the Wettabilities and Frictional Properties of Organic Thin Films. *Journal of the American Chemical Society* **122**, 7556-7563 (2000).

2. Shimazu, K., Kawaguchi, T. & Isomura, T. Construction of Mixed Mercaptopropionic Acid/Alkanethiol Monolayers of Controlled Composition by Structural Control of a Gold Substrate with Underpotentially Deposited Lead Atoms. *Journal of the American Chemical Society* **124**, 652-661 (2002).

3. Lopez, G. P. et al. Convenient methods for patterning the adhesion of mammalian cells to surfaces using self-assembled monolayers of alkanethiolates on gold. *J. Am. Chem. Soc.* **115**, 5877-8 (1993).

4. Abbott, N. L., Gorman, C. B. & Whitesides, G. M. Active Control of Wetting Using Applied Electrical Potentials and Self- Assembled Monolayers. *Langmuir* **11**, 16-18 (1995).

3. Bain, C. D. & Whitesides, G. M. Correlations between wettability and structure in monolayers of alkanethiols adsorbed on gold. *Journal of the American Chemical Society* **110**, 3665-6 (1988).

6. Bain, C. D. & Whitesides, G. M. Formation of two-component surfaces by the spontaneous assembly of monolayers on gold from solutions containing mixtures of organic thiols. *Journal of the American Chemical Society* **110**, 6560-1 (1988).

7. Bain, C. D. & Whitesides, G. M. Formation of monolayers by the coadsorption of thiols on gold: variation in the length of the alkyl chain. *Journal of the American Chemical Society* **111**, 7164-7175 (1989).

8. Folkers, J. P., Laibinis, P. E. & Whitesides, G. M. Self-assembled monolayers of alkanethiols on gold: comparisons of monolayers containing mixtures of short- and long-chain constituents with methyl and hydroxymethyl terminal groups. *Langmuir* **8**, 1330-41 (1992).

9. Whitesides, G. M. & Laibinis, P. E. Wet chemical approaches to the characterization of organic surfaces: self-assembled monolayers, wetting and the physical-organic chemistry of the solid-liquid interface. *Langmuir* **6**, 87-96 (1990).

10. Yang, Z., Engquist, I., Liedberg, B. & Kauffmann, J.-M. Electrochemical characterization of mixed monolayer assemblies of thiol analogs of cholesterol and fatty acids on gold. *Journal of Electroanalytical Chemistry* **430**, 189-195 (1997).

11. Hobara, D., Ota, M., Imabayashi, S.-i., Niki, K. & Kakiuchi, T. Phase separation of binary self-assembled thiol monolayers composed of 1-hexadecanethiol and 3-mercaptopropionic acid on Au(111) studied by scanning tunneling microscopy and cyclic voltammetry. *Journal of Electroanalytical Chemistry* **444**, 113-119 (1998).

12. Kang, J. F., Liao, S., Jordan, R. & Ulman, A. Mixed Self-assembled Monolayers of Rigid Biphenyl Thiols: Impact of Solvent and Dipole Moment. *Journal of the American Chemical Society* **120**, 9662-9667 (1998).

13. Ma, F. & Lennox, R. B. Potential-Assisted Deposition of Alkanethiols on Au: Controlled Preparation of Single- and Mixed-Component SAMs. *Langmuir* **16**, 6188-6190 (2000).

14. Nishizawa, M., Sunagawa, T. & Yoneyama, H. Selective desorption of 3-mercaptopropionic acid from a mixed monolayer with hexadecanethiol assembled on a gold electrode. *Journal of Electroanalytical Chemistry* **436**, 213-218 (1997).

13. Hobara, D., Sasaki, T., Imabayashi, S.-i. & Kakiuchi, T. Surface Structure of Binary Self-Assembled Monolayers Formed by Electrochemical Selective Replacement of Adsorbed Thiols. *Langmuir* **15**, 5073-5078 (1999).

16. Imabayashi, S.-i., Hobara, D., Kakiuchi, T. & Knoll, W. Selective Replacement of Adsorbed Alkanethiols in Phase-Separated Binary Self-Assembled Monolayers by Electrochemical Partial Desorption. *Langmuir* **13**, 4502-4504 (1997).

17. Stranick, S. J., Parikh, A. N., Tao, Y. T., Allara, D. L. & Weiss, P. S. Phase Separation of Mixed-Composition Self-Assembled Monolayers into Nanometer Scale Molecular Domains. *J. Phys. Chem.* **98**, 7636-46 (1994).

18. Biebuyck, H. A. & Whitesides, G. M. Interchange between monolayers on gold formed from unsymmetrical disulfides and solutions of thiols: evidence for sulfur-sulfur bond cleavage by gold metal. *Langmuir* **9**, 1766-70 (1993).

19. Troughton, E. B. et al. Monolayer films prepared by the spontaneous self-assembly of symmetrical and unsymmetrical dialkyl sulfides from solution onto gold substrates: structure, properties, and reactivity of constituent functional groups. *Langmuir* **4**, 365-85 (1988).

20. Shon, Y.-S., Lee, S., Perry, S. S. & Lee, T. R. The adsorption of unsymmetrical spiroalkanedithiols onto gold affords multi-component interfaces that are homogeneously mixed at the molecular level. *Journal of the American Chemical Society* **122**, 1278-1281 (2000).

21. Lahann, J.; Mitragotri, S.; Tran, T.-N.; Kaido, H.; Sundaram, J.; Choi, I. S.; Hoffer, S.; Somorjai, G. A.; Langer, R. A Reversibly Switching Surface. *Science (Washington, DC, United States)* **299**, 371-374 (2003).

22. Ulman. *Introduction to ultrathin organic films - from Langmuir-Blodgett to self-assembly* (Academic Press, Boston, 1991).

23. This approach was used to create a mixed SAM of MHA and *n*-butanethiol due to the fact that MHA and MPA are known to produce phase separated domains on co-adsorption. It was difficult to obtain phase-separated SAM of MHA and *n*-butanethiol directly via co-adsorption, probably due to the difference in adsorption kinetics. This method of selective electrochemical desorption of one component and backfilling with another has been used to obtain multiple component SAMs of varying compositions.[12,16] One of the advantages of this method is that the same domain size of the original co-adsorbed component can be preserved, and only domain sizes exceeding 15 nm^2 produced two desorption

waves.[12] Hence, homogeneously mixed monolayers with domain size of <15 nm^2 will not produce two waves on electrochemical desorption, and instead will show a single peak between that of the original two components.[2]

24. Frutos, A. G., Brockman, J. M. & Corn, R. M. Reversible Protection and Reactive Patterning of Amine- and Hydroxyl-Terminated Self-Assembled Monolayers on Gold Surfaces for the Fabrication of Biopolymer Arrays. *Langmuir* **16**, 2192-2197 (2000).

23. Porter, M. D., Bright, T. B., Allara, D. L. & Chidsey, C. E. D. Spontaneously Organized Molecular Assemblies. 4. Structural Characterization of n-Alkyl Thiol Monolayers on Gold by Optical Ellipsometry, Infrared Spectroscopy, and Electrochemistry. *Journal of the American Chemical Society* **109**, 3559 (1987).

26. Yan, L., Marzolin, C., Terfort, A. & Whitesides, G. M. Formation and Reaction of Interchain Carboxylic Anhydride Groups on Self-Assembled Monolayers on Gold. *Langmuir* **13**, 6704-6712 (1997).

27. Chapman, R. G., Ostuni, E., Yan, L. & Whitesides, G. M. Preparation of Mixed Self-Assembled Monolayers (SAMs) That Resist Adsorption of Proteins Using the Reaction of Amines with a SAM That Presents Interchain Carboxylic Anhydride Groups. *Langmuir* **16**, 6927-6936 (2000).

28. Hutt, D. A. & Leggett, G. J. Influence of Adsorbate Ordering on Rates of UV Photooxidation of Self-Assembled Monolayers. *Journal of Physical Chemistry* **100**, 6657-62 (1996).

29. Laibinis, P. E. et al. Comparison of the structures and wetting properties of self-assembled monolayers of n-alkanethiols on the coinage metal surfaces, copper, silver, and gold. *Journal of the American Chemical Society* **113**, 7152-67 (1991).

30. Castner, D. G., Hinds, K. & Grainger, D. W. X-ray Photoelectron Spectroscopy Sulfur 2p Study of Organic Thiol and Disulfide Binding Interactions with Gold Surfaces. *Langmuir* **12**, 5083-5086 (1996).

31. Yang, Z. et al. Preparation and Characterization of Mixed Monolayer Assemblies Composed of Thiol Analogs of Cholesterol and Fatty Acid. *Langmuir* **13**, 3210-3218 (1997).

32. Neumann, A. W. & Good, R. J. Thermodynamics of contact angles. I. Heterogeneous solid surfaces. *Journal of Colloid and Interface Science* **38**, 341-58 (1972).

33. Langmuir, I. Overturning and anchoring of monolayers. *Science* **87**, 493-500 (1938).

34. Chen, Y. L., Helm, C. A. & Israelachvili, J. N. Molecular mechanisms associated with adhesion and contact angle hysteresis of monolayer surfaces. *Journal of Physical Chemistry* **95**, 10736-47 (1991).

33. Yang, Z. P., Engquist, I., Kauffmann, J. M. & Liedberg, B. Thiocholesterol on Gold: A Nanoporous Molecular Assembly. *Langmuir* **12**, 1704-7 (1996).

36. Sato, Y. & Mizutani, F. Determination of real composition of 3-mercaptopropionic acid and 1-octadecanethiol mixed self-assembled monolayers

by using electrochemical and electrochemical quartz crystal microbalance measurements. *Electroanalysis* **10**, 633-637 (1998).

37. Miller, C., Cuendet, P. & Graetzel, M. Adsorbed w-hydroxy thiol monolayers on gold electrodes: evidence for electron tunneling to redox species in solution. *Journal of Physical Chemistry* **95**, 877-86 (1991).

38. Israelachvili, J. N. & Gee, M. L. Contact angles on chemically heterogeneous surfaces. *Langmuir* **5**, 288-9 (1989).

39. Fadeev, A. Y. & McCarthy, T. J. Trialkylsilane monolayers covalently attached to silicon surfaces: wettability studies indicating that molecular topography contributes to contact angle hysteresis. *Langmuir* **15**, 3759-3766 (1999).

40. Ulman, A. et al. Concentration-driven surface transition in the wetting of mixed alkanethiol monolayers on gold. *Journal of the American Chemical Society* **113**, 1499-506 (1991).

41. Evans, S. D., Sharma, R. & Ulman, A. Contact angle stability: Reorganization of monolayer surfaces? *Langmuir* **7**, 156-61 (1991).

42. This is expected due to the nature of thiol formation on gold surface. The thiols are believed to attach primarily to the threefold hollow sites of the gold surface, losing the proton in the process and forming the $(\sqrt{3} \times \sqrt{3})R30°$ overlayer structure. The distance between adsorption sites in this geometry is 5.0 Å, resulting in an available area for each molecule of 21.4 $Å^2$. Since the van der Waals diameter of the methylene chain is somewhat too small (4.6 Å) for the

chain to completely occupy that area, the chains will tilt towards the surface, forming an angle of approximately 30° with the surface normal for high density SAMs.[49-51] For low-density SAMs, such a tilt is not expected since the molecules have much more room (about 67 $Å^2$ per molecule) to move in, and hence exist in a random conformation. However, with the relatively rapid adsorption time, the *n*-butanethiol molecules will not have time to reorganize or pack densely. There are also steric limits as to what space they can fill into. According to previous studies[21], the space filling end group of CTC is about 67 $Å^2$, which allows for perhaps two or three octanethiol molecules to fill the empty molecular lattices. These geometric and steric constraints prevent complete coverage of the gold surface.

43. Widrig, C. A., Chung, C. & Porter, M. D. The electrochemical desorption of n-alkanethiol monolayers from polycrystalline gold and silver electrodes. *J. Electroanal. Chem. Interfacial Electrochem.* **310**, 335-59 (1991).

44. Walczak, M. M. et al. Reductive desorption of alkanethiolate monolayers at gold: a measure of surface coverage. *Langmuir* **7**, 2687-93 (1991).

43. Weisshaar, D. E., Lamp, B. D. & Porter, M. D. Thermodynamically controlled electrochemical formation of thiolate monolayers at gold: characterization and comparison to self-assembled analogs. *J. Am. Chem. Soc.* **114**, 5860-2 (1992).

46. Zhong, C.-J. & Porter, M. D. Fine structure in the voltammetric desorption curves of alkanethiolate monolayers chemisorbed at gold. *J. Electroanal. Chem.* **425**, 147-153 (1997).

47. Yang, D. F., Wilde, C. P. & Morin, M. Electrochemical Desorption and Adsorption of Nonyl Mercaptan at Gold Single Crystal Electrode Surfaces. *Langmuir* **12**, 6570-6577 (1996).

48. Yang, D. F., Wilde, C. P. & Morin, M. Studies of the Electrochemical Removal and Efficient Re-formation of a Monolayer of Hexadecanethiol Self-Assembled at an Au(111) Single Crystal in Aqueous Solutions. *Langmuir* **13**, 243-249 (1997).

49. Alves, C. A., Smith, E. L. & Porter, M. D. Atomic scale imaging of alkanethiolate monolayers at gold surfaces with atomic force microscopy. *J. Am. Chem. Soc.* **114**, 1222-7 (1992).

50. Chidsey, C. E. D., Liu, G. Y., Rowntree, P. & Scoles, G. Molecular order at the surface of an organic monolayer studied by low energy helium diffraction. *Journal of Chemical Physics* **91**, 4421-3 (1989).

51. Ulman, A. Formation and structure of self-assembled monolayers. *Chem. Rev.* **96**, 1533-1554 (1996).

CHAPTER FOUR

DESIGN OF OLIGONUCLEOTIDE ARRAYS USING HOMOGENEOUSLY MIXED SELF-ASSEMBLED MONOLAYERS

4.1. Introduction

The genomic revolution has created more demand for developing surface-based biosensors such as DNA hybridization biosensors for gene mapping, DNA sequencing, clinical diagnosis of genetic diseases, detection of infectious organisms and analysis of DNA-ligand interactions.[1-5] Heterogeneous hybridization of DNA from free solution on to an oligonucleotide microarrays (DNA chips or biosensors) has potential to become one of the most promising techniques in molecular biology and genomic analysis.[6] The inherent specificity in DNA base pairing, the sensitivity associated with various analytical detection schemes, and declining cost of sensor fabrication have made the development of DNA biosensors attractive.[7-10] The main research effort in the DNA sensor design has been focused on several issues, including the development of methods for the controlled immobilization of the oligonucleotides, the optimization of the ligand or hybridization efficiencies, and the introduction of sensitive techniques for signal detection and analysis.[11] Development of DNA biosensor often involved the tethering of DNA probes to a self-assembled monolayer (SAM) composed of functionalized alkanethiolates on gold.[6,11-22] These DNA microarrays can be used as a foundation for constructing nanostructured materials via self-assembly, where the spatial distribution of the DNA at the surface is critical to achieve stability at the interface.[23] Optimizing the surface density in the resulting DNA arrays permits a high hybridization efficiency to be achieved. Hybridization efficiencies are often tied to surface coverage, with densely tethered DNA probes providing lower hybridization efficiency due to increased steric hindrance and/or inappropriate oligo orientation for the complement hybridization.[11,15]

Many attempts have been done to improve DNA hybridization efficiencies, mostly involved in forming mixed SAM of the desired DNA-alkanethiol molecules and spacer molecules of "filler" alkanethiolates with varying amount of success.[11,12,24-31] Some studies, aimed at alleviating steric effects have used oligonucleotide spacers to move probes away from the surface and enhance hybridization.[32] Various other methods are also used where selective desorption of alkanethiols in mixed SAMs is employed for subsequent oligo attachment and DNA hybridization[33] to give improved DNA hybridization efficiency. Efforts at controlling surface probe density also involves varying the time of incubation of the thiolated probe, varying the solution ionic strength, and applying an attractive electrostatic field at the interface to assist in the immobilization of negatively-charged thiolated-DNA.[34] However, no controlled-design methods have been used to create a microarray of DNA SAM as often the mixed SAMs formed from coadsorption may phase separated, form small domains, and the ability to space apart functional group is very difficult in a controlled fashion with coadsorption.[11,35-38] We report a novel way to control DNA hybridization efficiency by tailoring the distance between functional groups in a mixed SAM using a new method for the formation of homogeneously-mixed SAM via a synthetic chemical method as outlined in Scheme 1.[39] Here, we used an assembly of precursor molecules containing a bulky endgroup that form a SAM that was densely packed with respect to the space-filling endgroup, but showed low-density packing with respect to the hydrophobic methylene chains (Step 1). These molecules were derived from 16-mercaptohexadecanoic acid (MHA). Cleavage of the endgroups gave a low density SAM, and backfilling this low-density layer with a second alkanethiol created a homogeneously-mixed SAM (Step

2-3). Using this method, we were able to space apart the functional group, this case – COOH, on the SAM surface.[39] This mixed SAM was then used as a platform for the attachment of oligonucleotides via the *N*-hydroxysulfosuccinimide (NHS)/1-(3-dimethylaminopropyl)-3-ethylcarbodiimide hydrochloride (EDC) reaction (Step 4). Subsequently, target oligonucleotides were introduced and the resulting DNA hybridization (Step 5) efficiency as compared to a surface composed of oligos attached to a dense layer of MHA SAM was determined via surface plasmon resonance (SPR) and quartz crystal microbalance with dissipation monitoring (QCM-D). SPR and QCM-D are surface-sensitive mass detection techniques that do not require added labeling. Using SPR, molecular interactions can be detected as changes to the refractive index over time, which is proportional to the mass of molecules bound to the surface and shown in sensorgram as resonance units (RU).[40,41] QCM is also a very sensitive mass-measuring device due to the changes in its resonance frequencies upon binding of molecules to the surface of QCM crystals, which can be detected at high sensitivity. In QCM-D, viscoelastic properties can also be detected, as the resonant frequency is not only sensitive to mass but also to viscosity, elasticity, surface roughness amongst other factors.[42,43]. These two techniques are complementary in the way that SPR allows for measurement of changes in the amount of mass absorbed to a surface, and QCM-D, while providing semi-quantitative mass changes, also provides additional information about both the structure of the immobilized nucleotides and the kinetics of the subsequent hybridization processes through energy dissipation monitoring.[43] The QCM-D technique measures simultaneously a change in mass via a change in resonant frequency f, and energy dissipation, D (cf. viscoelastic properties).[44] The magnitude of ΔD variations

provides information about viscoelastic properties, and determines if Δf can be directly converted to mass via the Sauerbrey equation (see subsequent discussion) or if modeling is required.[43]

Here, we used both SPR and QCM-D to measure the hybridization efficiency of oligos tethered to our homogeneously-mixed SAM vs. the dense MHA SAM. The use of short functionalized alkanethiol linkages has the added benefit of bringing the DNA closer to the QCM crystal surface, preventing large losses due to viscoelastic coupling and the resultant decrease in mass sensitivity.[45] This work represents a controlled method to improve hybridization efficiency via controlling the spatial distribution of oligos on the gold surface, and may lead to improvement in DNA arrays fabrication.

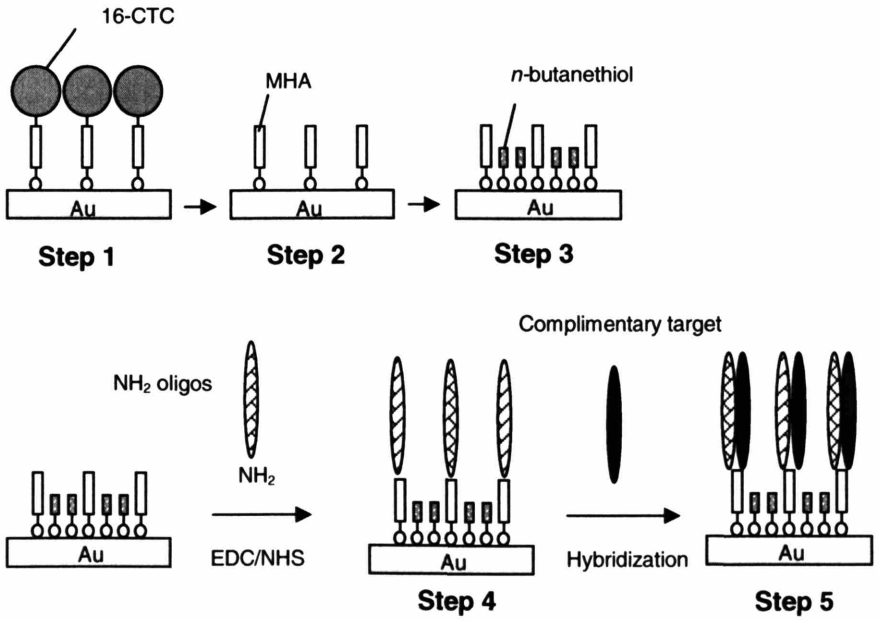

Scheme 4.1. Illustration of the formation of homogeneously-mixed (HM) SAM (steps 1-3) and the subsequent attachment of oligonucleotide probe via EDC/NHS reaction (step 4) and hybridization to a target sequence (step 5).

4.2. Surface Plasmon Resonance

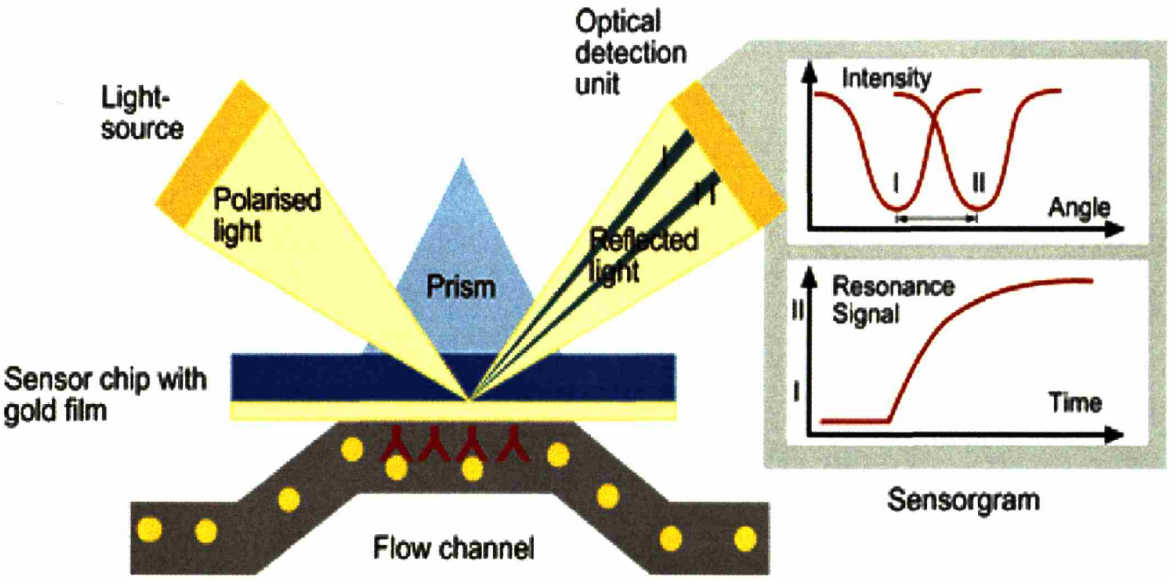

Scheme 4.2. The Biacore 2000: Operating principle.[a]

In the past decade, surface plasmon resonance (SPR) spectroscopy has become a powerful tool for *in situ* characterization of solid/liquid interfaces, and for studying the interactions of biological molecules with surfaces and has been widely used in recent years in biochemistry research to monitor events such as antibody-antigen binding,[46-48] DNA/RNA hybridization,[19,49-51] protein-DNA interactions,[28,52-58] and detection of conformational changes of immobilized proteins.[59,60] Surface plasmon resonance is a phenomenon which occurs when light is reflected off thin metal films. In SPR, a thin layer of metal film is placed between two media of different refractive indices. At the

[a] http://www.biacore.com

interface between these two transparent media (glass and water), light coming from the side of higher refractive index is totally reflected in a phenomenon called total internal reflection. However, there is an electromagnetic field component that penetrates a short distance into a medium of lower refractive index, creating an exponentially attenuating evanescent wave. If the interface is coated with a thin layer of metal, surface plamons (SPs) can be created when light energy from *p*-polarized incident photons is coupled into oscillating modes of free electron density present in the metal film. The SPs are evanescent waves that have their maximum intensity at the surface and decay exponentially away from the phase boundary to a penetration depth on the order of 200 nm.[24] When the wavevector for the photon and plasmon are equal in magnitude and direction, surface plasmons (SPs) or the collective oscillations of electrons at the boundary between conductors and insulators will be excited in the interface between the thin metal film and the medium having the lower refractive index. If the interface between the media is coated with a thin layer of metal (gold), and light is monochromatic and *p*-polarized, the intensity of the reflected light is reduced at a specific incident angle producing a sharp shadow (called surface plasmon resonance) due to the resonance energy transfer between evanescent wave and surface plasmons. The precise angle of incidence at which this occurs is determined by a number of factors, but in the Biacore devices the principal determinant becomes the refractive index close to the *backside* of the metal film, to which target molecules are immobilized and interacting with ligands that are being circulated via microfluidics. If binding occurs to the immobilized target the local refractive index changes, leading to a change in SPR angle, which can be monitored in real-time by detecting changes in the intensity of the reflected light, producing a

sensorgram. From this sensorgram, association and dissociation rate constants and equilibrium constant (affinity) can be derived from rates of change of the SPR signal, while mass information can be derived from the magnitude of change as the size of change in SPR signal is directly proportional to the mass immobilized (Scheme 4.1).[61-63]

4.3. Quartz Crystal Microbalance (QCM)

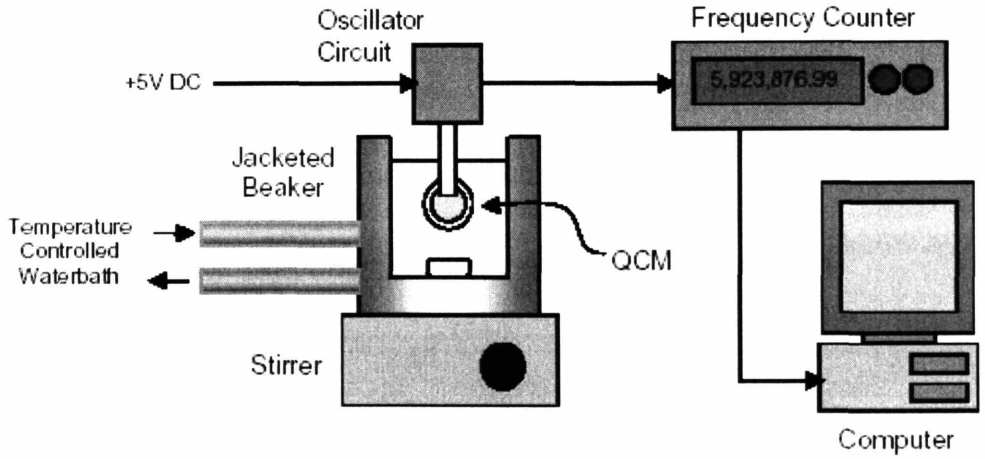

Scheme 4.3. Schematic of the experimental setup for the QCM apparatus.[b]

The piezoelectric quartz crystal microbalance (QCM) is a ultrasensitive weighing device, consisting of a thin disk of quartz crystal connected to metal electrodes.[64] When the electrodes are connected to an oscillator and an AC voltage is applied, the crystal oscillates at its resonance frequency. Most often, AT-cut crystal is used where the crystal

[b] http://poohbah.cem.msu.edu/courses/cem419/

oscillates in a shear mode.[44] The crystal is housed in a chamber where liquid can be exchanged, and the changes in resonance frequency can be detected by a frequency counter associated with a computer (Scheme 4.2). If a rigid layer is deposited on one or both of the electrodes, the resonant requency will decrease proportionally to the mass of the adsorbed layer according to the Sauerbrey equation:[65]

$$\Delta f = -\frac{\left[2 f_0^2 \Delta m\right]}{\left[A(\rho_q \mu_q)^{1/2}\right]} \tag{4.1}$$

Δf = measured frequency shift

f_0 = resonant frequency of the fundamental mode of the crystal

Δm = mass change per unit area (g/cm^2)

A = piezo-electrically active area (14 mm diameter)

ρ_q = density of quartz, 2.648 g/cm^3

μ_q = shear modulus of quartz, 2.947×10^{11} $g/(cm\ s^2)$

However, in the case where the mass is not rigidly deposited, slips on the surface, or is not evenly distributed, the Sauerbrey equation does not hold. The change in resonance frequency of a QCM taken from air into liquid is given by:[66]

$$\Delta f = -f_u^{2/3}\left[\frac{(\rho_L \eta_L)}{\pi \times (\rho_q \eta_q)}\right]^{1/2} \tag{4.2}$$

Δf = measured frequency shift

f_u = resonant frequency of the unloaded crystal

ρ_q = density of quartz, 2.648 g/cm^3

μ_q = shear modulus of quartz, 2.947×10^{11} $g/(cm\ s^2)$

ρ_L = density of liquid in contact with the crystal

μ_L = viscosity of the liquid in contact with the crystal

It was verified experimentally that quarz oscillators could respond to properties of a contacting liquid.[67,68] Those observations paved ways for investigations of the use of QCM in liquids.

In many situations the adsorbed film is not rigid and the Sauerbrey relation becomes invalid. A "soft" (viscoelastic) film will not fully couple to the oscillation of the crystal, and hence, dampens the crystal's oscillation. The dissipation (D) of the crystal's oscillation is a measure of the film's softness (viscoelasticity). D is defined as:[42,44]

$$D = \frac{E_{lost}}{2\pi E_{stored}} \tag{4.3}$$

where E_{lost} is the energy lost (dissipated) during one oscillation cycle and E_{stored} is the total energy stored in the oscillator.

The quartz crystal microbalance with dissipation monitoring (QCM-D) technique measures simultaneously the change in mass via changes in resonant frequency f, and energy dissipation, D (cf. viscoelastic properties).[69] The dissipation of the crystal is measured by recording the response of a freely oscillating crystal that has been vibrated at its resonance frequency and numerous overtones at 15, 25 and 35 MHz. By measuring at multiple frequencies and apply a viscoelastic model, the adhering film can be characterized in details and the viscosity, elasticity and correct thickness may be extracted.[42] The magnitude of ΔD variations provides information about the shear viscoelastic properties.[69] The information contained in both the frequency and dissipation changes have been shown to add unique information about structure and other properties of biomolecular films such as proteins,[70,71] lipid vesicles,[72,73] and DNA.[43]

4.4. Experimental Section

Materials. Anhydrous ethanol, *n*-butanethiol (BT), N-Hydroxysulfosuccinimide (NHS) were obtained from Aldrich and used as received. 1-(3-dimethylaminopropyl)-3-ethylcarbodiimide hydrochloride (EDC) was from Alfa Aesar. DNAse and RNAse-free water, phosphate-buffered saline were from Invitrogen. Tris-EDTA (TE) pH 8.0 buffer (20×) was obtained from Boston Scientific and diluted with water treated with a Millipore purification system (MilliQ water) to 1× prior to use. Amine modified oligo (NH_2-$(CH_2)_6$-5'- CAC-GAC-GTT-GTA-AAA-CGA-CGG-CCA-G-3'), and the target with a sequence complimentary to the 25-mer probe were all acquired from Integrated DNA Technologies, Inc. (Coralville, IA). All solutions were prepared with MilliQ water, filtered and degassed before use. 16-[[bis(4-methoxyphenyl)phenylmethyl]thio]-hexadecanoic acid (16-CTC) were synthesized in our lab as described previously.[39]

Solution preparation. TE buffer used in this work contained 1M NaCl (pH = 8.0). DNA solutions were prepared in this TE buffer. EDC/NHS solutions were produced by mixing 100 mM NHS and 400 mM EDC in water immediately before use. PBS pH 8.6 was made by adjusting the pH of PBS buffer with 1M NaOH.

Formation of SAMs and Subsequent DNA Attachment. Formation of homogeneously-mixed SAMs has been described previously.[39] SPR substrates were from the SIA Au Kit (BIAcore) and QSX sensor crystals were from Q-sense. Both the gold SPR substrates and the sensor crystals were cleaned for 1 min in piranha solution (7:3, H_2SO_4:H_2O_2), washed 3 times in MilliQ water and absolute ethanol, and blown dry under a stream of nitrogen; *caution: "piranha" solution reacts violently with organic materials, and should*

be handled carefully. The substrates were immersed in 1 mM solutions of the 16-CTC in anhydrous ethanol and allowed to equilibrate for a minimum of 16 h. The resultant SAMs were rinsed with ethanol and dried under a filtered stream of nitrogen. The CTC group was then cleaved, and the resulting low-density SAM backfilled with *n*-butanethiol to form a homogeneously-mixed SAM. Formation of the MHA SAM was achieved via a similar method, minus the cleavage and backfilling. Attachment of DNA to the SAM surface was carried out via the EDC/NHS method. In brief, the mixed monolayer was incubated for 5 min in PBS, pH 7.4, then 20 min in a fresh solution of EDC/NHS. Coupling of the 5'-modified oligos was performed by incubating the SAMs in 100 μM strands of oligos in TE buffer for 3-6 h. Subsequent incubation of the substrates for 1 min in PBS was followed by 20 min incubation in PBS pH 8.6. The DNA-covered substrates were used immediately for SPR or QCM-D measurements after rinsing with PBS pH 7.4 and water.

SPR. A BIAcore 2000 instrument (BIAcore, Upsala, Sweden) was used in all experiments. The SIA Au kit contains bare gold-coated substrates that can be used for surface modifications prior to assembling and running in the BIAcore. The running buffer is TE containing 1 M NaCl. The baseline was stabilized for at least 5 min to 1 h at a flow rate of 5 μl/min prior to injection of solution. EDC/NHS solution was made fresh right before the start of the injection. A dilute function was used to mix the two solutions. Typically, about 60 μl of EDC/NHS was injected at the flow rate of 5 μl/min. Oligonucleotide probe solution (150 μl of 1 μg/μl solution in TE buffer) was then injected at the same flow rate followed by 35 μl of PBS pH 8.6. Subsequently,

complimentary target oligos (600-750 μl of 0.0065 μmol/mL) was injected at 5 μl/min and hybridization was carried out for 3-4 h.

QCM-D. The QCM-D measurements were carried out in a Q-sense D300 measurement system (Q-sense AB, Gothenburg, Sweden). As described above, QCM is a mass detection technique in which changes in resonant frequency (*f*) of a quartz crystal is monitored as a material deposits on its suface.[65,74] QCM-D is a new technology that allows for the simultaneous measurements of both changes in mass and viscoelastic properties due to the ability to measure energy dissipation factor (D). The combined information recorded in a parallel fashion makes QCM-D a powerful technique to study viscoelastic monolayers, biofilms, and small proteins in liquid.[45] The QCM-D sensor crystals are gold coated, 14 mm in diameter, 5 MHz AT-cut quartz crystals. The crystal resonant frequency shift (Δf) and the dissipation factor (ΔD) were measured simultaneously at the fundamental frequency (5 MHz) and 3 other over tones at 15, 25, and 35 MHz. All samples were thermally equilibrated to 23 ± 0.1 ^{o}C for 2 min in an axial flow chamber (QAFC 301) which comprised of a T-loop that can hold upto 1.5 mL of liquid. The sample (0.4-0.5 mL) was introduced to the measurement chamber after it had been thermally equilibrated, resulting in small pressure changes evident on the *f* and *D* traces. A steady baseline was acquired prior to staring all measurements.

DNA hybridization was carried out as follows: 0.4 mL of PBS buffer for 5 minutes, 0.4 mL of complementary oligos 3-4 ×, waiting 2 min between each injection, incubate for at least 6 hours, flush with buffer until baseline stabilize.

4.5. Results and Discussion

4.5.1. QCM-D. The QCM-D technique was used to examine the hybridization efficiency of 25-mer oligos immobilized on both the homogeneously-mixed (HM) SAM generated as described versus the dense MHA layer. If we assume that the absorbed film is thin, not too viscoelastic, and fulfilling certain conditions about the coupling to certain medium, then the Sauerbrey equation can be applied: [6,71]

$$\Delta m_{QCM} = \rho_{film}\delta_{film} = \frac{C_{QCM}}{n}\Delta f \tag{4.4}$$

where ρ_{film} and δ_{film} are the effective density and film thickness, respectively, C_{QCM} (=17.7 ng cm^{-2} Hz^{-1}) is the mass sensitivity constant, and n (=1,3,5,7) are the overtone number.[42,43] This calculation is complicated in liquid due to the fact that liquid may absorb a considerably high amount of water, which is sensed as a mass uptake by all QCMs. The QCM-D technique allows users to determine whether the absorbed film is rigid or water-rich (soft) by measuring several frequencies and the dissipation (D). [75] Viscous loss of energy in the film can lead to a non-trivial reduction in measured surface mass of the film.[76] Other theoretical considerations need to be accounted when the film is not rigid and the results deviate from what predicted by the Sauerbrey equation. Figure 4.1 shows the frequency vs time (A) and dissipation vs time (B) for the oligo-modified HM & MHA SAMs upon hybridization. The HM SAM shows a Δf of 43.0 vs 24.2 for the MHA SAM for the third harmonic at 15 MHz (which will use throughout the analysis). First, using the approximation that the monolayer is fairly rigid and applying the Sauerbrey equation, mass changes of 253.8 ng cm^{-2} and 143.1 ng cm^{-2} are obtained for the HM SAMs and MHA SAM respectively. The HM SAM shows an improvement

of 1.77 times more than the MHA monolayer. Since the change in dissipation (ΔD) is small ($1.5 \times 10^{=7}$ and 6.2×10^{-7} for the HM and MHA SAMs respectively) and within detection limits, we can assume that the covalently bound nucleotides form fairly rigid film at the surface.[45,70] The change in ΔD is a little small to assign confidently to hybridization process, however, we consistently observe a change in dissipation in all the samples, ranging between 1×10^{-7} to 1×10^{-6} for HM samples and similarly for MHA SAMs.

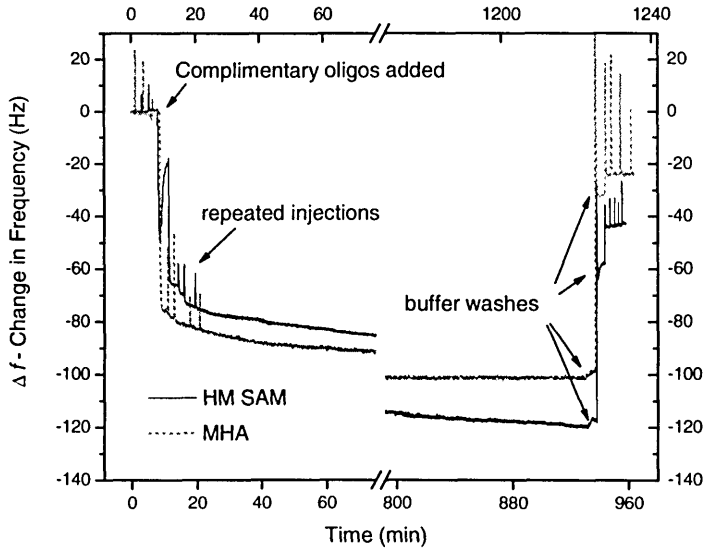

Figure 4.1. Change in frequency vs. time for the hybridization of complimentary strands to oligos tethered to homogeneously mixed (HM) monolayers (black straight line) and MHA monolayer (gray dotted line).

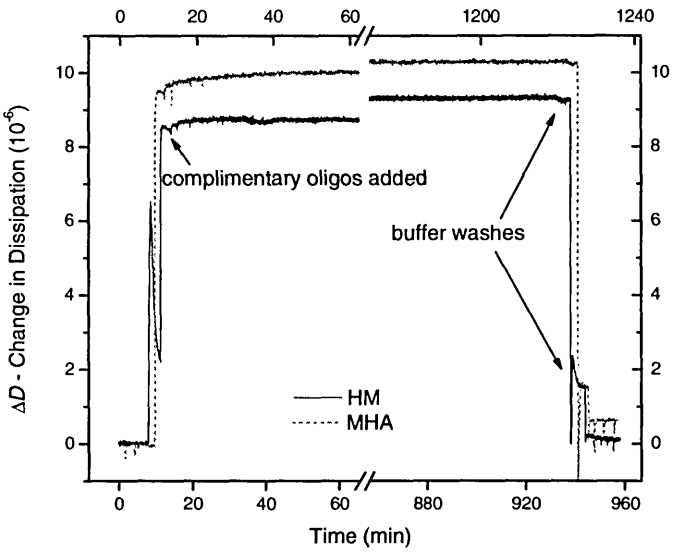

Figure 4.2. Change in dissipation vs. time for the hybridization of complimentary strands to oligos tethered to homogeneously mixed (HM) monolayers (black straight line) and MHA monolayer (gray dotted line).

The change in ΔD is higher for the MHA monolayers than for HM. This may be due to the oligos on the HM surfaces lying down as they are not so densely tethered, and therefore reducing the dissipative effects by not protruding into the solution. The opposite is true for the MHA monolayer, where oligos are so densely tethered and hence more rigid that they protrude into the solution, increasing ΔD. Similar observations was noted by other reseachers where higher ΔD was observed for more rigid protein formation.[77] or to increased duplex length, increased close-packing the resulting energy losses through chain entanglement.[45] While this is speculative, support for this interpretation can be drawn from comparison with the work of Kim *et al.* who showed a

relationship between energy dissipation in a polymeric film on a QCM sensor and the level of molecular entanglement within the film.[78]

4.5.2. SPR. The hybridization efficiency is expressed as the ration of hybridized and immobilized nucleotides per square centimeter. This is obtained from the SPR spectra, with the difference between pre- and post-oligo immobilization serves as the amount of immobilized probes, and the difference between pre- and post-target hybridization as the amount of oligo bound to its complimetary sequence on the surface. Figure 4.3 and 4.4 show the SPR spectra for the HM and MHA monolayers, respectively, post hybridization. The hybridization efficiency for HM monolayers is approximately 93-96% whereas for the MHA monolayer is 48-65%.

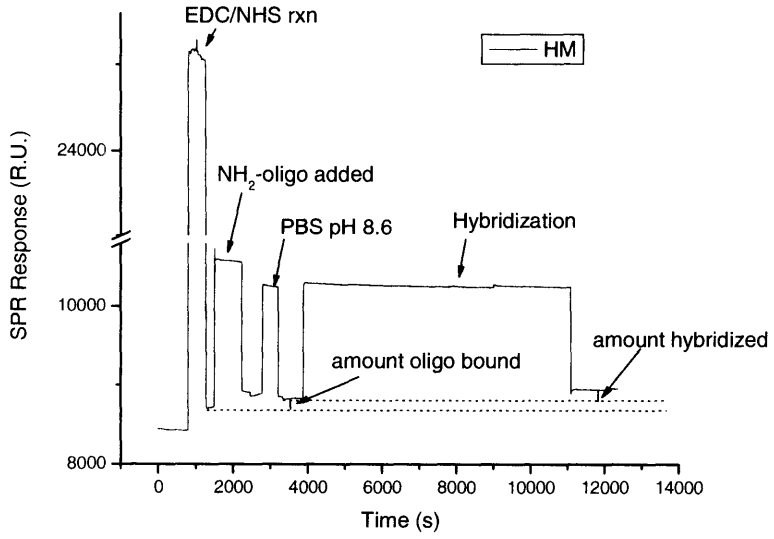

Figure 4.3. SPR spectra for the immobilization of oligo on to HM SAM via EDC/NHS reaction and the subsequent hybridization of complimentary target oligos.

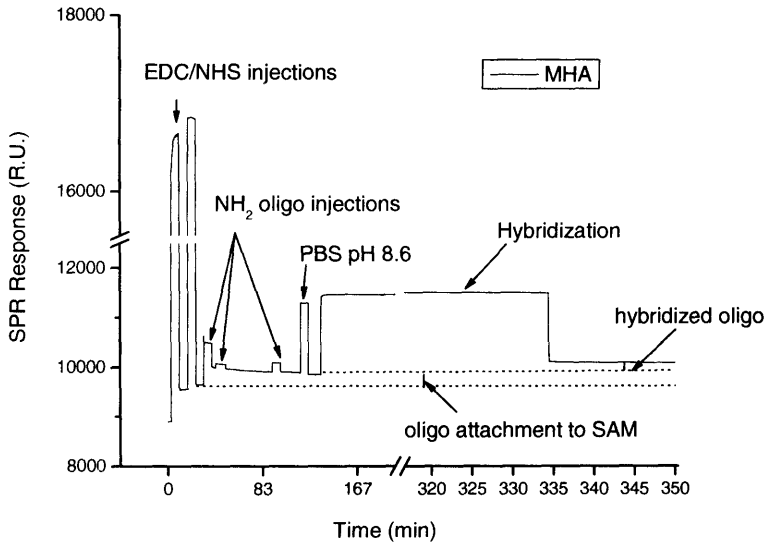

Figure 4.4. SPR spectra for the immobilization of oligo on to MHA SAM via EDC/NHS reaction and the subsequent hybridization of complimentary target oligos.

As expected, and in agreement with earlier reports[15,30,34,79], the hybridization efficiency depends strongly on the probe density. The immobilization of probe results in changes of 90-350 RU, where 1000 RU corresponds to approximately 1ng/mm^2 (Biacore manual) and have been used by other authors for estimating the amount of immobilized probes,[80,81] although this method has originally been employed for proteins. Using this approximation, the probe density for the MHA monolayer is approximately 2.71×10^{12} molecules per cm^2 (RU of 353.4 and a molecular weight for the oligo of 7864.2 g/mol) and that for the HM monolayer is 9.03×10^{11} molecules per cm^2 (RU of 117.9). The amount of hybridized oligo is 1.62×10^{12} and 8.70×10^{11} molecules per cm^2 with the corresponding hybridization efficiency of 58.2 % and 93.6% for the MHA and HM monolayers respectively. This is in good agreement with earlier results where a 90% efficiency was observed for a mixed monolayer of 11-mercaptoundecanoic acid and 1-

decanethiol, where the maximum surface density of the DNA probe is 3×10^{12} molecules. For higher density probes (up to 12×10^{12}) molecules per cm^2, much lower efficiency was found (about 40%).[11] Another group reported coupling efficiency of ~50 % for the high density probe (3.0×10^{12} probes per cm^2) and a much better improvement in hybridization efficiency up to 100% for lower density probes (1.5×10^{12} probes per cm^2).[82] Demers *et al.*[83] used a fluorescent-based measurement to detect probe coverage and target hybridization on planar gold. Over night incubation, which likely led to higher-density probe coverage, the reported target hybridization was 33% even after 40 h of incubation.[83] Steel *et al.* also showed a similar trend: higher-density probe films have reduced target hybridization efficiency.[30] However, our results are only an estimate, and to exactly quantify the amount of immobilized probes, labeling of probes may be necessary.

4.6. Conclusions

We have employed two quantitative techniques, quart-crystal microbalance with dissipation monitoring (QCM-D) and surface plasmon resonance imaging (SPR) to quantify the hybridization efficiency of a 25-mer oligonucleotide probe to two different surfaces: a dense MHA monolayer and a homogeneously-mixed (HM) SAM generated from a method that allows for regular spacing of functional –COOH groups. The HM SAMs are about a third as dense in terms of –COOH groups as the MHA SAM based on earlier study.[39] This reduced density of functional groups led to reduced attachment of oligonucleotide probes to the surface, increasing the area per probe, and allowed more space in which complimentary sequence can bind. Reducing the density of immobilized

probes led to the improvement in hybridization efficiency as demonstrated in both SPR and QCM-D results, which are comparable to previous reports. Our method paves the way for customizing binding efficiency and target probe density based on the distance between functional groups. By changing the headgroup size of the precursor monolayer, different distances between functional group can be formed, allowing for an ability to tailor distances between molecules. This method may allow for improvement in DNA array technology.

4.7. References

1. Bier, F. F. & Furste, J. P. *Frontiers in Biosensorics* (eds. Scheller, F., Schubert, F. & Ferdowitz, J.) (Birkhauser Verlag, Basel, Switzerland, 1997).

2. Luther, A., Brandsch, R. & von Kiedrowski, G. Surface-promoted replication and exponential amplification of DNA analogs. *Nature (London)* **396**, 245-248 (1998).

3. Ziegler, C. & Gopel, W. Biosensor development. *Current Opinion in Chemical Biology* **2**, 585-91. (1998).

4. Maskos, U. & Southern, E. M. Oligonucleotide hybridizations on glass supports: a novel linker for oligonucleotide synthesis and hybridization properties of oligonucleotides synthesised in situ. *Nucleic Acids Research* **20**, 1679-84. (1992).

5. Pease, A. C. et al. Light-generated oligonucleotide arrays for rapid DNA sequence analysis. *Proceedings of the National Academy of Sciences of the United States of America* **91**, 5022-6 (1994).

6. Huang, E., Zhou, F. & Deng, L. Studies of Surface Coverage and Orientation of DNA Molecules Immobilized onto Preformed Alkanethiol Self-Assembled Monolayers. *Langmuir* **16**, 3272-3280 (2000).

7. Lerman, L. S. *DNA Probes: Applications in Genetic and Infectious Disease and Cancer* (UMI, Ann Arbor, MI, 1986).

8. Watson, J., Gilman, M., Witkowski, J. & Zoller, M. *Recombinant DNA* (W. H. Freeman and Company, New York, 1992).

9. Wetmur, J. G. DNA probes: applications of the principles of nucleic acid hybridization. *Critical Reviews in Biochemistry and Molecular Biology* **26**, 227-59 (1991).

10. Chan, V., Graves, D. J. & McKenzie, S. E. The biophysics of DNA hybridization with immobilized oligonucleotide probes. *Biophysical Journal* **69**, 2243-55. (1995).

11. Boncheva, M., Scheibler, L., Lincoln, P., Vogel, H. & Aakerman, B. Design of Oligonucleotide Arrays at Interfaces. *Langmuir* **15**, 4317-4320 (1999).

12. Satjapipat, M., Sanedrin, R. & Zhou, F. Selective desorption of alkanethiols in mixed self-assembled monolayers for subsequent oligonucleotide attachment and DNA hybridization. *Langmuir* **17**, 7637-7644 (2001).

13. Wang, J. et al. Amplified Voltammetric Detection of DNA Hybridization via Oxidation of Ferrocene Caps on Gold Nanoparticle/Streptavidin Conjugates. *Analytical Chemistry* **75**, 3941-3945 (2003).

14. Kerman, K. et al. Voltammetric determination of DNA hybridization using methylene blue and self-assembled alkanethiol monolayer on gold electrodes. *Analytica Chimica Acta* **462**, 39-47 (2002).

15. Huang, E., Satjapipat, M., Han, S. & Zhou, F. Surface Structure and Coverage of an Oligonucleotide Probe Tethered onto a Gold Substrate and Its Hybridization Efficiency for a Polynucleotide Target. *Langmuir* **17**, 1215-1224 (2001).

16. Gu, J., Lu, X. & Ju, H. DNA sensor for recognition of native yeast DNA sequence with methylene blue as an electrochemical hybridization indicator. *Electroanalysis* **14**, 949-954 (2002).

17. Caruso, F., Rodda, E., Furlong, D. N., Niikura, K. & Okahata, Y. Quartz Crystal Microbalance Study of DNA Immobilization and Hybridization for Nucleic Acid Sensor Development. *Analytical Chemistry* **69**, 2043-2049 (1997).

18. Bajaj, M. G. & Laibinis, P. E. in *Abstracts of Papers, 225th ACS National Meeting, New Orleans, LA, United States, March 23-27, 2003* COLL-100 (2003).

19. Brockman, J. M., Nelson, B. P. & Corn, R. M. Surface plasmon resonance imaging measurements of ultrathin organic films. *Annual Review of Physical Chemistry* **51**, 41-63. (2000).

20. Goodrich, G. P., Nicewarner, S. R., He, L., Natan, M. J. & Keating, C. D. Nanoparticle-amplified surface plasmon resonance for detection of DNA hybridization. *Proceedings of SPIE-The International Society for Optical Engineering* **4258**, 80-85 (2001).

21. Bamdad, C. The use of variable density self-assembled monolayers to probe the structure of a target molecule. *Biophysical Journal* **75**, 1989-1996 (1998).

22. Bamdad, C. A DNA self-assembled monolayer for the specific attachment of unmodified double- or single-stranded DNA. *Biophysical Journal* **75**, 1997-2003. (1998).

23. Erts, D., Polyakov, B., Olin, H. & Tuite, E. Spatially distributed 2-dimensional DNA arrays on Au (111): AFM characterisation. *Latvian Journal of Physics and Technical Sciences*, 63-72 (2001).

24. Brockman, J. M., Frutos, A. G. & Corn, R. M. A Multistep Chemical Modification Procedure To Create DNA Arrays on Gold Surfaces for the Study of Protein-DNA Interactions with Surface Plasmon Resonance Imaging. *Journal of the American Chemical Society* **121**, 8044-8051 (1999).

25. Nakamura, F. et al. Preparation of a Branched DNA Self-Assembled Monolayer toward Sensitive DNA Biosensors. *Nano Letters*, ACS ASAP.

26. Riepl, M. et al. Functionalized surfaces of mixed alkanethiols on gold as a platform for oligonucleotide microarrays. *Langmuir* **18**, 7016-7023 (2002).

27. Nakamura, F., Mitsui, K. & Hara, M. Adsorption behavior of DNA onto self-assembled monolayer containing intercalator. *Molecular Crystals and Liquid Crystals Science and Technology, Section A: Molecular Crystals and Liquid Crystals* **370**, 359-362 (2001).

28. Peterlinz, K. A., Georgiadis, R. M., Herne, T. M. & Tarlov, M. J. Observation of Hybridization and Dehybridization of Thiol-Tethered DNA Using Two-Color Surface Plasmon Resonance Spectroscopy. *Journal of the American Chemical Society* **119**, 3401-3402 (1997).

29. Levicky, R., Herne, T. M., Tarlov, M. J. & Satija, S. K. Using Self-Assembly To Control the Structure of DNA Monolayers on Gold: A Neutron Reflectivity Study. *Journal of the American Chemical Society* **120**, 9787-9792 (1998).

30. Steel, A. B., Herne, T. M. & Tarlov, M. J. Electrochemical Quantitation of DNA Immobilized on Gold. *Analytical Chemistry* **70**, 4670-4677 (1998).

31. Herne, T. M. & Tarlov, M. J. Characterization of DNA Probes Immobilized on Gold Surfaces. *Journal of the American Chemical Society* **119**, 8916-8920 (1997).

32. Shchepinov, M. S., Case-Green, S. C. & Southern, E. M. Steric factors influencing hybridization of nucleic acids to oligonucleotide arrays. *Nucleic Acids Research* **25**, 1155-1161 (1997).

33. Erts, D., Polyakov, B., Olin, H. & Tuite, E. Spatial and Mechanical Properties of Dilute DNA Monolayers on Gold Imaged by AFM. *Journal of Physical Chemistry B* **107**, 3591-3597 (2003).

34. Peterson, A. W., Heaton, R. J. & Georgiadis, R. M. The effect of surface probe density on DNA hybridization. *Nucleic Acids Research* **29**, 5163-5168 (2001).

35. Shimazu, K., Kawaguchi, T. & Isomura, T. Construction of Mixed Mercaptopropionic Acid/Alkanethiol Monolayers of Controlled Composition by Structural Control of a Gold Substrate with Underpotentially Deposited Lead Atoms. *Journal of the American Chemical Society* **124**, 652-661 (2002).

36. Folkers, J. P., Laibinis, P. E., Whitesides, G. M. & Deutch, J. Phase behavior of two-component self-assembled monolayers of alkanethiolates on gold. *Journal of Physical Chemistry* **98**, 563-71 (1994).

37. Folkers, J. P., Laibinis, P. E. & Whitesides, G. M. Self-assembled monolayers of alkanethiols on gold: comparisons of monolayers containing mixtures of short- and long-chain constituents with methyl and hydroxymethyl terminal groups. *Langmuir* **8**, 1330-41 (1992).

38. Hobara, D., Ota, M., Imabayashi, S.-i., Niki, K. & Kakiuchi, T. Phase separation of binary self-assembled thiol monolayers composed of 1-hexadecanethiol and 3-mercaptopropionic acid on Au(111) studied by scanning tunneling microscopy and cyclic voltammetry. *Journal of Electroanalytical Chemistry* **444**, 113-119 (1998).

39. Tran, T.-N. et al. A Synthetic Chemical Route for the Formation of Homogeneously-Mixed Self-Assembled Monolayers. *Submitted for review.* (2003).

40. Joensson, U. et al. Introducing a biosensor based technology for real-time biospecific interaction analysis. *Annales de Biologie Clinique* **51**, 19-26 (1993).

41. Stenberg, E., Persson, B., Roos, H. & Urbaniczky, C. Quantitative determination of surface concentration of protein with surface plasmon resonance using radiolabeled proteins. *Journal of Colloid and Interface Science* **143**, 513-26 (1991).

42. Q-Sense Technology Notes - Q-sense.com

43. Hook, F., Ray, A., Norden, B. & Kasemo, B. Characterization of PNA and DNA Immobilization and Subsequent Hybridization with DNA Using Acoustic-Shear-Wave Attenuation Measurements. *Langmuir* **17**, 8305-8312 (2001).

44. Rodahl, M., Hook, F., Krozer, A., Brzezinski, P. & Kasemo, B. Quartz crystal microbalance setup for frequency and Q-factor measurements in gaseous and liquid environments. *Review of Scientific Instruments* **66**, 3924-30 (1995).

45. Pope, L. H. et al. Probing DNA Duplex Formation and DNA-Drug Interactions by the Quartz Crystal Microbalance Technique. *Langmuir* **17**, 8300-8304 (2001).

46. Adamczyk, M., Moore, J. A. & Yu, Z. Application of surface plasmon resonance toward studies of low-molecular-weight antigen-antibody binding interactions. *Methods* **20**, 319-28. (2000).

47. Kaganer, E., Pogreb, R., Davidov, D., Willner & Itamar. Surface Plasmon Resonance Characterization of Photoswitchable Antigen-Antibody Interactions. *Langmuir* **15**, 3920-3923 (1999).

48. Rahn, J. R. & Hallock, R. B. Antibody Binding to Antigen-Coated Substrates Studied with Surface Plasmon Oscillations. *Langmuir* **11**, 650-4 (1995).

49. Shumaker-Parry, J. S., Campbell, C. T., Stormo, G. D., Silbaq, F. S. & Aebersold, R. H. Probing protein: DNA interactions using a uniform monolayer of DNA and surface plasmon resonance. *Proceedings of SPIE-The International Society for Optical Engineering* **3922**, 158-166 (2000).

50. Nelson, B. P., Grimsrud, T. E., Liles, M. R., Goodman, R. M. & Corn, R. M. Surface plasmon resonance imaging measurements of DNA and RNA hybridization adsorption onto DNA microarrays. *Analytical Chemistry* **73**, 1-7. (2001).

51. He, L. et al. Colloidal Au-enhanced surface plasmon resonance for ultrasensitive detection of DNA hybridization. *Journal of the American Chemical Society* **122**, 9071-9077 (2000).

52. Tsoi Pui, Y. & Yang, M. Kinetic study of various binding modes between human DNA polymerase beta and different DNA substrates by surface-plasmon-resonance biosensor. *Biochemical Journal* **361**, 317-25. (2002).

53. Tsoi, P. Y. & Yang, M. Kinetic study of various binding modes between human DNA polymerase b and different DNA substrates by surface-plasmon-resonance biosensor. *Biochemical Journal* **361**, 317-325 (2002).

54. Tsoi, P. Y., Yang, J., Sun, Y.-t., Sui, S.-f. & Yang, M. Surface Plasmon Resonance Study of DNA Polymerases Binding to Template/Primer DNA

Duplexes Immobilized on Supported Lipid Monolayers. *Langmuir* **16**, 6590-6596 (2000).

55. Gotoh, M. et al. Rapid method for detection of point mutations using mismatch binding protein (MutS) and an optical biosensor. *Genetic Analysis* **14**, 47-50. (1997).

56. Thiel, A. J., Frutos, A. G., Jordan, C. E., Corn, R. M. & Smith, L. M. In situ surface plasmon resonance imaging detection of DNA hybridization to oligonucleotide arrays on gold surfaces. *Analytical Chemistry* **69**, 4948-4956 (1997).

57. Caruso, F., Rodda, E., Furlong, D. N. & Haring, V. DNA binding and hybridization on gold and derivatized surfaces. *Sensors and Actuators, B: Chemical* **B41**, 189-197 (1997).

58. Jin-Lee, H., Goodrich, T. T. & Corn, R. M. SPR imaging measurements of 1-D and 2-D DNA microarrays created from microfluidic channels on gold thin films. *Analytical Chemistry* **73**, 5525-31. (2001).

59. Sota, H., Hasegawa, Y. & Iwakura, M. Detection of Conformational Changes in an Immobilized Protein Using Surface Plasmon Resonance. *Analytical Chemistry* **70**, 2019-2024 (1998).

60. Hasegawa, Y., Shinohara, Y. & Sota, H. Structure analysis of saccharides using a biosensor based on molecular recognition. *Trends in Glycoscience and Glycotechnology* **9**, S15-S24 (1997).

61. BIACore Technology Notes -BIAcore.com

62. Malmqvist, M. Biospecific interaction analysis using biosensor technology. *Nature* **361**, 186-7. (1993).

63. Loefaas, S. et al. Bioanalysis with surface plasmon resonance. *Sensors and Actuators, B: Chemical* **B5**, 79-84 (1991).

64. Czanderna, A. W. & Lu, C. *Applications of Piezoelectric Quartz Crystal Microbalances* (eds. Lu, C. & Czanderna, A. W.) (Elsevier, Amsterdam, 1984).

65. Sauerbrey, G. The use of quartz oscillators for weighing thin layers and for microweighing. *Zeitschrift fuer Physik* **155**, 206-22 (1959).

66. Kanazawa, K. K. & Gordon, J. G., II. Frequency of a quartz microbalance in contact with liquid. *Analytical Chemistry* **57**, 1770-1 (1985).

67. Konash, P. L. & Bastiaans, G. J. Piezoelectric crystals as detectors in liquid chromatography. *Analytical Chemistry* **52**, 1929-31 (1980).

68. Nomura, T. & Minemura, A. Behavior of a piezoelectric quartz crystal in an aqueous solution and its use for the determination of minute amounts of cyanide. *Nippon Kagaku Kaishi*, 1621-5 (1980).

69. Cans, A. S. et al. Measurement of the dynamics of exocytosis and vesicle retrieval at cell populations using a quartz crystal microbalance. *Analytical Chemistry* **73**, 5805-11. (2001).

70. Hook, F., Rodahl, M., Kasemo, B. & Brzezinski, P. Structural changes in hemoglobin during adsorption to solid surfaces: effects of pH, ionic strength, and ligand binding. *Proceedings of the National Academy of Sciences of the United States of America* **95**, 12271-12276 (1998).

71. Cans, A.-S. et al. Measurement of the dynamics of exocytosis and vesicle retrieval at cell populations using a quartz crystal microbalance. *Analytical Chemistry* **73**, 5805-5811 (2001).

72. Keller, C. A. & Kasemo, B. Surface specific kinetics of lipid vesicle adsorption measured with a quartz crystal microbalance. *Biophysical Journal* **75**, 1397-1402 (1998).

73. Keller, C. A., Glasmastar, K., Zhdanov, V. P. & Kasemo, B. Formation of Supported Membranes from Vesicles. *Physical Review Letters* **84**, 5443-5446 (2000).

74. Rodahl, M. & Kasemo, B. Frequency and dissipation-factor responses to localized liquid deposits on a QCM electrode. *Sensors and Actuators, B: Chemical* **B37**, 111-116 (1996).

75. Rodahl, M. et al. Simultaneous frequency and dissipation factor QCM measurements of biomolecular adsorption and cell adhesion. *Faraday Discussions* **107**, 229-246 (1997).

76. Voinova, M. V., Jonson, M. & Kasemo, B. 'Missing mass' effect in biosensor's QCM applications. *Biosensors & Bioelectronics* **17**, 835-841 (2002).

77. Hoeoek, F., Ray, A., Norden, B. & Kasemo, B. Characterization of PNA and DNA Immobilization and Subsequent Hybridization with DNA Using Acoustic-Shear-Wave Attenuation Measurements. *Langmuir* **17**, 8305-8312 (2001).

78. Kim, J.-M., Chang, S.-M. & Muramatsu, H. Monitoring changes in the viscoelastic properties of thin polymer films by the quartz crystal resonator. *Polymer* **40**, 3291-3299 (1999).

79. Southern, E., Mir, K. & Shchepinov, M. Molecular interactions on microarrays. *Nature Genetics* **21**, 5-9. (1999).

80. Mariotti, E., Minunni, M. & Mascini, M. Surface plasmon resonance biosensor for genetically modified organisms detection. *Analytica Chimica Acta* **453**, 165-172 (2002).

81. Nilsson, P., Persson, B., Uhlen, M. & Nygren, P. A. Real-time monitoring of DNA manipulations using biosensor technology. *Analytical Biochemistry* **224**, 400-8. (1995).

82. Peterson, A. W., Wolf, L. K. & Georgiadis, R. M. Hybridization of Mismatched or Partially Matched DNA at Surfaces. *Journal of the American Chemical Society* **124**, 14601-14607 (2002).

83. Demers, L. M. et al. A Fluorescence-Based Method for Determining the Surface Coverage and Hybridization Efficiency of Thiol-Capped Oligonucleotides Bound

to Gold Thin Films and Nanoparticles. *Analytical Chemistry* **72**, 5535-5541 (2000).

CHAPTER FIVE

LONG-TERM STABILITY OF SELF-ASSEMBLED MONOLAYERS IN BIOLOGICAL MEDIA

5.1. Introduction

Recently, biological microelectromechanical systems (bioMEMS) have received significant attention.[1,2] These devices find potential applications in areas as diverse as biosensing and artificial organ generation. One interesting potential application is the use of bioMEMS devices for drug delivery.[3] These bioMEMS drug delivery vehicles incorporate many of the typical materials encountered with microfabricated devices such as silicon, silicon oxide, silicon nitride, and gold.[4-6] Since many of these proposed uses for these devices necessitate moderate to long-term exposure to a biological medium *in vivo*, the material-environment interactions are important for the device's ultimate performance.

Although initial tests of biocompatibility look promising for these types of devices,[7,8] concerns over biofouling remain. To minimize biofouling effects, researchers have investigated protein/cell adhesion resistant surface-bound materials such as poly(ethylene glycol) or oligo(ethylene glycol) terminated self-assembled monolayers (SAMs).[9,10] The SAMs have several advantageous properties. Alteration of functional groups from thiols to trialkoxysilanes allows the monolayers to be prepared on myriad surfaces including gold, silicon oxide, and metal oxides, which are commonly encountered in MEMS. Additionally, these materials show increased resistance to adsorption of numerous proteins including ribonuclease A, chymotrypsinogen, pyruvate kinase, fibrinogen, lysozyme, and □-globulin.[11-14] The total adhesion of cell lines such as glial, fibronectin, and bovine and human endothelial is also reduced due to the reduction

of pre-adsorbed protein.[15-17] It is this property of SAMs, along with their application to many surfaces, which make them useful to bioMEMS devices.

Despite intense interest in SAMs for modifying biocompatibility/biofouling relatively little on the long-term stability of the monolayers is known. The majority of studies involving *in vitro* testing of oligo(EG) terminated alkanethiols are conducted after immersion in media for periods ranging from 15 minutes to several hours.[11,13,14,18,19] One study investigating moderate time length cell adhesion resistance of oligo(EG) terminated alkanethiols is that by Mrksich and co-workers.[20] The researchers found that the ability to resist adhesion of 3T3 fibroblasts diminishes significantly at times longer than 7 days in culture. No investigation of changes in monolayer structure or integrity was conducted, however. Little else is known concerning the long-term exposure of these potentially useful materials to biological media. The air stability of highly crystalline alkanethiol monolayers has also been debated.[21-24]

To address the issue of moderate to long-term stability of SAMs for bioMEMS device modification, alkanethiol and oligo(EG) terminated alkanethiol monolayers were prepared and studied after immersion in either phosphate buffer saline (PBS) or calf serum. Electrochemical response to a probe molecule, ferricyanide ($FeCN_6^{3-}$), is determined at time points over the course of five weeks. The specific interest here is in the modification of gold features on a electrochemically activated MEMS based drug delivery device.[4] This application has importance for other electrode-based MEMS devices such as cardiac pacemakers[25] and biosensors. Additionally, this work may serve as a starting point for further studies of surface chemical modification methods for moderate to long-term minimization of biofouling for *in vivo* applications.

5.2. Experimental Section

Materials. 1-Undecanethiol ($C_{11}SH$) and Na_2SO_4 (Aldrich), $K_3Fe(CN)_6$ (Mallinkrodt), and 200 proof ethanol (Pharmco), 10X phosphate buffered saline (Roche), and uric acid (Sigma) were all used as received. $HO(C_2H_4O)_3C_{11}H_{22}SH$ ($EG_3C_{11}SH$) was a gift from Dr. Insung Choi (KAIST, Daejon Korea) and was synthesized according to literature procedures.[26] All water was purified using a Milli-Q UV system (Millipore, Bedford, MA). Calf serum, Fungizone Antimycotic, and Penicillin-Streptomycin were all from GIBCO. Calf serum solutions used here contained 1.0 % (v/v) Penicillin-Streptomycin and 0.2 % (v/v) Fungizone Antimycotic. Glassware was cleaned by rinsing with aqua regia (3:1 $HCl:HNO_3$) followed by rinsing with Milli-Q water.

Surface and Self-Assembled Monolayer Preparation. Gold on silicon surfaces were fabricated by the following method outlined below. The electrodes consisted of two pads, 0.5 cm × 0.5 cm and 0.75 cm × 0.5 cm connected by one gold strip, 0.1 cm × 0.5 cm. This electrode design was chosen to simultaneously prepare a series of electrodes with the same geometric area. The electrodes were fabricated using standard lithographic techniques, producing electrodes with a macroscopic surface area of 0.25 cm^2 and 0.375 cm^2. The electrodes were prepared by evaporation of titanium (100 Å) as an adhesion layer and gold (1000 Å) on test grade silicon wafer (SiliconQuest) precoated with a 3000 Å layer of Si_3N_4 as an electrically insulating layer. The ebeam was carried out in a Temescal Semiconductor Products VES 2550 electron beam evaporator under high vacuum (10^{-7} Torr) at the slowest rate of 1 Å/sec to ensure smooth gold deposition. The root-mean square roughness of the surface from atomic force microscopy (AFM) using the Nanoscope IIIa Scanned Probe Microscope (Digital Instruments) is approximately 15 Å. Prior to self-assembly, the gold surfaces were cleaned in piranha solution (4:1 ratio of

H_2SO_4 to 30% H_2O_2). (Safety note: Piranha solutions can react violently with organic materials.) The surfaces were withdrawn from piranha, vigorously rinsed in a water then ethanol stream, and dried in a N_2(g) stream. Immediately after piranha cleaning, gold surfaces were placed in an electrochemical cell containing 5.0 mM $K_3Fe(CN)_6$ and 0.10 M Na_2SO_4 and characterized with cyclic voltammetry as outlined below. Surfaces were again cleaned with water and ethanol and dried in a N_2(g) stream.

Gold surfaces were immersed in 2.0 mM $EG_3C_{11}SH$ or 2.0 mM $C_{11}SH$ in ethanol solution after cleaning. The samples were immersed for 48 hours at minimum to enable formation of monolayers with minimal defects. After self-assembly, surfaces were withdrawn, cleaned with the normal protocol (water, ethanol, N_2(g) dried), and characterized with contact angle goniometry and cyclic voltammetry as outlined below. Samples were then stored in one of three solutions: phosphate buffered saline (PBS), calf serum, or deoxygenated-PBS with 1.0 mM uric acid.

Contact Angle Measurements. Contact angle measurements were made using a VCA2000 (AST Products, Inc.) system. The SAM/Au samples were withdrawn from solution, washed in a high flow rate water and then ethanol stream, and subsequently dried in a filtered N_2(g) stream. Devices were placed on the sample stage and the advancing contact angle of Milli-Q water was recorded. The values reported here represent the average of at least two distinct spots on two separate samples along with the corresponding standard deviations.

Electrochemical Analysis. Cyclic voltammetry was performed on a Solartron 1287 electrochemical system interfaced to a PC for data acquisition. A three electrode electrochemical system employing a Au film counter electrode (100 nm Au on silicon with a 10 nm Ti adhesion layer) and a Ag|AgCl|saturated KCl reference electrode

(BioAnalytical Systems) were used. Contact was made to the larger pad of the electrode with a flat clip. Solutions of 5.0 mM $K_3Fe(CN)_6$ and 0.10 M Na_2SO_4 were freshly prepared in Milli-Q water and deoxygenated for 20 minutes minimally. The working SAM/Au surface and the Au counter electrode film were reproducibly place ~4 mm apart. The reference electrode was then placed in close proximity, less than 1 cm, from the other electrodes.

Infrared Spectroscopy. IR spectra were recorded with a Bio-Rad FTS 175 spectrometer fitted with the Universal Reflectance Attachment. The spectra were recorded in a single reflection mode with the p-polarized light incident at 80° from the surface normal. The reflected light was collected with a narrow-band MCT detector. Octadecanethiol-d_{37} on gold served as a spectral reference. A minimum of 512 scans was acquired for all samples. After triangular apodization, resolution was 2 cm^{-1}.

X-ray Photoelectron Spectroscopy. X-ray photoelectron spectra were recorded using a Kratos AXIS Ultra spectrometer. Spectra were obtained with a monochromatic Al K X-ray source and a pass energy of 10.0 eV. Spectra were recorded with similar settings (number of sweeps, integration times, etc.) from sample to sample to enable comparisons to be made. The S 2p peak heights in Figures 5.6 and 5.7 have scales that have been normalized to the Au 4f peak. Samples for XPS were cleaned using the water, ethanol, $N_2(g)$ method after emmersion from solution and then transferred to the vacuum environment of the spectrometer.

5.3. Results

Contact Angle Measurements. Figure 5.1 shows the surface wettability of SAM/Au samples as measured by the advancing contact angle. Initial contact angles for the

$C_{11}SH$/Au (99 ± 3°) and $EG_3C_{11}SH$/Au (31 ± 2°) systems were similar to those previously observed for these surfaces.[13,26] Samples immersed in PBS (solid circles and squares in Figure 5.1) show only mild alteration of contact angle through 21 days. After that time, however, an abrupt change in contact angle is observed. The $C_{11}SH$/Au contact angle exhibited a drop in contact angle from ~100° to 31 ± 1° at 35 days. Similarly, the $EG_3C_{11}SH$/Au samples increased from approximately 30° to 42 ± 3° over the same period.

SAM-coated gold surfaces immersed in calf serum differ in contact angle behavior from the PBS immersed counterparts, as shown in the open circle and square data in Figure 5.1. Here, samples show a dramatic change in contact angle from the initial value before immersion to the first sample recorded at 24 hours. Both $C_{11}SH$ and $EG_3C_{11}SH$ have advancing contact angles that vary between 80° and 59° from day 1–35.

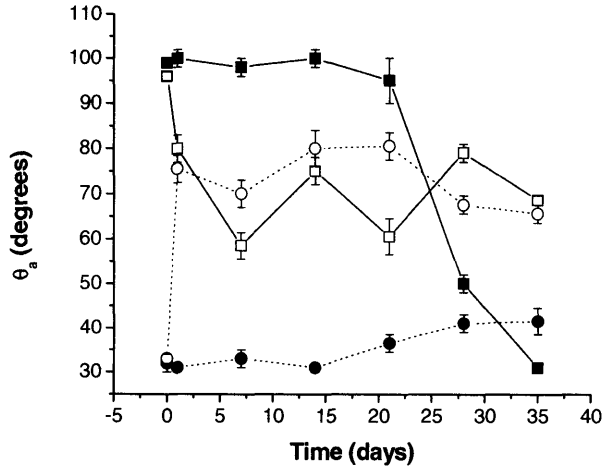

Figure 5.1. Surface wettability measured as the advancing contact angle for $C_{11}SH$ (solid squares) and $EG_3C_{11}SH$ (solid circles) in PBS and $C_{11}SH$ (open squares) and $EG_3C_{11}SH$ in calf serum. Measurements were made following withdrawal of the sample at the indicated time from PBS or calf serum followed by the cleaning procedure outlined in the Experimental Section.

Cyclic Voltammetry. Figure 5.2 shows voltammetric results from the (a) $C_{11}SH/Au$ and (b) $EG_3C_{11}SH/Au$ samples immersed in PBS over the course of 35 days. The initial voltammetry for the $Fe(CN_6)^{3-/4-}$ couple at the SAM covered gold surface is shown as the 0 day sample. Voltammetry after immersion for 1, 7, 14, 21, 28, and 35 days in PBS is also shown in Figure 5.2. The peak current densities at 1 day were similar to that obtained immediately following SAM formation. Both samples deviated from the initial behavior, however, by the seven-day time point. Current densities for anodic and cathodic peaks continued to increase over the course of the 35 days.

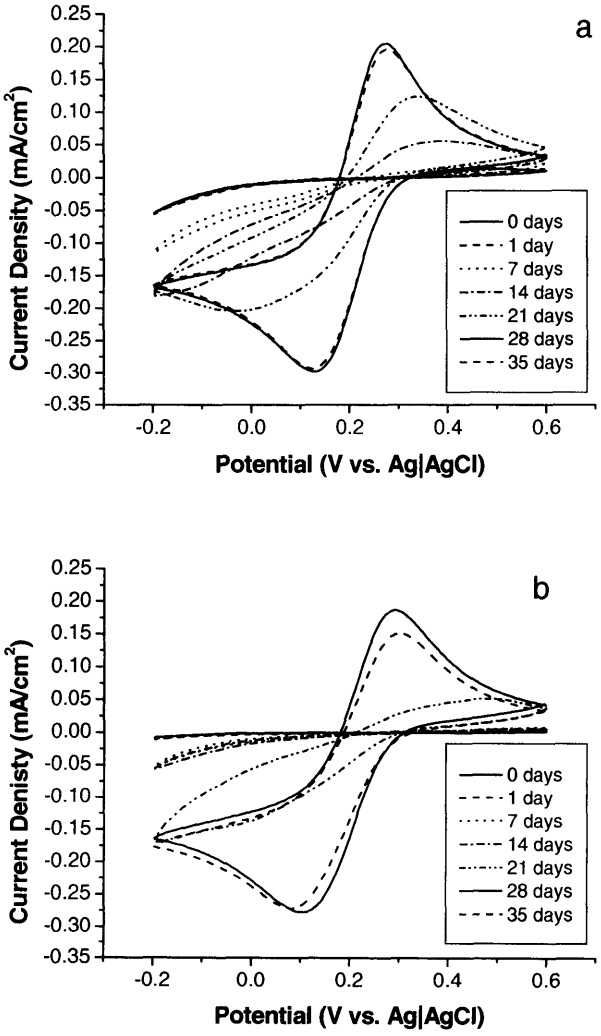

Figure 5.2. Cyclic voltammograms of 5.0 mM $K_3Fe(CN)_6$ + 0.10 M Na_2SO_4 at (a) $C_{11}SH/Au$ and (b) $EG_3C_{11}SH/Au$ after immersion for 0–35 days in PBS. The scan rate was 10 mV/s.

The percentage of current density maximum obtained in voltammetry from PBS-immersed samples is shown in Figure 5.3(a). The percentage represents the average of the absolute value of cathodic and anodic peak current densities divided by the same value calculated from a clean, unmodified surface. As Figure 5.3(a) shows, the average current density increases for both $C_{11}SH/Au$ and $EG_3C_{11}SH/Au$ systems over the course of 35 days. Data are also presented for the $C_{11}SH/Au$ and $EG_3C_{11}SH/Au$ samples immersed in calf serum in Figure 5.3(b). In serum the percentage of peak current density maximum increases from 0–21 days after which decreases from 21–35 days are observed. Finally, similar data are presented in Figure 5.3(c) for samples placed in deoxygenated PBS containing 1.0 mM uric acid. Here little variation in the maximum current densities occurred over the course of 35 days.

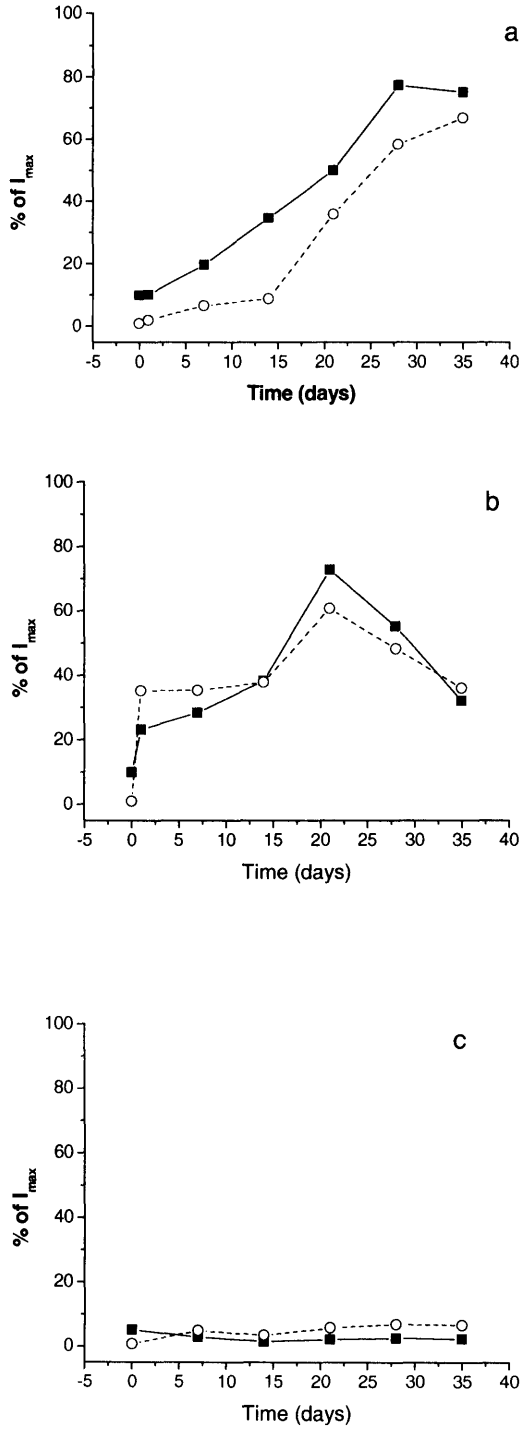

Figure 5.3. Peak current densities measured as a percentage of the average of cathodic and anodic currents for the sample divided by initial peak current densities of clean gold for surfaces immersed in (a) PBS, (b) calf serum, (c) deoxygenated PBS containing 1.0 mM uric acid for $C_{11}SH$ (solid squares) and $EG_3C_{11}SH$ (open circles).

Infrared Spectroscopy. Figure 5.4 shows selected infrared spectra for the $C_{11}SH/Au$ system after immersion for 0, 7, 21, and 35 days in PBS saline. The 0 day spectrum (bottom trace) has predominate peaks centered at 2965.9 cm^{-1}, 2919.6 cm^{-1}, 2879.1 cm^{-1}, and 2851.1 cm^{-1}. These bands have previously been assigned to the CH_3 asymmetric (ν_a-CH_3), CH_2 asymmetric (ν_a-CH_2), CH_3 symmetric (ν_s-CH_3), and CH_2 symmetric (ν_s-CH_2) vibrations, respectively, for other alkanethiol SAM systems on gold.[27] The spectrum seen here for the $C_{11}SH/Au$ system match that previously observed in IR studies for well formed monolayers.[28] Significant changes in spectral features occur after immersion in PBS for as little as 7 days as seen in the second trace from bottom in Figure 5.4. All four peaks have all increased in magnitude as is illustrated in Figure 5.5, where peak heights are plotted as a function of immersion time for the four bands. Additionally, the peaks have broadened significantly and the ν_a-CH_2 and ν_s-CH_2 peaks have shifted position slightly to 2925.4 cm^{-1} and 2854.9 cm^{-1}, respectively. The spectral signature is maintained for the 14 and 21 days samples. At 28 and 35 days, however, a second change is observed. Peaks decrease in height to approximately half there initial value, as seen in Figure 5.5, with substantial peak broadening. Also with the final two time points, the ν_a-CH_2 mode is more intense than the ν_a-CH_3 mode.

Three main peaks at 2921.5 cm^{-1}, 2851.1 cm^{-1}, and 1140 cm^{-1} characterize the initial IR spectrum for $EG_3C_{11}SH/Au$. These peaks have previously been assigned to the ν_a-CH_2, ν_s-CH_2 and C-O and C-C stretching modes in the ethylene glycol groups, respectively.[18] The alteration of the peak intensities for the $EG_3C_{11}SH/Au$ samples immersed in PBS mimics that observed in the $C_{11}SH/Au$ system (data not show).

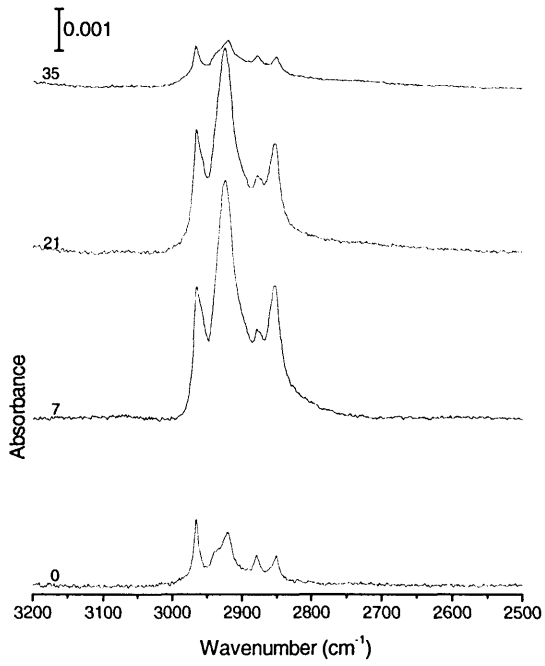

Figure 5.4. IR spectra of $C_{11}SH$/Au SAM after immersion for 0, 7, 21, and 35 days in PBS solution. Spectra have been vertically offset for clarity, but all share the same absorbance scale indicated by the vertical bar.

Temporal changes to spectra for both the $C_{11}SH$/Au and $EG_3C_{11}SH$/Au samples were also investigated in calf serum. Here, however, peaks associated with biological component adsorption (as assigned from bare gold controls aged in calf serum) dominated the spectra from the 1-day point onward.

Controls for the $C_{11}SH$/Au and $EG_3C_{11}SH$/Au monolayers placed in ethanol indicated only minimal decreases in signal over the course of the 35-day experiment. The two monolayer systems immersed for 35 days in deoxygenated PBS containing 1.0 mM uric acid exhibited changes similar to those of the ethanol controls (data not shown).

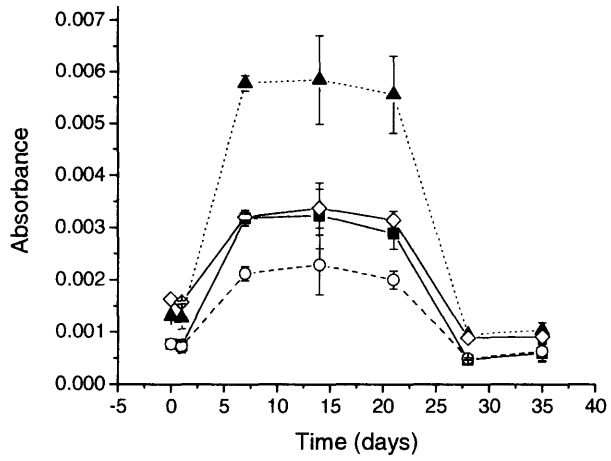

Figure 5.5. Temporal changes in IR peak intensities for the $C_{11}SH/Au$ system immersed in PBS for the 2850 cm^{-1} (solid squares), 2880 cm^{-1} (open circles), 2920 cm^{-1} (solid triangles), and 2965 cm^{-1} (open diamonds) vibrational bands. Values represent the average of at least 3 samples and errors represent the corresponding standard deviations.

X-ray Photoelectron Spectroscopy. Figure 5.6(a) shows the S 2p region of the X-ray photoelectron spectrum for $C_{11}SH/Au$ both immediately after monolayer formation (solid line) and after 35 days immersed in PBS (dashed line). The count rates were normalized so that the count rate for the Au $4f_{7/2}$ peak was the same for each sample. The position of the S 2p peak corresponds well with the reported values for other self-assembled monolayer systems on gold surfaces.[24] The position of the S 2p falls within the range (160–165) expected for thiols.[29] Similarly, Figure 5.6(b) shows the S 2p region of the spectrum for the $EG_3C_{11}SH/Au$ immediately after monolayer formation (solid line) and after 35 days immersed in PBS (dashed line), again with normalized count rate. Both the $C_{11}SH/Au$ and $EG_3C_{11}SH/Au$ spectra show appreciable loss of the S 2p peaks after 35 days immersion in PBS. Control experiments with freshly prepared SAM/Au immersed in ethanol over the same period of time showed no similar loss in S 2p signal.

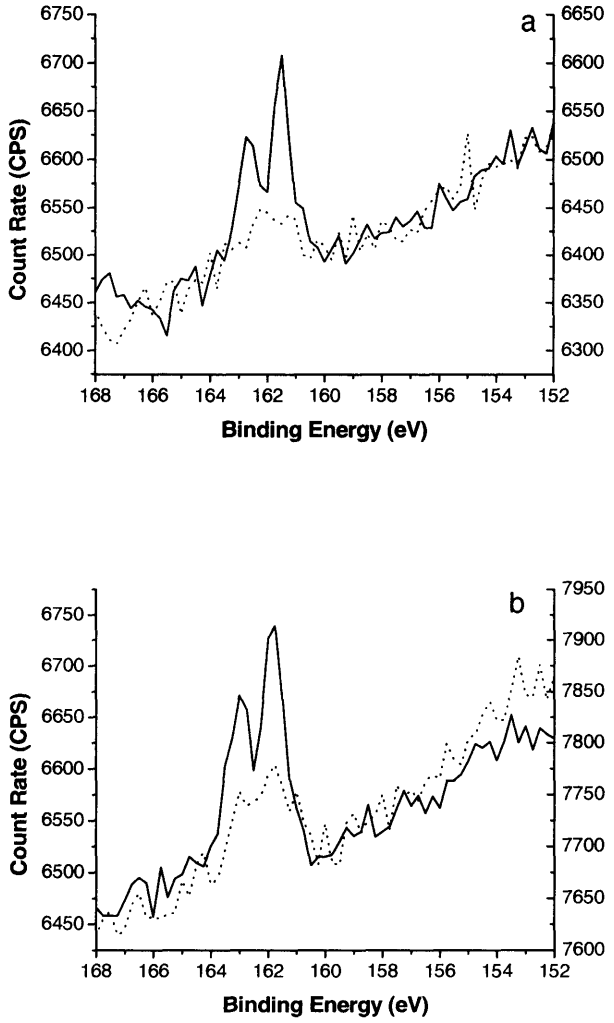

Figure 5.6. XPS of S 2p region for freshly prepared SAM/Au (solid lines) and samples emmersed (dotted lines) after 35 days in PBS for (a) $C_{11}SH/Au$ and (b) $EG_3C_{11}SH/Au$.

Spectra for the $C_{11}SH/Au$ and $EG_3C_{11}SH/Au$ samples immersed for 35 days in deoxygenated PBS with 1.0 mM uric acid present are shown in Figure 5.7, solid and dashed lines respectively. Here, both the samples retain their initial peak heights over the course of 35 days.

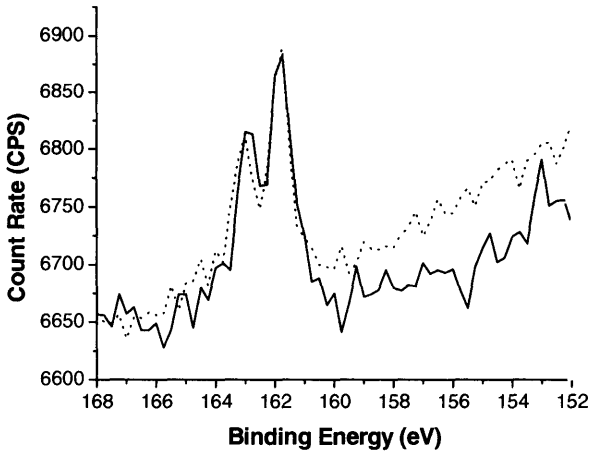

Figure 5.7. XPS of S 2p region of $C_{11}SH/Au$ (solid line) and $EG_3C_{11}SH/Au$ (dotted line) after 35 days in deoxygenated PBS solution containing 1.0 mM uric acid.

5.5. Discussion

Integrity of the as-formed SAMs. The $C_{11}SH/Au$ and $EG_3C_{11}SH/Au$ monolayer systems both exhibit characteristics associated with well-formed monolayers prior to immersion in PBS or serum. The initial advancing contact angles of water for the two samples, 99 ± 3° $C_{11}SH/Au$ and 31 ± 2° $EG_3C_{11}SH/Au$, correspond well to previously observed values.[13,26] Strong passivation of the gold electrode surface is also observed in electrochemical experiments using 5.0 mM $Fe(CN_6)^{3-/4-}$ as a redox probe as illustrated in the 0 day voltammograms in Figure 5.2 (a) and (b). The $C_{11}SH/Au$ system exhibits a maximum current density that is less than 10% of that seen for a clean gold surface and the $EG_3C_{11}SH/Au$ sample is less than 1% that value. Additionally, both the cathodic current density maxima are dramatically shifted toward more negative potentials. Again, the voltammetric features for the straight chain alkanethiol system are similar to those observed in well-formed SAM systems previously.[30-33] Although little electrochemical

characterization of oligo(ethylene glycol) terminated SAMs is available in the literature, the degree of initial passivation indicates formation of monolayers with low defect density.

Initial contact angle measurements indicate the expected hydrophobic and hydrophilic nature of the $C_{11}SH/Au$ and $EG_3C_{11}SH/Au$ monolayers, respectively. Similarly, voltammetry of $Fe(CN_6)^{3-}$ at these monolayers reveals that the surfaces as formed are largely defect free. The importance of surface preparation on long-term stability of SAMs in air has been noted.[24,34,35] To test the robustness of SAMs used in these studies, RSH/Au samples were immersed in alkanethiol-free ethanol and stored for 35 days. After that time, samples were withdrawn and probed using contact angle goniometry and electrochemistry. The contact angles measured and the currents observed in voltammetry both indicate little loss in the initial monolayer integrity (data not shown). Specifically, the contact angle for both samples was within the error of the initial readings and the peak cathodic current density from voltammetry was within 5% of that observed initially. Therefore, the monolayers appear to have stability in ethanol over the course of five weeks.

FT-IR spectroscopy serves as an excellent measure of the initial integrity of a SAM. In particularly, the ν_a-CH_2 band is strongly sensitivity to monolayer order occurring at 2916-2917 cm^{-1} for highly crystalline, long-chain alkanethiols and shifting toward 2925 cm^{-1} or above for more disordered monolayers.[36] The initial position of the band for the $C_{11}SH/Au$ sample at 2919.6 cm^{-1} indicates that this relatively short chain alkanethiol is well-formed. The $EG_3C_{11}SH/Au$ asymmetric methylene stretch at 2921.5 cm^{-1} is somewhat shifted from the crystalline value, but this is expected for ordered

oligo(ethylene glycol) terminated SAMs where the peak is typically found near 2921 cm^{-1}.

SAM Behavior in PBS and Serum. The long-term immersion of SAM/Au in PBS and serum causes significant alteration in properties. In PBS, $C_{11}SH$/Au shows slightly different time scales of alteration in contact angle and electrochemical analyses. The advancing contact angle drops precipitously from ~100° to > 50° after 21 days as seen in Figure 5.1. Voltammetry results, however, reveal a steady increase in current densities measured beginning with the first time point at 1 day (closed squares in Figure 5.3a). Similar, though not as pronounced, differences between contact angle and electrochemistry results are observed for the $EG_3C_{11}SH$/Au system. The origin of the difference may lie in the length scale over which these techniques probe. Cyclic voltammetry using a solution-based redox active probe is a technique that allows the identification of nanoscopic defects within the self-assembled monolayer.[37,38] On the other hand, contact angle measures large area properties. One likely explanation, then, is that the monolayer slowly degrades by removal of alkanethiol molecules from the surface. Figure 5.6 indicates this loss for both $C_{11}SH$/Au (a) and $EG_3C_{11}SH$/Au (b) monolayers by the substantial decrease in S 2p signal between days 1 and 35. A mechanism for this proposed loss is outline below. As SAM molecules desorb, current densities immediately increase due to small-scale defects allowing access of the redox probe to the gold surface. The contact angle, however, remains relatively constant because chains simply tilt further from the surface normal while retaining their hydrophobic or hydrophilic nature.

This mechanism of SAM loss is supported by infrared spectroscopy. Significant increases in peak intensities are seen between days 0 and 7 as Figure 5.4 shows. Figure 5.5 illustrates the temporal changes in peak intensity for each of the four major bands of

the $C_{11}SH$/Au system. These increases in intensity, in particular those of the CH_2 vibrations, are correlated with the increase in tilt angle of the SAM molecules away from the surface normal or an increase in disorder along the alkanethiol backbone.[39] Previous studies of methyl-terminated SAMs in air have shown similar changes in peak intensities as a function of time and attributed these changes to increases in molecular tilt angle.[21] Additionally, between days 0 and 7 the ν_a-CH_2 band shifted position form 2919.6 cm^{-1} to 2925.4 cm^{-1} signifying a decrease in monolayer crystallinity.[36] Over the first week in PBS, the $C_{11}SH$ monolayer appears to rapid become less well ordered along the hydrocarbon backbone and tilt farther from the surface normal. These changes likely occur through the loss of some fraction of the molecules within the monolayer.

After 21 days, the peak intensities decrease and bands broaden significantly as illustrated by the 35-day spectrum in Figure 5.4. The behavior here differs from the case of alkanethiol monolayers oxidation in air, where only increases in peak intensity are observed. [21] The difference lies in the presence of a low energy pathway for removal of the oxidized head group from the surface. In air, the oxidized adsorbates become increasingly disordered with time. In PBS, however, the molecules can simply desorb from the surface into the surrounding medium leading to a loss of signal after longer periods of time.

Results for the monolayers immersed in calf serum vary substantially from those seen with PBS-immersed samples as Figures 5.1 and 5.3 indicate. Figure 5.1 (open circles and squares) shows a precipitous change in contact angle for both SAMs immediately following immersion. The rapid change is followed by contact angles that vary substantially between 60° and 80° over the next 34 days. The rapid change results from the difficulty of removing serum components from the device surface. Despite vigorous

washing in water and ethanol streams, serum components likely remained on the surface. The variability in contact angle over the 35-day period also has its genesis in the difficulties associated with adequate removal of biological components.

Electrochemical results in Figure 5.3(b) show variation substantially different from that observed for PBS (Figure 5.3a). An increase in current density occurs over the first 21 days, followed by a decrease between 21 and 35 days. The origins of the current density increases over the first 21 days likely arise through the same method as that used above to describe the increases with PBS-immersed samples. Specifically, the alkanethiol molecules within the self-assembled monolayer desorb and make the surface more electrochemically accessible for the $Fe(CN_6)^{3-}$ species. Near 21 days, however, enough of the monolayer has been removed so that biological molecules within the serum can easily adsorb causing a subsequent decrease in current densities.

Mechanism of SAM Desorption. An understanding of the mechanism of desorption is necessary both to evaluate the viability of this surface modification method and to point to other surface chemistries that resist this mechanism and may exhibit higher long-term stability for *in vivo* applications. The contact angle, cyclic voltammetry, FT-IR and XPS results for both SAM samples are consistent with the loss of monolayer integrity over 35 days. One likely explanation for this loss is through a mechanism similar to that proposed for alkanethiols that lose integrity in air. Researchers have attributed the process to oxidation of the thiolate head group. Specifically, infrared,[21] Raman,[24] and X-ray photoelectron[23,24] spectroscopies all indicate changes in the monolayer that are consistent with conversion of the thiolate head group to species such as sulfinates and sulfinites. The extent of this oxidation is also found to vary based on exposure to ozone.[24] In XPS, the S 2p peak is seen to shift from a binding energy of 162 eV to 168 eV. Similar shifts are not

observed here because of a fundamental experimental difference. The oxidized head group in the current study can easily desorb from the surface and become solubilized in the PBS or serum medium. This is in contrast to the situation in air where there is a large energetic barrier to removal from the gold surface.

The PBS immersion experiments were repeated in a solution that was deoxygenated with N_2(g) and contained the mild antioxidant uric acid to test the oxidation hypothesis.[40] Figure 5.3(c) shows electrochemical results for these samples. Here, no long-term increase in peak current densities occurred over the 35-day experiment. Also, the infrared spectra of the 35-day C_{11}SH/Au and EG_3C_{11}SH/Au samples immersed in deoxygenated PBS containing 1.0 mM uric acid were indistinguishable from the ethanol controls. Finally, Figure 5.7 shows the S 2p region for the C_{11}SH/Au and EG_3C_{11}SH/Au samples after immersion for 35 days. Again, no indication of loss of the monolayer is seen with XPS as opposed to the results seen for the standard conditions in Figure 5.7. From these experiments, we conclude that the most likely mechanism for loss of the monolayer integrity is through oxidation of the thiolate head group followed by desorption into the surrounding medium.

5.6. Conclusions

The multiweek stability of C_{11}SH/Au and EG_3C_{11}SH/Au self-assembled monolayers was investigated after immersion in either PBS or calf serum. Contact angle, electrochemical, FT-IR, and XPS measurements all indicate that the integrity of both monolayer systems is compromised over the course of 35 days of immersion. The most likely origin of the monolayer loss is through the oxidation of the thiolate head group and its subsequent desorption from the gold surface. Controls with deoxygenated PBS

containing an antioxidant substantially improved the monolayer integrity, supporting this conclusion. The results here suggest that the use of SAMs for alleviation of biofouling issues faced by MEMS devices is usefully over a time scale of several weeks. Systems requiring longer durations may necessitate the use of modified systems such as a cross-linked,[41] oligo(EG) terminated SAMs or other methods of surface passivation such as that involving block copolymers[42], which may exhibit better long-term stability.

5.7. References

1. Voldman, J., Gray, M. L. & Schmidt, M. A. Microfabrication in biology and medicine. *Annu. Rev. Biomed. Eng.* **1**, 401-425 (1999).
2. Dario, P., Carrozza, M. C., Benvenuto, A. & Menciassi, A. Micro-systems in biomedical applications. *J. Micromech. Microeng.* **10**, 235-244 (2000).
3. Shawgo, R. S., Richards Grayson, A. C., Li, Y. & Cima, M. J. BioMEMS for drug delivery. *Curr. Opin. Solid State Mater. Sci.* **6**, 329-334 (2002).
4. Santini, J. T., Jr., Cima, M. J. & Langer, R. A controlled-release microchip. *Nature (London)* **397**, 335-338 (1999).
5. Santini, J. T., Jr., Richards, A. C., Scheidt, R., Cima, M. J. & Langer, R. Microchips as controlled drug-delivery devices. *Angew. Chem., Int. Ed.* **39**, 2396-2407 (2000).
6. Ahmed, A., Bonner, C. & Desai, T. A. Bioadhesive microdevices for drug delivery: a feasibility study. *Biomedical Microdevices* **3**, 89-95 (2001).
7. Voskerician, G. et al. *In vivo* inflammatory and wound healing effects of gold electrode voltammetry for MEMS micro-reservoir drug delivery device. *IEEE Transactions on Biomedical Engineering*, in press (2003).
8. Voskerician, G. et al. Biocompatibility and biofouling of MEMS drug delivery devices. *Biomaterials* **24**, 1959-1967 (2003).
9. Blawas, A. S. & Reichert, W. M. Protein patterning. *Biomaterials* **19**, 595-609 (1998).
10. Kingshott, P. & Griesser, H. J. Surfaces that resist bioadhesion. *Curr. Opin. Solid State Mater. Sci.* **4**, 403-412 (1999).

11. Prime, K. L. & Whitesides, G. M. Self-assembled organic monolayers: model systems for studying adsorption of proteins at surfaces. *Science (Washington, D. C., 1883-)* **252**, 1164-1167 (1991).

12. Mrksich, M., Sigal, G. B. & Whitesides, G. M. Surface Plasmon Resonance Permits in Situ Measurement of Protein Adsorption on Self-Assembled Monolayers of Alkanethiolates on Gold. *Langmuir* **11**, 4383-4385 (1995).

13. Sigal, G. B., Mrksich, M. & Whitesides, G. M. Effect of Surface Wettability on the Adsorption of Proteins and Detergents. *Journal of the American Chemical Society* **120**, 3464-3473 (1998).

14. Benesch, J. et al. Protein adsorption to oligo(ethylene glycol) self-assembled monolayers: experiments with fibrinogen, heparinized plasma, and serum. *Journal of Biomaterials Science, Polymer Edition* **12**, 581-597 (2001).

15. Mrksich, M. et al. Controlling cell attachment on contoured surfaces with self-assembled monolayers of alkanethiolates on gold. *Proceedings of the National Academy of Sciences of the United States of America* **93**, 10775-10778 (1996).

16. Roberts, C. et al. Using mixed self-assembled monolayers presenting RGD and (EG)3OH groups to characterize long-term attachment of bovine capillary endothelial cells to surfaces. *Journal of the American Chemical Society* **120**, 6548-6555 (1998).

17. Cox, J. D., Curry, M. S., Skirboll, S. K., Gourley, P. L. & Sasaki, D. Y. Surface passivation of a microfluidic device to glial cell adhesion: a comparison of hydrophobic and hydrophilic SAM coatings. *Biomaterials* **23**, 929-935 (2001).

18. Harder, P., Grunze, M., Dahint, R., Whitesides, G. M. & Laibinis, P. E. Molecular Conformation in Oligo(ethylene glycol)-Terminated Self-Assembled Monolayers

on Gold and Silver Surfaces Determines Their Ability To Resist Protein Adsorption. *Journal of Physical Chemistry B* **102**, 426-436 (1998).

19. Ostuni, E. et al. Self-assembled monolayers that resist the adsorption of proteins and the adhesion of bacterial and mammalian cells. *Langmuir* **17**, 6336-6343 (2001).

20. Luk, Y.-Y., Kato, M. & Mrksich, M. Self-Assembled Monolayers of Alkanethiolates Presenting Mannitol Groups Are Inert to Protein Adsorption and Cell Attachment. *Langmuir* **16**, 9604-9608 (2000).

21. Horn, A. B., Russell, D. A., Shorthouse, L. J. & Simpson, T. R. E. Ageing of alkanethiol self-assembled monolayers. *J. Chem. Soc., Faraday Trans.* **92**, 4759-4762 (1996).

22. Zhang, Y., Terrill, R. H., Tanzer, T. A. & Bohn, P. W. Ozonolysis Is the Primary Cause of UV Photooxidation of Alkanethiolate Monolayers at Low Irradiance. *Journal of the American Chemical Society* **120**, 2654-2655 (1998).

23. Lee, M.-T., Hsueh, C.-C., Freund, M. S. & Ferguson, G. S. Air oxidation of self-assembled monolayers on polycrystalline gold. The role of the gold substrate. *Langmuir* **14**, 6419-6423 (1998).

24. Schoenfisch, M. H. & Pemberton, J. E. Air Stability of Alkanethiol Self-Assembled Monolayers on Silver and Gold Surfaces. *J. Am. Chem. Soc.* **120**, 4502-4513 (1998).

25. Schoenfisch, M. H., Ovadia, M. & Pemberton, J. E. Covalent surface chemical modification of electrodes for cardiac pacing applications. *J. Biomed. Mater. Res.* **51**, 209-215 (2000).

26. Pale-Grosdemange, C., Simon, E. S., Prime, K. L. & Whitesides, G. M. Formation of self-assembled monolayers by chemisorption of derivatives of oligo(ethylene glycol) of structure HS(CH2)11(OCH2CH2)mOH on gold. *J. Am. Chem. Soc.* **113**, 12-20 (1991).

27. Laibinis, P. E. et al. Comparison of the structures and wetting properties of self-assembled monolayers of n-alkanethiols on the coinage metal surfaces, copper, silver, and gold. *Journal of the American Chemical Society* **113**, 7152-67 (1991).

28. Yam, C.-M. et al. Labelling and binding of poly-(L-lysine) to functionalised gold surfaces. Combined FT-IRRAS and XPS characterisation. *Colloids and Surfaces, B: Biointerfaces* **21**, 317-327 (2001).

29. Ulman, A. Ultrathin organic films: from Langmuir-Blodgett to self-assembly. *J. Mater. Educ.* **11**, 205-80 (1989).

30. Miller, C., Cuendet, P. & Graetzel, M. Adsorbed .omega.-hydroxy thiol monolayers on gold electrodes: evidence for electron tunneling to redox species in solution. *Journal of Physical Chemistry* **95**, 877-886 (1991).

31. Takehara, K., Takemura, H. & Ide, Y. Electrochemical studies of the terminally substituted alkanethiol monolayers formed on a gold electrode: effects of the terminal group on the redox responses of Fe(CN)63-, Ru(NH3)63+ and ferrocenedimethanol. *Electrochim. Acta* **39**, 817-22 (1994).

32. Cheng, J., Saghi-Szabo, G., Tossell, J. A. & Miller, C. J. Modulation of Electronic Coupling through Self-Assembled Monolayers via Internal Chemical Modification. *Journal of the American Chemical Society* **118**, 680-684 (1996).

33. Janek, R. P., Fawcett, W. R. & Ulman, A. Impedance Spectroscopy of Self-Assembled Monolayers on Au(111): Sodium Ferrocyanide Charge Transfer at Modified Electrodes. *Langmuir* **14**, 3011-3018 (1998).

34. Creager, S. E., Hockett, L. A. & Rowe, G. K. Consequences of microscopic surface roughness for molecular self-assembly. *Langmuir* **8**, 854-861 (1992).

35. Yang, Z. et al. Analytical application of self assembled monolayers on gold electrodes: critical importance of surface pretreatment. *Biosens. Bioelectron.* **10**, 789-795 (1995).

36. Porter, M. D., Bright, T. B., Allara, D. L. & Chidsey, C. E. D. Spontaneously organized molecular assemblies. 4. Structural characterization of n-alkyl thiol monolayers on gold by optical ellipsometry, infrared spectroscopy, and electrochemistry. *Journal of the American Chemical Society* **109**, 3559-68 (1987).

37. Sabatani, E. & Rubinstein, I. Organized self-assembling monolayers on electrodes. 2. Monolayer-based ultramicroelectrodes for the study of very rapid electrode kinetics. *J. Phys. Chem.* **91**, 6663-6669 (1987).

38. Baker, W. S. & Crooks, R. M. Independent Geometrical and Electrochemical Characterization of Arrays of Nanometer-Scale Electrodes. *J. Phys. Chem. B* **102**, 10041-10046 (1998).

39. Allara, D. L. & Nuzzo, R. G. Spontaneously organized molecular assemblies. 2. Quantitative infrared spectroscopic determination of equilibrium structures of solution-adsorbed n-alkanoic acids on an oxidized aluminum surface. *Langmuir* **1**, 52-66 (1985).

40. Van der Vliet, A., O'Neill, C. A., Eiserich, J. P. & Cross, C. E. Oxidative damage to extracellular fluids by ozone and possible protective effects of thiols. *Archives of Biochemistry and Biophysics* **321**, 43-50 (1995).

41. Peanasky, J. S. & McCarley, R. L. Surface-Confined Monomers on Electrode Surfaces. 4. Electrochemical and Spectroscopic Characterization of Undec-10-ene-1-thiol Self-Assembled Monolayers on Au. *Langmuir* **14**, 113-123 (1998).

42. Bearinger, J. P. et al. Chemisorbed poly(propylene sulphide)-based copolymers resist biomolecular interactions. *Nature Materials* **2**, 259-264 (2003).

CHAPTER SIX

CONCLUSIONS AND FUTURE DIRECTIONS

This thesis represents an effort to understand the phenomena occurring at the interfaces of self-assembled monolayers (SAMs) and solutions, to explore the ability to control SAM properties by modifying surface functionalities, and to develop means of improving technologies related to biosensing, drug delivery, implantable biochips, as well as other nanotechnological applications. SAMs are good candidates for studying of interfacial phenomena, since they are relatively easy to form, and has structural order that allows surface properties to be fine-tuned and interfaces to be designed according to specific requirements. One of the original goals of the project is to investigate the feasibility of controlling surface wettability by applying an external force, in this case an electrical potential. In developing this goal, we have synthesized a new class of SAM containing a globular endgroup that is densely packed with respect to the space-filling endgroup, yet shows low-density packing with respect to the methylene chains. Cleavage of this endgroup leads to formation of a low-density monolayer. The low-density monolayer was then used as a template of surface-confined, single-layered molecules undergoing conformational transitions in response to an electrical potential. This type of surface enables amplification of conformational transitions at a molecular level to macroscopic changes in surface properties without altering chemical identity. We observed changes in both a microscopic scale with Sum-Frequency Generation Spectroscopy and the macroscopic scale with dynamic contact angles measurements. The changes are reversible (up to four cycles) and the macroscopic change from a hydrophilic to a moderately hydrophobic state is observable in receding contact angle measurements. This reversibility is of importance in developing lab-on-a-chip, biosensor, and drug delivery technologies, where capture and release of cells, biomolecules, and drugs are desirable. However, this is a proof-of-principle. In order to develop further the technology, new class of molecules that can amplify these effects is needed. This new class of molecules may involve, for

example, a flip-flop module that can reversibly switch between a hydrophobic and hydrophilic state, or it may involve two crown ether molecules with a "thread" in-between that contains a planar compound with hydrophobic/hydrophilic sides and an ability to rotate around its axis. A "state change" as close as possible from 0 to 1 is most desirable (ie from a completely hydrophobic to completely hydrophilic state). Once a more robust system with a larger change in surface property in response to an external force is developed, one can think about developing switches in biological properties, introducing functional groups, enzymes, proteins at the right temporal pattern. This has interesting applications in the study of the dynamics of cell-surface interactions, where turning on and off charges on a surface, increase or decrease hydrophobicity, hydrophilicy, as well as introduction and withdrawal of extracellular-matrix binding elements may lead to interesting insights regarding how cells interact with its environment. Other applications involve drug delivery, microfabricated cell-sorter with an ability to capture and release cells, biosensing devices, and microfluidics devices, where a change in hydrophobicity and/or hydrophilicity can act as a nanovalve, redirecting fluid flows in a desired direction.

The development of a new class of low-density monolayers led us to some interesting projects. One involves backfilling the low-density assembly with a second alkanethiol molecules, therefore forming a homogeneously-mixed self-assembled monolayer. This method of forming mixed SAMs has implications in the ability to tailor-make and space apart functionalities on a surface, as well as varying the composition of the different components in the SAM. This is an improvement over some previous methods, where the control of surface composition involves trial-and-error, and one has little control over the spacing between each molecules. The development of the homogeneously-mixed SAMs can lead to applications in oligonucleotide and proteins arrays, where reduced density often leads to improvement in hybridization or binding

efficiency. We tested this hypothesis by tethering oligos to our homogeneously-mixed SAM and investigated its hybridization efficiency with complimentary target oligonucleotides versus the same procedure on a densely-packed SAM of the same functional group (in this case, a carboxylic acid compound – 16-mercaptohexadecanoic acid). Both quartz-crystal microbalance with dissipation monitoring (QCM-D) and surface plasmon resonance (SPR) measurements support the hypothesis that oligo tethered to a backfilled low dense layer has improved hybridization efficiency versus a dense layer. This observation may be attributable to decrease steric hindrance and/or more appropriate oligo orientation for complement hybridization. Future applications can be in tailoring the distance between molecules for specific needs, depending on the size of the molecules being tethered, and development of protein arrays using similar technologies. The ability to isolate single molecule from each other may have implications in studying single-molecule dynamics, charge transfer properties, etc.

The final piece of the project involves the study of the long-term stability of SAMs in biological media. SAMs have many interesting applications in modifying surface properties, rendering it biocompatible by attachment of extracellular matrix peptides, or in preventing adsorption of proteins, in decreasing adhesion of cells, etc., most often through the use of poly(ethylene glycol) (PEG) terminated endgroups. These properties render them desirable for possible uses in implantable bio-microelectromechanical system (bioMEMs), drug delivery, and artificial organs devices, which often have prolonged exposure to bodily fluids and tissue. We investigated the electrochemical and surface properties of PEG-terminated SAM versus undecanethiol SAMs after 35 days immersion in either PBS or calf serum. The results show that both surfaces are compromised over the course of 35 days, with desorption of monolayer through a possible oxidative process, implying that the use of SAM in MEMs devices are useful over the

time scale of several weeks. System requiring longer duration may necessitate the use of polymeric or cross-linked monolayers. This particular project ties in nicely with the rest of the thesis, since it addresses long-term issues in the use of SAMs for implantable devices purposes, and may serve as a starting point for further studies of surface chemical modifications methods for moderate to long-term minimization of biofouling in *in vivo* applications.